AD NUMBER

AD838802

NEW LIMITATION CHANGE

TO

Approved for public release, distribution unlimited

FROM

Distribution authorized to U.S. Gov't. agencies and their contractors; Administrative/Operational Use; AUG 1968. Other requests shall be referred to Air Force Materials Lab., Wright-Patterson AFB, OH 45433.

AUTHORITY

AFML ltr, 12 Jan 1972

AD638802

STUDY OF MICROPLASTIC PROPERTIES AND DIMENSIONAL STABILITY OF MATERIALS

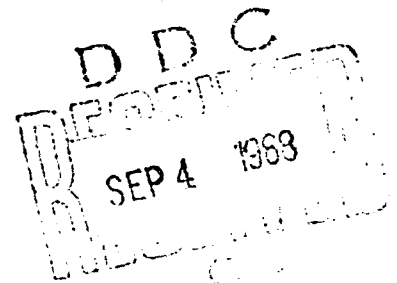A. G. Imgram, M. E. Hoskins, J. H. Sovik, R. E. Maringer,
and F. C. Holden

BATTELLE MEMORIAL INSTITUTE
Columbus Laboratories

TECHNICAL REPORT AFML-TR-67-232, Part II

August, 1968

Air Force Materials Laboratory
Air Force Systems Command
Wright-Patterson Air Force Base, Ohio

D D C

SEP 4 1968

AFML-TR-67-232
Part II

STUDY OF MICROPLASTIC PROPERTIES AND DIMENSIONAL STABILITY OF MATERIALS

A. G. Imgram, M. E. Hoskins, J. H. Sovik, R. E. Maringer,
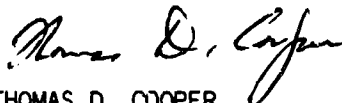and F. C. Holden

FOREWORD

    This report was prepared by Battelle Memorial Institute, Columbus, Ohio under USAF Contract No. AF 33(615)5218. The contract was initiated under Project No. 7351 "Metallic Materials", Task No. 735103 "Unique Metallic Materials". The work was administered under the direction of the Air Force Materials Laboratory, Directorate of Laboratories with Mr. George Saul (MAMN) acting as project engineer.

    The report covers work conducted during the period July 1967 - June 1968.

    The manuscript was released by the authors 7 June 1968 for publication as an AFML Technical Documentary Report.

    This technical report has been reviewed and is approved.

THOMAS D. COOPER
Chief, Processing &
Nondestructive Testing Branch
Metals & Ceramics Division

ABSTRACT

Average microyield strengths of 39,000 psi for Ni-Span-C, 70,000 psi for 440 C stainless steel, 7,500 psi for A356 cast aluminum, 75,000 psi for Ti-5Al-2.5Sn, 47,000 psi for Super PEL beryllium, and 29,000 psi for AD995 aluminum oxide were measured. The microcreep behavior of these materials at 50 and 75 percent of their microyield strengths was evaluated also. Experiments showed that plastic strains of 20-40 μin./in. increased the microyield strength of Ni-Span-C and 440 C stainless steel, but plastic strains of 2.5 and 5 percent decreased the microyield strength of Ni-Span-C. Electron-microscope studies indicated that microplastic deformation of Ni-Span-C is the result of dislocation generation at second-phase particles in grain boundaries. For A356 cast aluminum, the generation of dislocations at Mg_2Si particles appeared to be the controlling mechanism.

Dimensional-stability studies showed that plastic strains of 20-40 μin./in. did not result in any significant deterioration in dimensional stability, but extensive contraction of specimens strained 2 percent was noted. The mild stress and thermal cycling treatments employed in this research sometimes caused a small change in length upon cycling, but showed no effect on subsequent dimensional stability over a period of at least 6 months.

Machining experiments revealed that the residual stresses introduced by machining can exceed the microyield strength of an alloy. Furthermore, the highest residual stresses are frequently associated with the finest finishing cuts.

A capacitor strain gage was designed, constructed, and used to measure the microyield strength of Ti-5Al-2.5Sn.

A phenomenological theory has been devised which is selfconsistent with the bulk of the observed behavior.

iii

TABLE OF CONTENTS

v

TABLE OF CONTENTS
(Continued)

LIST OF ILLUSTRATIONS

LIST OF ILLUSTRATIONS
(Continued)

LIST OF TABLES

INTRODUCTION

The designers of precision instruments, such as inertial guidance units and optical devices, frequently require that the critical components of these instruments retain their dimensions to very close tolerances under storage and service conditions. Reversible dimensional changes attributable to thermal expansion and elastic deformation can usually be compensated for. Control of permanent dimensional changes due to other sources presents a much more serious problem, and requires an understanding of material behavior heretofore left largely unexplored.

Both external and internal factors can cause small dimensional changes. The most important external factor is an applied load. Most materials deform plastically in response to an externally applied load of a sufficient magnitude, and it is known that microplastic deformation (i.e., plastic deformation on the order of microinches per inch) can occur at stresses well below the conventional 0.2 percent offset yield strength. Consequently, the designer of precision instruments requires mechanical-property data quite different from those derived from an ordinary tensile test.

The microplastic deformation of a material is frequently evaluated by the microyield-strength test. This test involves loading a tensile specimen to successively higher stresses and determining the residual strain in the specimen upon removal of the load from each stress increment. The microyield strength itself is defined as the stress necessary to cause a residual plastic strain of 1 μin./in. Microplastic deformation is similar to macroplastic deformation (i.e., deformation resulting from loading to significantly higher strains) in that it is presumably a result of the stress-induced and thermally activated generation and movement of dislocations. However, the specific mechanisms controlling dislocation generation and motion resulting in microplastic deformation at relatively low stresses can differ from those accounting for macroplastic deformation at higher stresses.

If microplastic deformation is a thermally activated process, it can be expected that microplastic deformation will occur at stresses below the microyield strength if the material remains loaded for extended periods. This property of a material can be evaluated by the microcreep test in which a tensile specimen is loaded to a fraction of the microyield strength, and the increase in total strain is determined as a function of time.

Two major internal factors leading to dimensional instability are residual stresses and metallurgical instabilities. Residual stresses are usually developed by processing (i.e., mechanical working, heat treatment, and machining, etc.). A material can respond to these internal, residual stresses in much the same way that it reacts to an externally applied load. Therefore, one manifestation of residual-stress relaxation will be microplastic deformation, and consequent dimensional change. Mechanical vibrations should accelerate residual-stress relaxation. The vibrational stresses are superimposed on the preexisting residual stresses and can provide the additional energy necessary to activate dislocation generation and movement.

Rapid thermal cycling can produce a thermal gradient severe enough to develop internal stresses of a sufficient magnitude to cause microplastic deformation. Also, high internal stresses can be created by slow thermal cycling if the material is anisotropic with respect to its thermal expansion coefficients or if it contains two or more microstructural phases each of which has a different thermal expansion coefficient. Even if these stresses produced by thermal cycling are not high enough by themselves to cause

1

microplastic deformation, they will be superimposed on preexisting residual stresses and the combined stresses may exceed the microyield strength and cause dimensional changes.

Metallurgical alterations such as recrystallization, grain growth, polygonization, second-phase precipitation, ordering, and allotropic phase transformations are accompanied by a volume change. Therefore, metallurgical instabilities can also result in dimensional changes.

Methods for eliminating, or at least minimizing, dimensional instability resulting from residual stresses and metallurgical transformations are known in principle and have been used in practice.[1,2,3] Residual stresses are reduced by stress-relief annealing, and by thermal and stress cycling, whereas metallurgical stability is promoted by approaching thermodynamic equilibrium. Difficulties arise in the application of these principles because the optimum thermal treatments for metallurgical stability and stress-relief annealing may not be compatible. Furthermore, other requirements for strength, hardness, or corrosion resistance etc., may preclude their use.

This report summarizes the results obtained in a 2-year research program designed to obtain increased knowledge of the microplastic properties and dimensional stability of materials of potential interest for the construction of precision instruments. The materials studied were Ni-Span-C, 440 C stainless steel, A356 cast aluminum, Ti-5Al-2.5Sn, Super PEL beryllium, and AD995 aluminum oxide. The microyield strength and microcreep behavior of each material was evaluated. Insight was gained into the effects of plastic strain on microplastic deformation and into the dislocation mechanisms involved in microplastic flow. In addition, the dimensional stability of the above metallic materials was investigated as a function of plastic strain, load cycling, thermal cycling, and residual stresses developed by machining.

2

SUMMARY

The purpose of this research program was to evaluate the microplastic proper-
ties and dimensional stability of Ni-Span-C, 440 C stainless steel, A356 cast aluminum,
Ti-5Al-2.5Sn, Super PEL beryllium, and AD995 aluminum oxide.

Table I summarizes the microyield-strength and microcreep behavior of the
above materials. Experiments showed that plastic strains of 20-40 μin./in. significantly
increased the microyield strengths of Ni-Span-C and 440 C stainless steel. However,
plastic strains of 2.5 and 5 percent greatly reduced the microyield strength of Ni-Span-C.

TABLE I. MICROYIELD STRENGTH AND MICROCREEP PROPERTIES

Material	Average MYS, 1000 psi	Creep Stress, 1000 psi	Approximate Percent of MYS	Creep Strain in 1000 hours, μin./in.
Ni-Span-C	39.0	20.0	50	12
		30.0	75	16
440 C	70.0	33.5	50	(b)
		50.0	75	6
A356	7.5	4.0	50	15
		6.0	75	12
Ti-5Al-2.5Sn	75.0	–	–	–
Super PEL Be	47.0	23.5	50	4
		35.0	75	5
AD995 Aluminum Oxide	29.0[a]	16.5	50	(b)

(a) Fracture stress.
(b) No creep strain observed in 1000 hours.

Electron-microscope studies indicated that microyielding in Ni-Span-C is the re-
sult of dislocation generation at second-phase particles in grain boundaries. For A356,
the generation of dislocations at Mg_2Si particles appeared to be the controlling mecha-
nism.

Dimensional-stability experiments revealed that the inherent stability of all of the
materials studied, as processed for this research, was good. Furthermore, the rela-
tively mild stress cycles (loaded to 75 percent MYS ten consecutive times) and thermal
cycles (10 min at 212 F, 10 min at RT, 10 min at -100 F, 10 min at RT repeated five
times) employed in this research sometimes caused slight immediate dimensional
changes, but did not lead to a change in the time-dependent dimensional stability. No
severe dimensional instability was observed in specimens strained 20 to 40 μin./in.,
but rapid contractions continuing over some weeks, were noted after specimens were
strained approximately 2 percent (20,000 μin./in.).

The residual stresses introduced by machining were frequently greater for fine finishing cuts than for heavier cuts. In addition, the residual stresses introduced by machining in Ni-Span-C and A356 cast aluminum exceeded the microyield strengths of these two alloys.

A capacitor strain gage was constructed and used to determine the microyield strength of Ti-5Al-2.5Sn. Although this gage offers somewhat less precision in strain measurement than electrical-resistance strain gages, it is useful for measuring micro-strains in materials that exhibit unusually high elastic strains below the microyield strength, where the limit of resistance gages is exceeded.

These results are discussed in terms of a hypothesis involving the stress and the thermally activated generation and motion of dislocations.

4

EXPERIMENTAL PROCEDURES

All micromechanical-property testing and precision-length measurements were performed in a Sheffield Modulab in which the temperature is maintained at 68 ±1/4 F.

Materials

Five metals and one ceramic material were selected for study. The five metals, along with their chemical analyses supplied by the vendors, are given in Table II.

Ni-Span-C is an age-hardenable iron-nickel-chromium alloy with an austenite matrix. Its modulus of elasticity can be maintained constant or varied over a given temperature range by controlling the thermomechanical processing history. This property has led to its use in a number of precision-instrument applications.

440 C stainless steel is a high-chromium, high-carbon, iron-base alloy. It has a martensite matrix and contains dispersed carbide particles. This steel offers a superior combination of high strength, wear resistance, and corrosion resistance, and is seeing increasing use as a bearing material.

Ti-5Al-2.5Sn is an all-alpha, nonheat-treatable titanium alloy offering moderate strength and high fracture toughness. Fusion welds can provide the same strength and toughness as the base metal. These properties have led to considerable use in missile applications.

A356 cast aluminum possesses good castability and better corrosion resistance than most other high-strength aluminum casting alloys. Highest strength is achieved with permanent-mold castings. It is widely used for precision castings where both weight and cost must be minimized.

Beryllium has a very low density and a high modulus of elasticity. This combination of properties makes beryllium exceptionally useful for structures such as gyroscopes or telescope mirrors that must be light in weight but provide high rigidity to applied loads. Super PEL beryllium is a fine-grained, high-strength beryllium in which the powder particles are coated with chromium prior to hot pressing.

Ni-Span-C, 440 C stainless steel, and Ti-5Al-2.5Sn were procured as wrought bar stock. A356 aluminum was purchased in the form of pigs and was subsequently cast into two leg "keel blocks" at Battelle. Specimen blanks were sliced from the legs which had a 1-inch diameter cross section. The Super PEL beryllium was received in the form of rods machined from a powder metallurgy ingot.

The ceramic evaluated was AD995 aluminum oxide.

TABLE II. CHEMICAL ANALYSIS

Element	Composition, weight percent				
	Ni-Span-C[a]	440 C Stainless Steel	Ti-5Al-2.5Sn	A356 Cast Aluminum[b]	Beryllium
Al	0.30-0.80		5.0	Balance	0.043
Mn	<0.80	0.42	0.006		
P	<0.04	0.016			
S	<0.04	0.012			
Si	<1.0	0.40		6.98	0.040
Cr	4.9-5.75	17.43			
Ni	41.0-43.5	0.49			
Mo		0.48			
Zn				0.02	
Ti	2.2-2.75		Balance	0.21	
Fe	Balance	Balance	0.27	0.10	0.081
Mg				0.36	0.059
C	<0.06	1.04	0.023		0.300
N			0.016		
O			0.19		
H			0.008		
Sn			2.6		
Be					Balance
BeO					5.77

(a) Nominal composition.
(b) Ingot analysis.

6

Mechanical-Property Evaluation

Three different mechanical-property tests have been conducted as follows:

(1) Microyield strength:* stress required to cause a residual plastic strain of 1 μin./in.

(2) Microcreep: the strain observed in specimens loaded to a fraction of their microyield strength for 1000 hours

(3) Conventional tensile properties: ordinary 0.2 percent offset yield stress, ultimate tensile strength, elongation, and reduction in area.

A full description of testing procedures and conditions is given in a later section of this report.

Specimen Preparation

Figure 1 gives the specifications of the specimens used for the determination of the above mechanical properties of the metals being studied. The specimens were first rough machined to 0.010 inch larger than final dimensions, and then heat treated to produce a microstructure characteristic of each alloy. After heat treatment, the specimens were finish machined to final specifications. Any distortion or surface contamination due to heat treatment was eliminated by the finish machining.

The heat treatments employed for each alloy are described in Table III. They are based on those recommended by MIT for maximum dimensional stability.[4] Microstructures of heat-treated material are shown in Figure 2.

Specimens of aluminum oxide were given no preliminary heat treatment. They were prepared and successfully tested by cementing metallic loading shoulders on uncontoured rods of the ceramic as shown in Figure 3. This technique appears to be an excellent approach for the testing of brittle materials to minimize geometric stress concentrations and consequent premature fracture.

TABLE III. HEAT TREATMENTS

Alloy	Heat Treatment
Ni-Span-C	1-1/4 hr at 1800 F, water quench; 21 hr at 1250 F, air cool
440 C Stainless Steel	1/2 hr at 1900 F, oil quench, hold for 2 min; immerse in liquid nitrogen for 30 minutes;[a] 1 hr at 500 F, air cool
Ti-5Al-2.5Sn	1 hr at 1500 F in argon, furnace cool
A356 Cast Al	16 hr at 1000 F, boiling water quench; 4 hr at 310 F, air cool
Super PEL Beryllium	1 hr at 1450 F, furnace cool

(a) Recommended in Metals Handbook, Vol. II, to reduce retained austenite content.

* Formerly denoted as the "precision elastic limit".
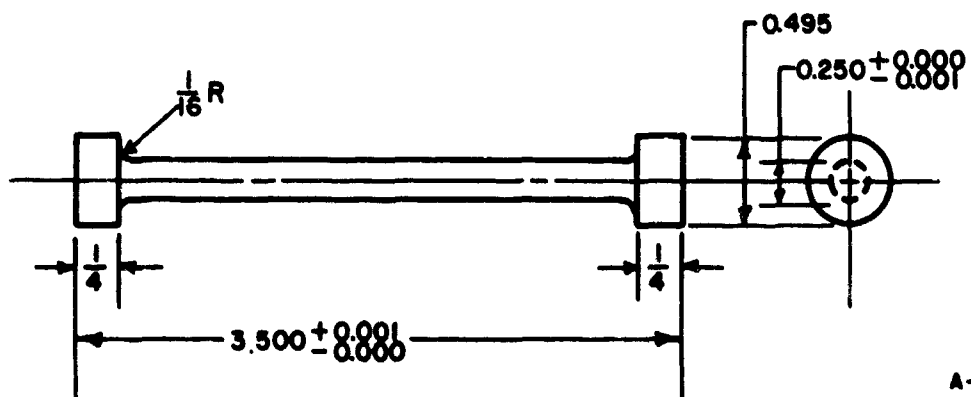
FIGURE 1. SPECIMEN FOR MICROPLASTIC PROPERTY, CONVENTIONAL
TENSILE PROPERTY, AND LOAD- AND THERMAL-CYCLE
DIMENSIONAL-STABILITY TESTS

8
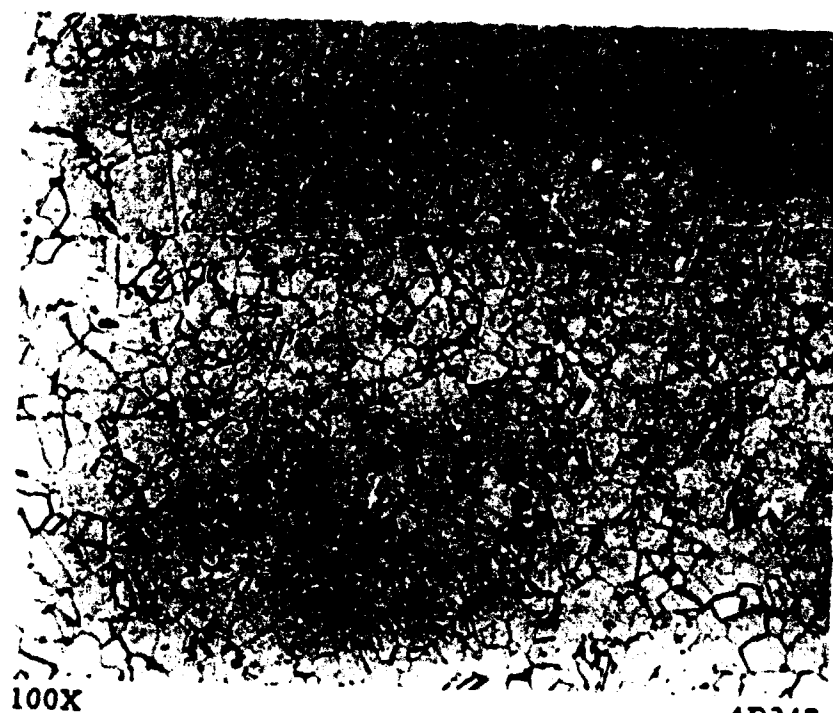
100X   4B247

a. Ni-Span-C
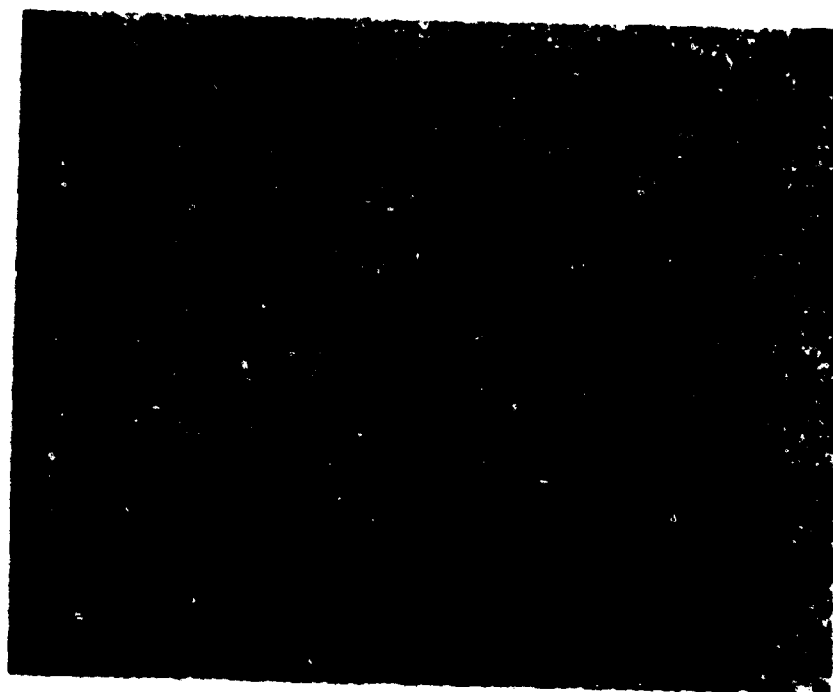
100X   4B243

b. 440C Stainless Steel

FIGURE 2. MICROSTRUCTURE OF HEAT-TREATED MATERIALS

9
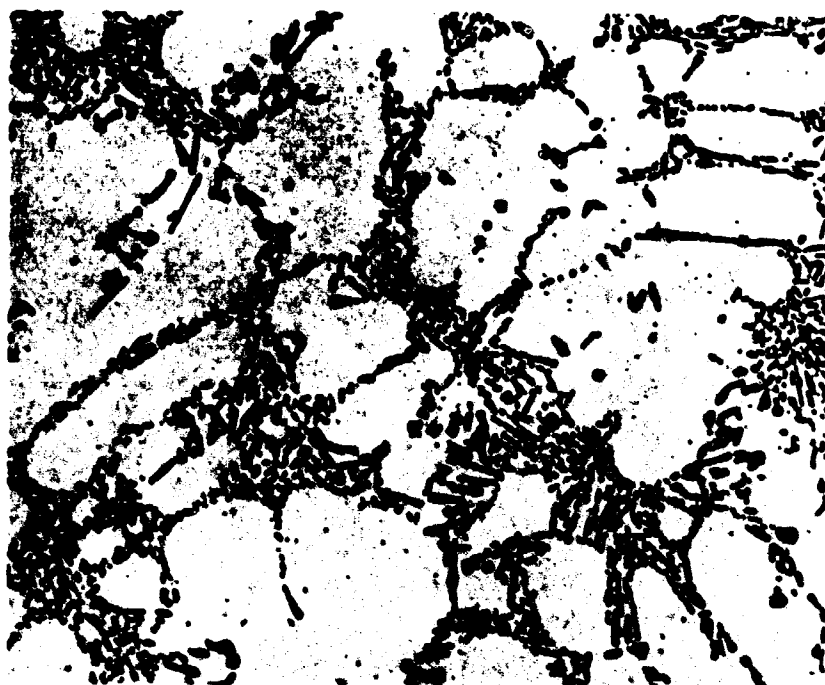
4B245

c. A356 Cast Aluminum

FIGURE 2. (CONTINUED)

100X   2C433

d.   Ti-5Al-2.5 Sn
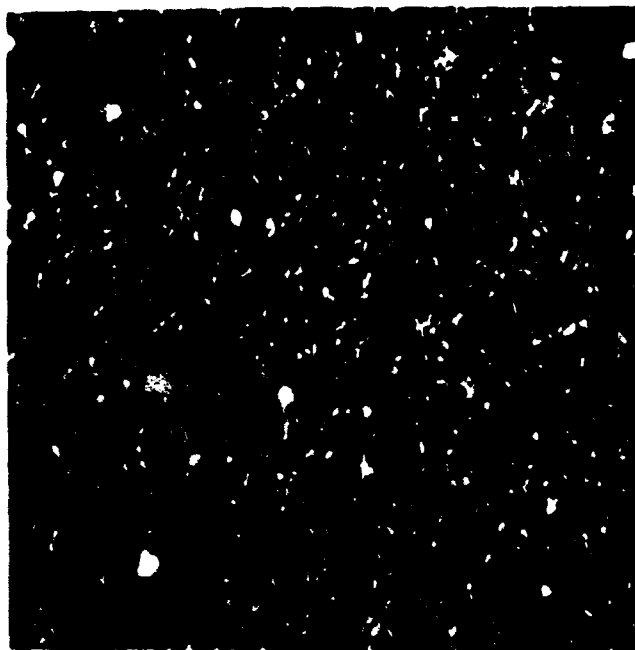
500X   9C819

e.   Super PEL   Be

FIGURE 2.   (CONTINUED)

11
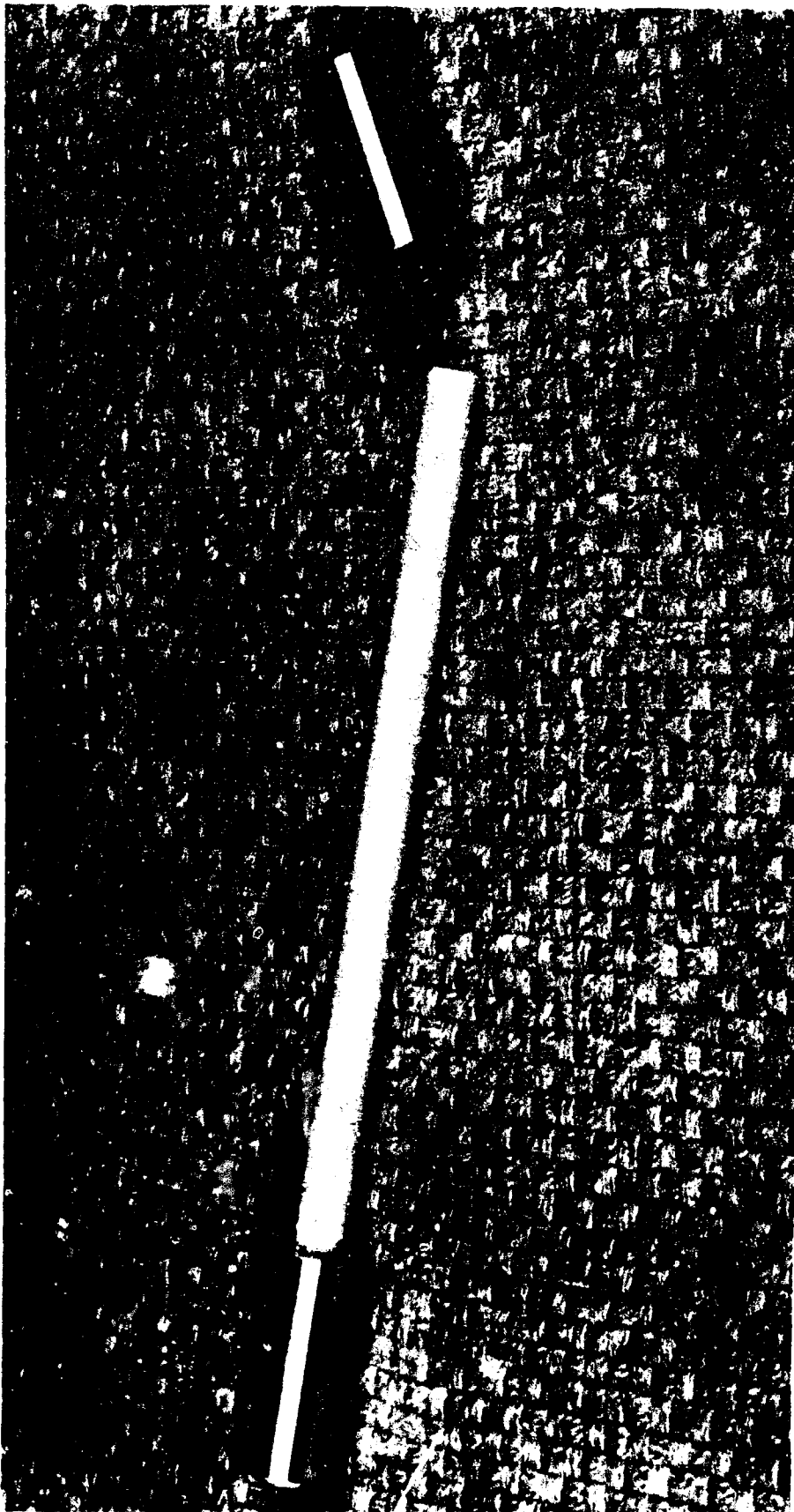
FIGURE 3.   A D995 ALUMINUM OXIDE TENSILE SPECIMEN WITH ALUMINUM LOADING SHOULDERS

38797

12

Strain-Gage Application

Three strain gages were applied to each specimen and were spaced 120 degrees apart around the circumference.

Materials. The strain gages used in this study were SR-4, epoxy base, constantan foil gages, type FA-2SN-12S. The gage configuration is shown in Figure 4, and the manufacturer's specifications are given below:

Resistance, ohms	120.0 ±0.2
Nominal gage factor	2.1 ±1 percent
Grid length, inch	0.25
Grid width, inch	0.02

The temperature compensation of the gages was matched as closely as possible to the thermal expansion of each material as shown in Table IV.

The adhesive used to apply the gages was BR-600, an epoxy cement with excellent stability and creep characteristics.

TABLE IV. THERMAL EXPANSION AND STRAIN-GAGE COMPENSATION

Material	Coefficient of Thermal Expansion, μin./in./F	Gage Compensation, μin./in./F
A356 Aluminum	11.5	13.0
Ni-Span-C	4.5	4.7
440 C Stainless Steel	5.6	6.0
Super PEL Beryllium	6.5	6.0
Al_2O_3	4.0	3.0

Specimen Preparation. Before gaging, approximately 10 mils was removed from the diameter of the gage length of each specimen (excluding the Al_2O_3) by chemical etching. The shoulders of the specimens were protected with Microwax Stop-off C-562. The solutions, temperatures, and techniques used for each material are given in Table V.

Gage Application. The gage backing was first trimmed to a width of approximately 0.2 inch so that three gages would fit around the specimen without overlapping. Each gage was attached to a paper handling tab with a small piece of mylar tape. Three of these gages were then layed out on a grid as shown in Figure 5 to assure proper spacing for the 120 degree separation, and another piece of mylar tape was placed over the gages to hold their spacing. This assembly was then lifted from the grid and the excess tape was trimmed off.

SR-4
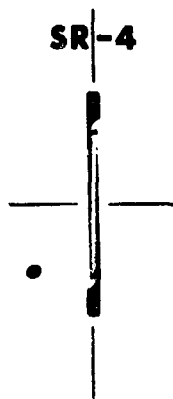
38141

FIGURE 4. STRAIN GAGE USED IN THIS STUDY
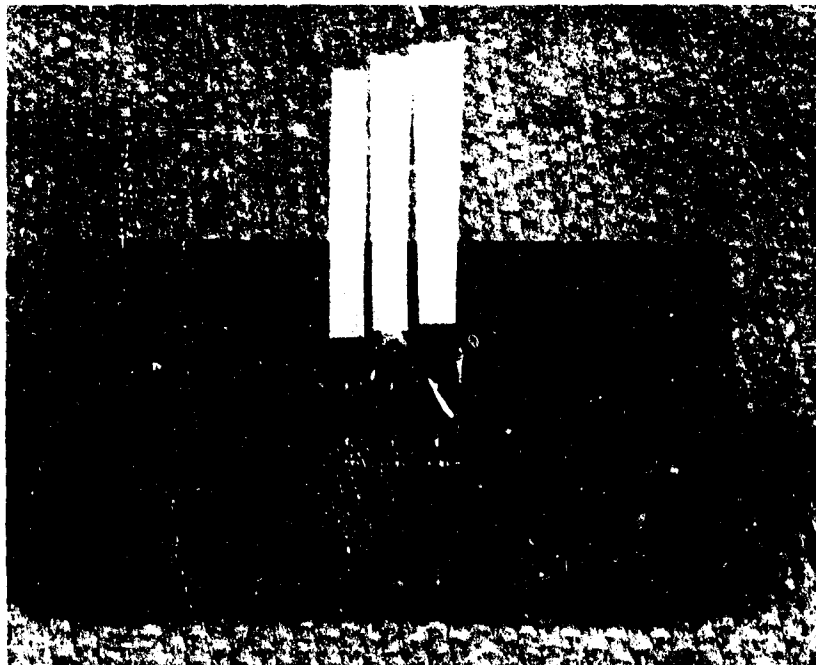
38142

FIGURE 5. STRAIN-GAGE ASSEMBLY ON GRID USED TO
OBTAIN 120-DEGREE SPACING

TABLE V. CHEMICAL-MILLING PROCEDURES

Material	Solution	Etching Temperature	Technique
A356 Al	100 grams sodium hydroxide in 500 cc water	115 F	Stir slowly
Ni-Span-C and 440 C Stainless	3 parts water 1 part hydrochloric acid	Room temp.	Make specimen an anode in an electrolytic bath with a current density of 0.9 amp/cm^2
Super PEL Beryllium	410 cc phosphoric acid 27 cc sulphuric acid 70 grams chromium trioxide	115 F	Stir slowly
Titanium	240 cc lactic acid 80 cc nitric acid 80 cc hydrofluoric 130 cc water	Room temp.	Stir slowly
Al_2O_3	Not etched		

At this point, the gage assembly was laid aside, and the specimen to be gaged was cleaned, first by swabbing with acetone followed by washing with a "metal conditioner" (a weak acid solution) and finally by rinsing with neutralizer (ammonia). The gages in the assembly described above were also cleaned with the neutralizer.

A thin layer of cement was then applied to the gages and allowed to air dry for 5 minutes. The gage assembly was carefully aligned on the specimen using a specially marked V-block and one end was tacked down with the tape. At this point, the specimen was lifted from the V-block and appeared as shown in Figure 6. The entire assembly was then wrapped securely around the specimen, smoothing each gage with thumb pressure. A silicone rubber pad and a thin aluminum plate were placed over each of the three gages and were held in place by a "hose clamp". The cement was then cured for 1 hour at 225 F.

After curing, the clamp and pads were removed and the tape was stripped off. A copper terminal strip on fiber-glass backing was installed near each tab using Eastman 910 contact cement. Both the terminal strips and gage tabs were tinned with 300 F solder. The lead wires (26 ga. stranded copper) were soldered to the terminal strips with a single strand of wire extending over to the gage tabs. The entire installation is shown in Figure 7. Gagecote #1, a solvent-thinned resin, was applied as waterproofing prior to testing.
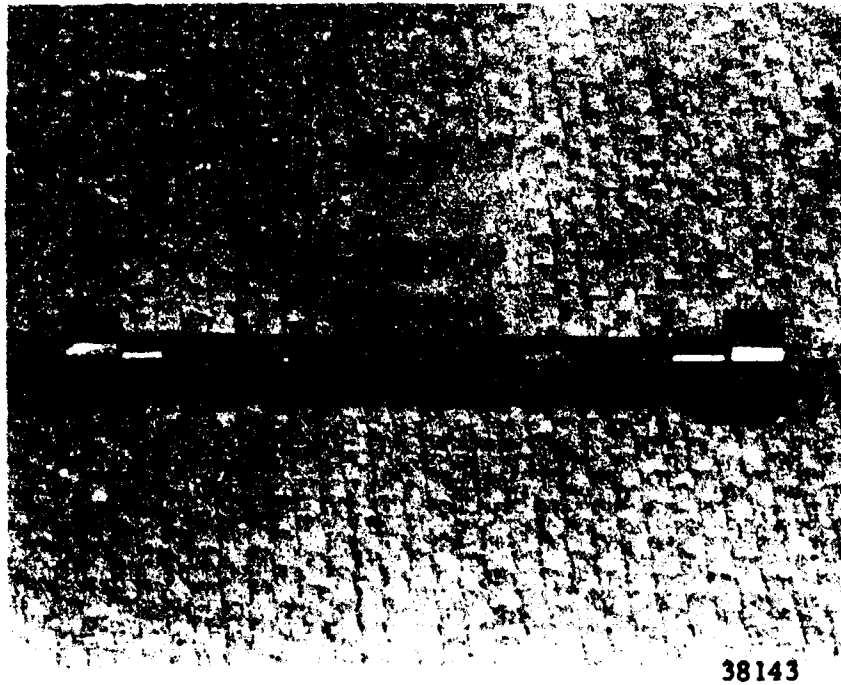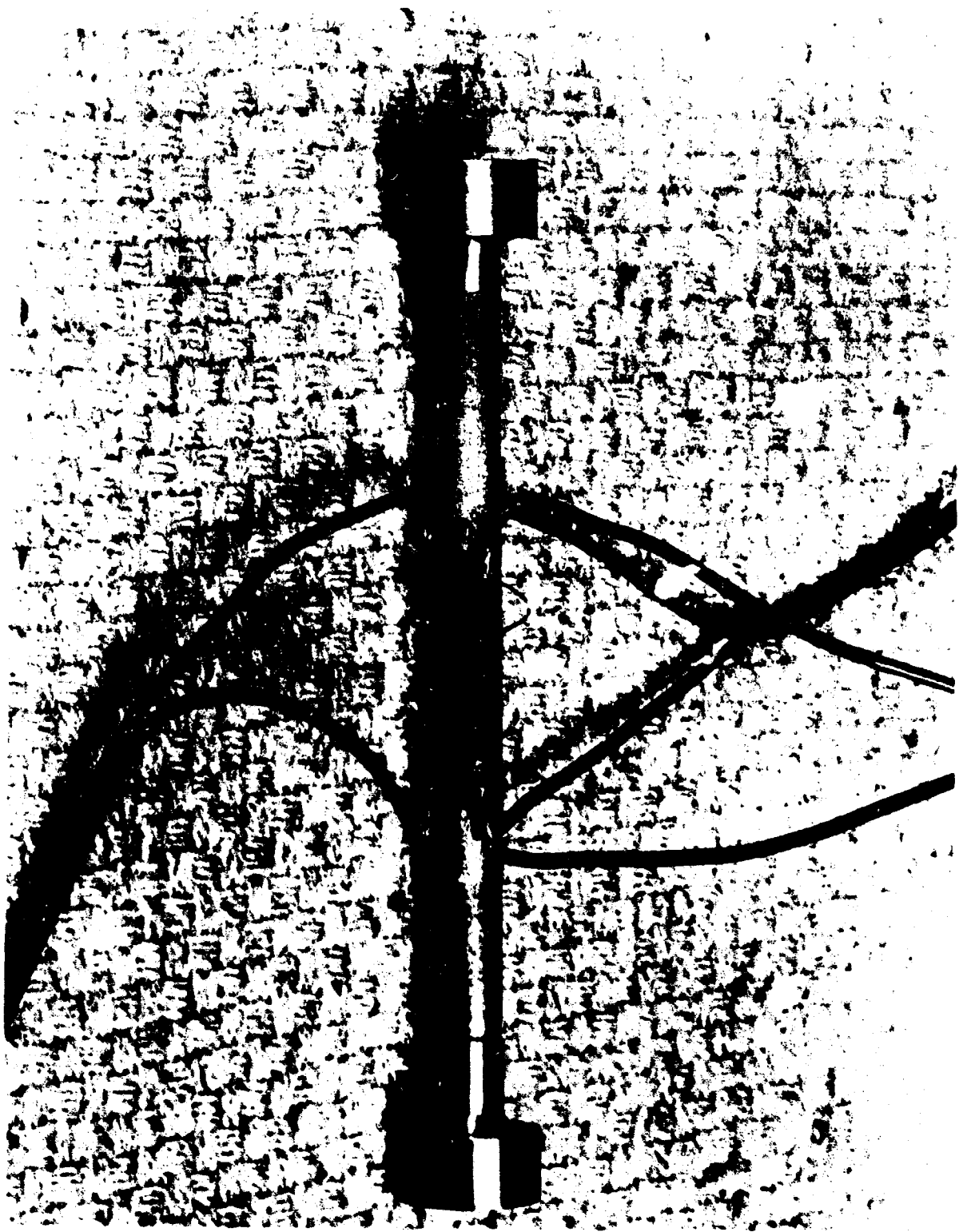
15

38143

FIGURE 6. STRAIN-GAGE ASSEMBLY READY TO WRAP AROUND SPECIMEN

38090

FIGURE 7. COMPLETED INSTALLATION PRIOR TO WATERPROOFING

Testing Procedures

Microyield strength. The microyield strength of each material was evaluated by loading specimens to successively higher stress levels and measuring the residual strain after removal of the load from each stress increment. The load was relaxed immediately upon attainment of the desired stress levels. Each specimen was loaded to stress levels sufficient to cause 20-40 μin./in. residual strain.

All tests were performed in an Instron Testing Machine. A photograph of the load train is shown in Figure 8. The load was applied to the specimens through a universal joint and a thrust bearing to minimize bending and torsion moments. The specimen loading shoulders were gripped in a spherical seat employing a split-collar as shown in Figure 9. Specimens were loaded using a constant cross-heat speed of 0.05 inch per minute.

Prior to actual testing, a small load (approximately 25 to 100 pounds) was applied to the specimen, and eccentricity of loading was minimized by adjusting the specimen and load train until the strains on the three gages were as nearly identical as possible. Some eccentricity always remained, probably due largely to slight bending of the specimens and/or nonparallelism of the loading shoulders.

Residual-strain measurements were made by measuring the strain on each of the three gages individually with a BLH Strain Indicator. This instrument was modified at the factory to have increased sensitivity. The gages and strain indicator are capable of measuring residual strains with a sensitivity of 0.1 μin./in. Each gage was wired into a four-arm bridge network external from the strain indicator. A schematic of the strain-measuring circuit is illustrated in Figure 10. Strain gages cemented on another specimen of the same material as that being tested were used as dummy gages. Additional strain gages cemented on a stainless steel plate were used to complete the measuring bridge network. In this manner, all switching from gage to gage was accomplished outside of the measuring bridge network. Therefore, the strain indicator detected only the imbalance of the measuring bridges due to strain in the gages on the test specimen, and changes in contact resistance due to switching were effectively bypassed. Furthermore, using a gaged specimen of the same material for a dummy reduced the possibility of obtaining false strain indications due to thermal fluctuations and consequent changes in length of the specimen. Switching was performed with a four-deck rotary switch.

The microyield strength of each tested specimen was calculated by plotting the average residual strain of the three gages versus stress. An appropriate vertical line was fitted to the data points obtained at low stress levels (i.e., below stresses at which significant residual strains were apparent. A second vertical line was then drawn offset from the reference line by a positive strain of 1 μin./in. The point at which this second line intersected a smooth curve drawn through the data points not falling on the reference line was taken as the microyield strength of the specimen.

Microcreep

The microcreep behavior of each material was evaluated by loading tensile specimens to 50 and 75 percent of their microyield strength for 1000 hours and measuring the
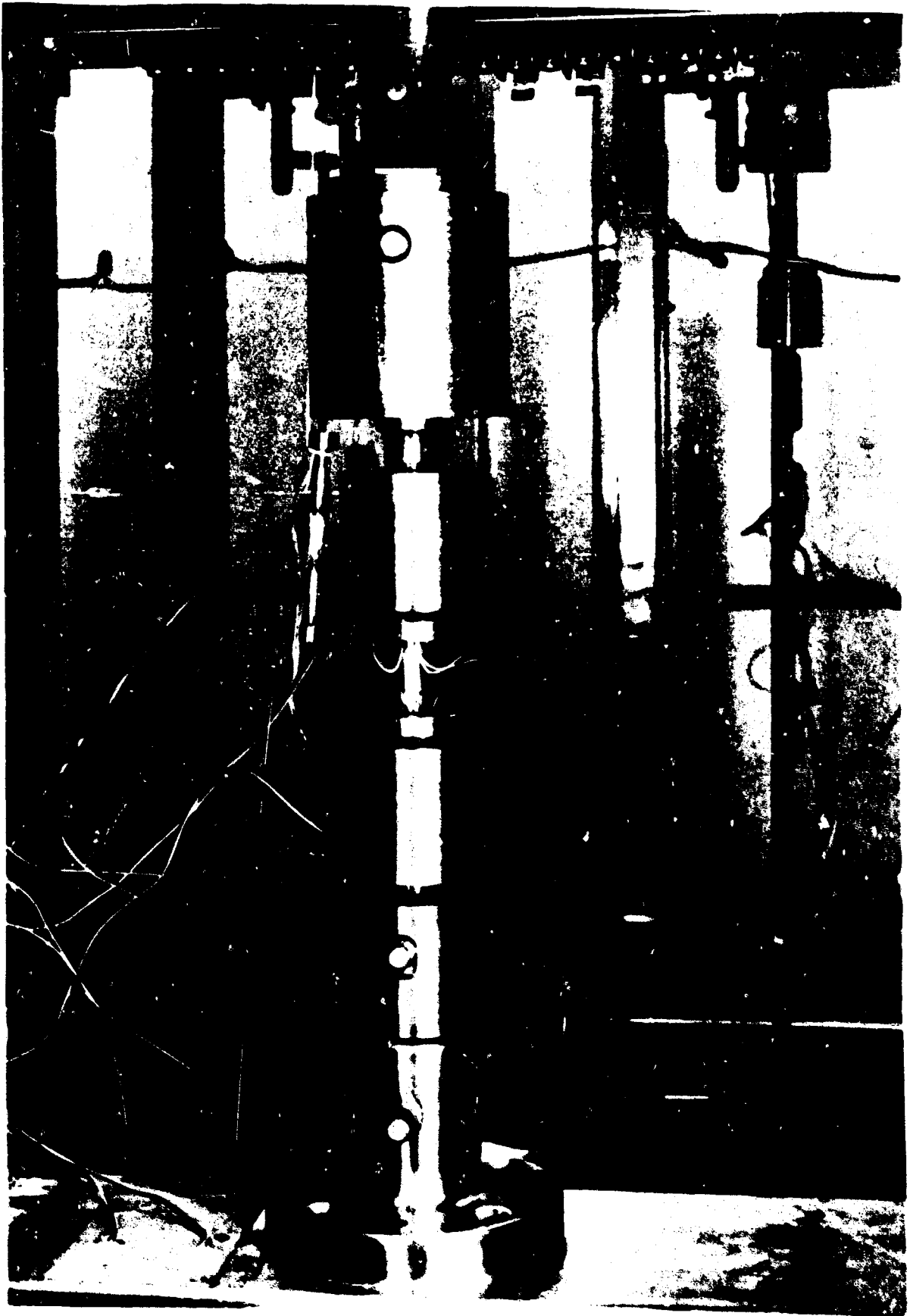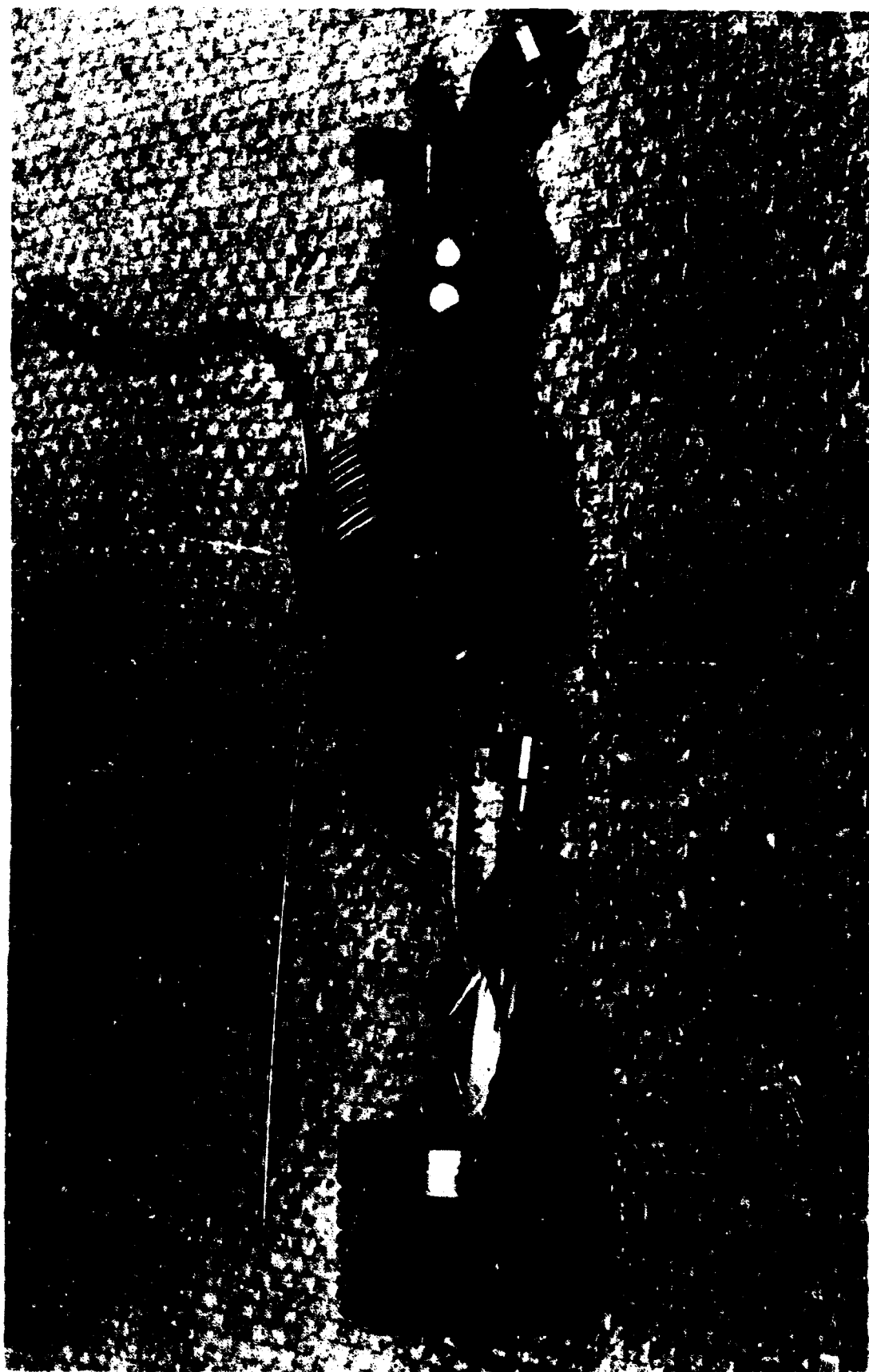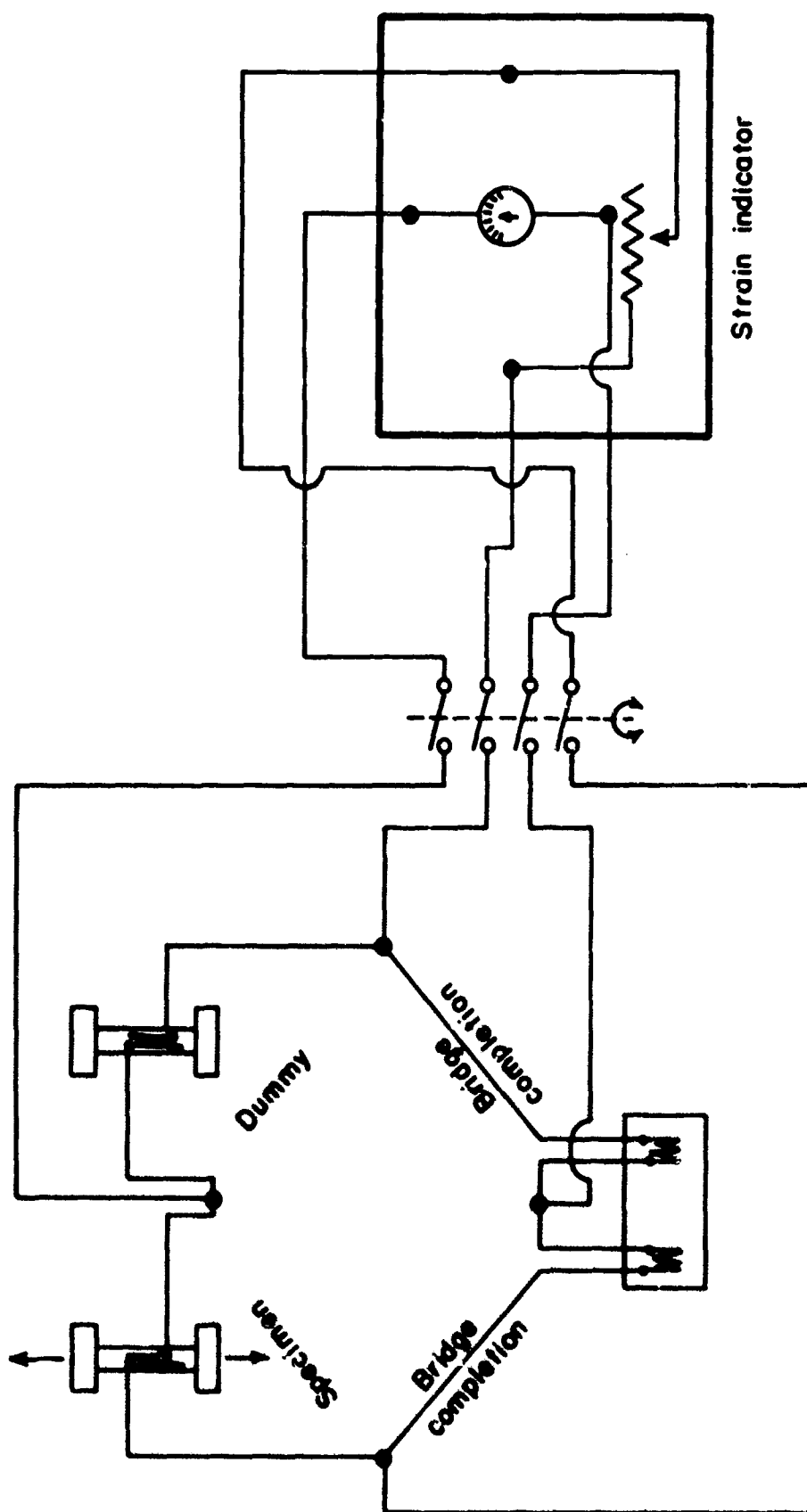
FIGURE 8.   MICROMECHANICAL PROPERTY TESTING LOAD TRAIN

38140

FIGURE 9. SPHERICAL SEAT

20

FIGURE 10. SCHEMATIC OF STRAIN-MEASURING CIRCUIT

A-55949

21

increase in strain with time. Figure 11 illustrates the creep machines used for these tests. Specimen-preparation and strain-measuring techniques were identical to those described for the microyield-strength tests.

The precision of strain measurement in the microcreep test was approximately ± 1 μin./in. as compared to the ± 0.1 μin./in. previously noted for the microyield-strength test. Subtle variables such as small electronic instabilities and stress relaxation in the gages that do not interfere with the short-duration microyield-strength test, can account for the lower precision of strain measurement in the extended-time microcreep tests. Variations in ambient humidity were observed to have a marked affect on strain measurement. Anomalously low and high strains were recorded during periods of low and high humidity, respectively. A humidity-control system was installed in the constant-temperature facility to minimize this difficulty.

Conventional Tensile Properties. The 0.2 percent offset yield stress, ultimate tensile strength, elongation, and reduction in area were measured by standard techniques and need not be elaborated upon here.

Dimensional-Stability Evaluation

Machining Studies

Residual stresses introduced by machining were evaluated by measuring the length of a machined specimen, chemically etching away the machined surface, and measuring the length a second time. The change in length upon chemical etching is a function of the average residual stress in the removed layer. This stress (σ) can be calculated by the equation,

$$\sigma = \frac{(d_F)^2 \, E \, \dfrac{L_F - L_o}{L_o}}{d_o{}^2 - d_F{}^2} \quad , \tag{1}$$

where E is the modulus of elasticity, d_o is the initial diameter, d_F is the final diameter, L_o is the initial length, and L_F is the final length.[5]

Specimen Preparation. Figure 12 illustrates the design of the specimen used for the machining studies. These specimens were prepared by the same procedures previously described for the mechanical-property specimens with the exception that the ends were lapped flat and parallel. The various machining procedures evaluated were performed on the large-diameter central portion of the specimens. The small-diameter ends of the specimens were used only to support the specimens in a specimen holder, and were not machined during the course of the study.

Etching Procedures. The etching procedures employed were similar to those used to prepare the tensile specimens for strain-gage application described in Table IV. However, greater control was exercised over the process to maintain roundness and taper to tolerances of less than 0.001 inch to facilitate subsequent machining operations. The electrochemical-etching procedure was modified so that specimens of Ni-Span-C and 440 C stainless steel were revolved at 7 rpm between two copper-strip cathodes. No
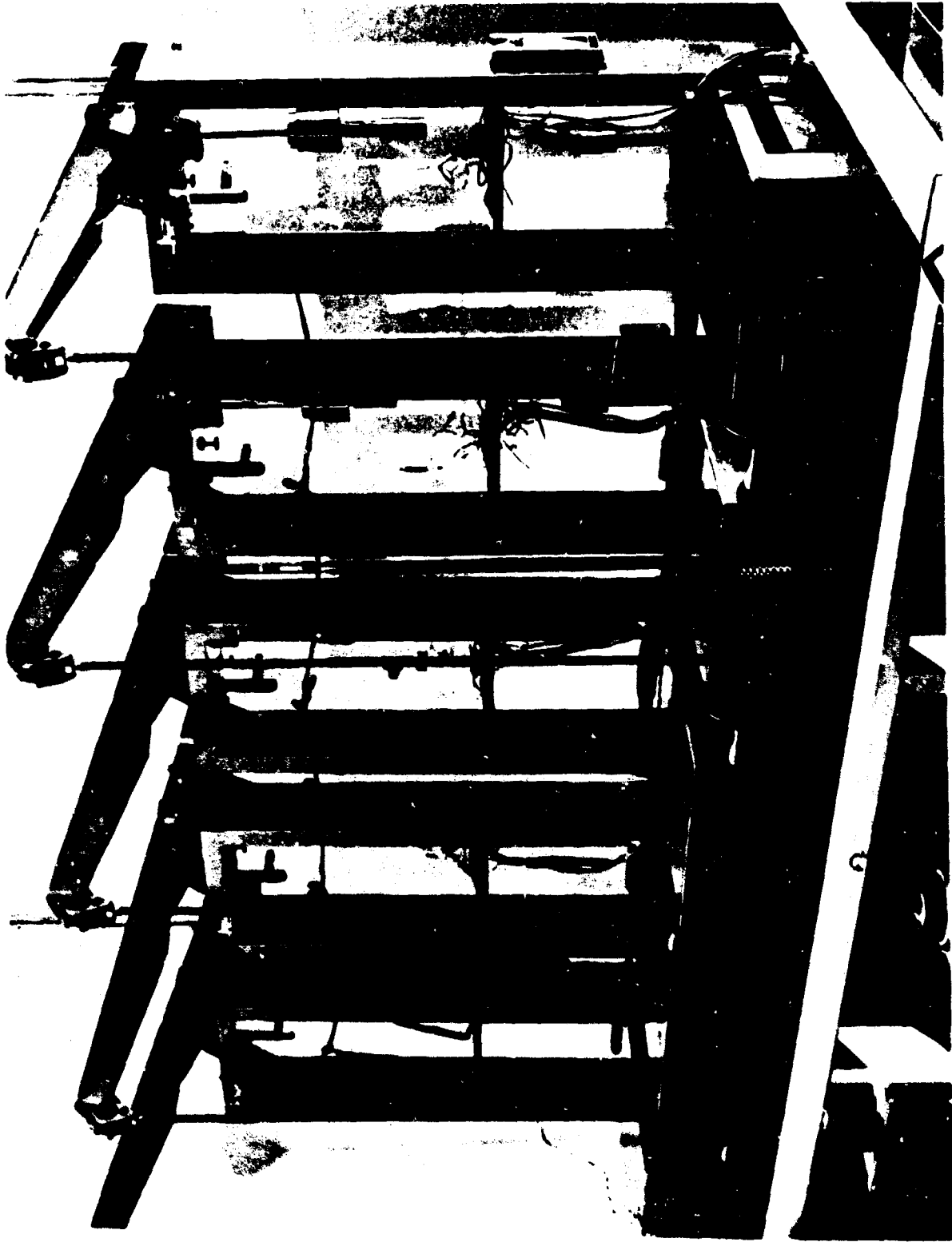
FIGURE 11. CREEP MACHINES

121367-37
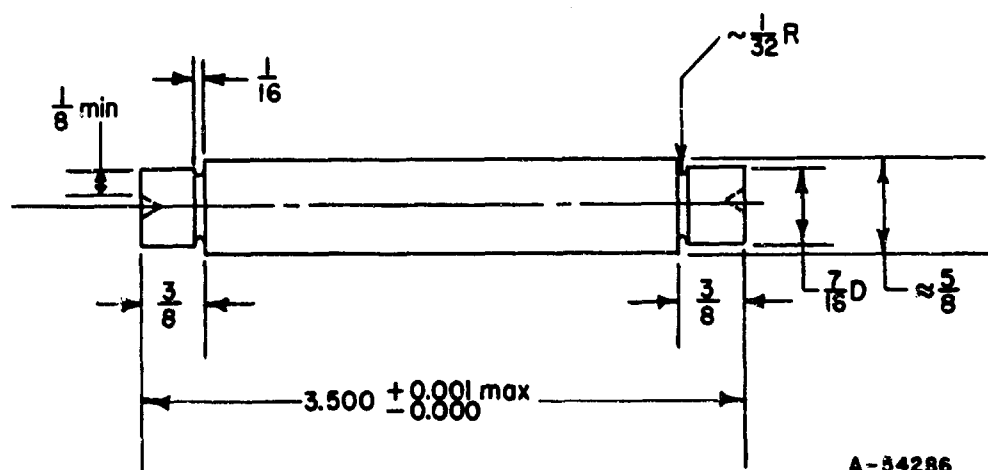
FIGURE 12. SPECIMEN FOR MACHINING STUDIES

major modifications were necessary for the chemical etching of A356 cast aluminum and Super PEL beryllium. The lapped ends of the specimens were protected from the etching solutions by wax.

Effects of Load Cycles, Thermal Cycles, and Plastic Strain

The influence of load and thermal cycling and of plastic strain on dimensional stability was studied by applying various mechanical and thermal treatments to specimens and observing their change in length over a period up to 6 months. The specimen design illustrated in Figure 1 for mechanical-property testing was used. However, the ends were lapped flat and parallel to facilitate making length measurements. Load cycles and plastic strains were applied with a tensile-testing machine.

Instrumentation

The length measurements of all the tensile and machining specimens undergoing the dimensional-stability tests were made in an electromechanical gage-block comparator having a precision capability of one microinch.

The technique and procedure employed was designed to assure as much accuracy and repeatability as practicable in the positioning of the specimens and corrections for coefficient-of-expansion differences.

The gage-block comparator was modified slightly from the standard specifications of such an instrument. The gaging pressure was 2 ounces and the radius of the gaging tips was 1 inch, which prevented marring of surfaces at the point of measurement.

The specimens were compared in length to laboratory-grade gage blocks, both steel and chromium carbide, which were wrung together in the appropriate lengths and, in most cases, left wrung together during the 6-month testing period to eliminate possible variations in length due to wringing errors. Extreme care in cleanliness and proper wringing was employed and only the chromium carbide blocks were used in the long-term buildups.

Figure 13 illustrates the test setup. The specimens were held vertically in specially designed V-blocks. The reference gage-block buildup was placed against a positioning fixture on the instrument table and the back of the specimen holder was placed against the gage-block buildup. This entire assembly rested on a base plate that is moved by a screw thread to sequentially pass the gage block and specimen between two measuring contacts in the instrument. One measuring contact is inert and serves to position the second head that is coupled to an induction transformer that electrically amplifies the difference in length between the reference gage-block buildup and the specimen. Angular alignment of the specimen was achieved by index marks on V-block and specimen. Lateral positioning was established by the fixture on the base plate. Travel of the base plate was indicated by a dial indicator that contacted the back surface of the gage block. Each specimen was measured at least twice for each step in the program; the second measurement was made after removing the specimen from the V-block holder and reassembling, usually a minimum of 1 hour later. This procedure was followed to assure that all positions and alignments could be repeated and that temperature corrections were properly determined.

25
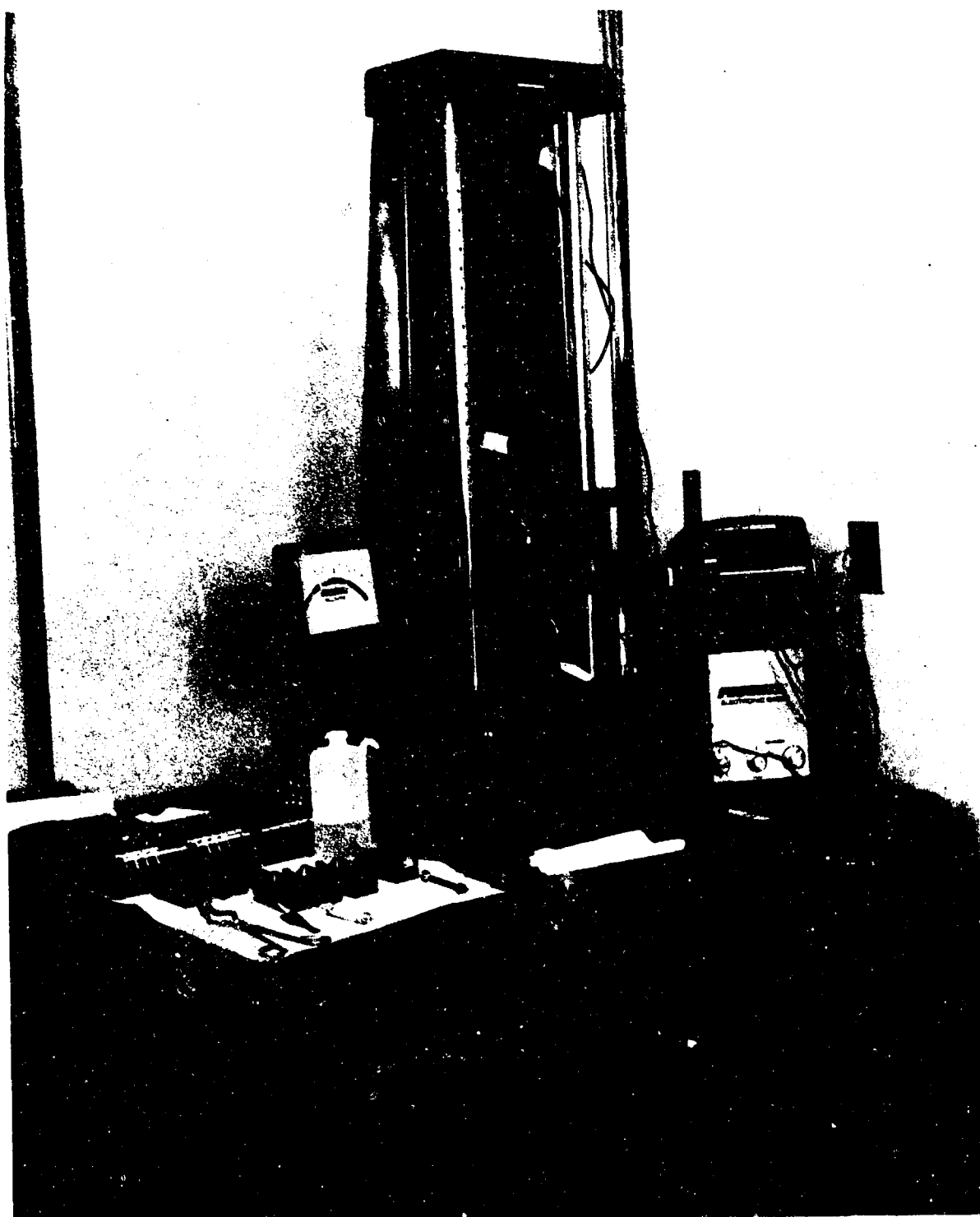
42641

FIGURE 13.   PRECISION LENGTH MEASURING TEST SET-UP

The coefficients of thermal expansion of the various specimens and gage blocks were of such difference that although the laboratory was controlled to 68 F ±0.25 F the customary 24-hour cool out did not afford enough control. A digital thermometer with four thermistor probes and a range of 10 C to 30 C having a least significant digit read-out to 0.02 C to an accuracy of ±0.05 C was used for determinations of the temperature for correction. One probe was positioned in the base plate, one probe was used for ambient-air temperature at the point of measurement and another probe was attached to a specimen to assure its thermal equilibrium with the base plate. If the ambient-air temperature and the base-plate-table temperature differed by more than 0.2 C at the time of measurement, the measurement was repeated after thermal equilibrium was re-attained. It is normal for some difference between air and plate temperature to exist due to mass differences and probe designs. In computing the thermal-expansion correction values to 68 F (20 C) the temperature at the base plate was used. Figure 14 shows the formula and coefficient-of-expansion values used for these corrections.

Taking into consideration the uncertainties possible in the measurements, the accuracy of the dimensional data reported is estimated to be ±2 μin./in. for all specimens except the grossly strained specimens where loss of parallelism degrades the accuracy possible.
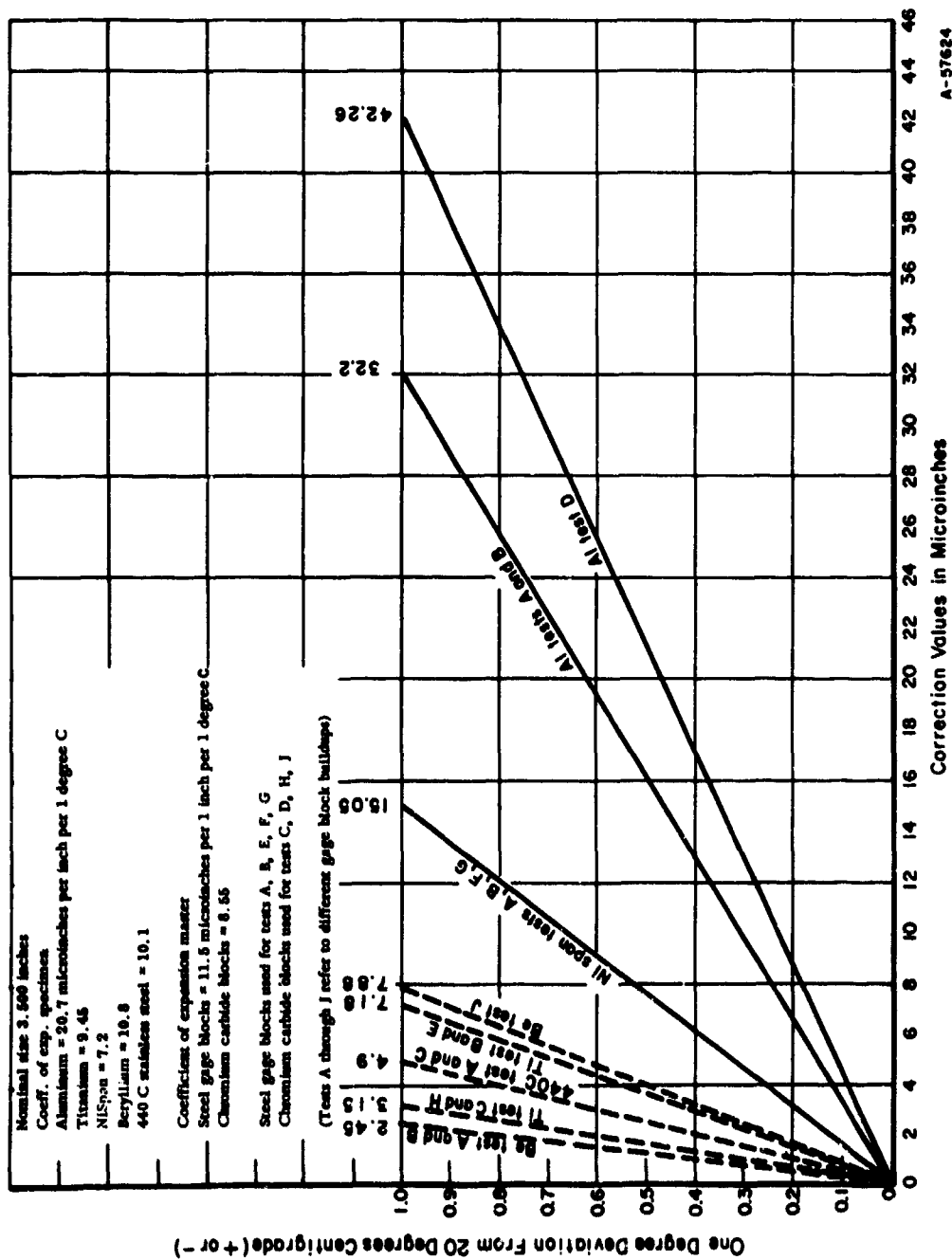
FIGURE 14. COEFFICIENT OF EXPANSION CORRECTION VALUES

Formula: Gage reading − [(coeff. of exp. specimen − coeff. of exp. master) x nom. size x (temperature −20)] .

Nominal size 3.500 inches
Coeff. of exp. specimen
Aluminum = 20.7 microinches per inch per 1 degree C
Titanium = 9.45
NiSpan = 7.2
Beryllium = 10.8
440 C stainless steel = 10.1

Coefficients of expansion master:
Steel gage blocks = 11.5 microinches per 1 inch per 1 degree C
Chromium carbide blocks = 8.65

Steel gage blocks used for tests A, B, E, F, G
Chromium carbide blocks used for tests C, D, H, J

(Tests A through J refer to different gage block buildups)

Correction Values in Microinches

One Degree Deviation From 20 Degrees Centigrade (+ or −)

A-57624

28

MICROMECHANICAL PROPERTIES

Microyield-Strength Studies

The microyield strengths of Ni-Span-C, 440 C stainless steel, A356 cast aluminum, Ti-5Al-2.5Sn, Super PEL beryllium, and AD995 aluminum oxide were evaluated.

Ni-Span-C

Microyield strength data for Ni-Span-C are illustrated in Figures 15, 16, and 17. The individual tests are in good agreement. An average microyield strength of 39 ksi is indicated. This is somewhat lower than the value of 47.0 reported by Schetky.[4]

440 C Stainless Steel

Microyield strength data for 440 C stainless steel are presented in Figures 18, 19, and 20. The three separate tests are in excellent agreement, and an average microyield strength of 69-70 ksi is indicated. This value is significantly lower than the value of 190.0 reported by Schetky.[4]

A356 Cast Aluminum

Figures 21 and 22 illustrate microyield strength data for A356 cast aluminum. The percentage variation in the observed microyield strength is somewhat greater than that obtained with Ni-Span-C and 440 C stainless steel, but this is considered to be normal for cast aluminum. An average microyield strength of approximately 7.5 ksi is indicated. This is slightly lower than the value of 12.0 ksi reported by Schetky.[4] It is known, however, that the MYS of A356 is strongly affected by the temperature of the quenching medium[6], and this may account for some of the difference.

Ti-5Al-2.5Sn

Electrical resistance strain gages were found to be unsuitable for measuring the microyield strength of Ti-5Al-2.5Sn. The combination of high strength and low modulus of elasticity, characteristic of titanium alloys, resulted in the gages being strained upon loading beyond their ability to respond elastically in the load-unload microyield-strength test. Negative residual strains were indicated after unloading from stress levels above approximately 20,000 psi. As a consequence, the microyield strength of Ti-5Al-2.5Sn was evaluated with a capacitor strain gage. This capacitor strain gage, described in a later section of this report, gave somewhat less precision (± 1 μin./in.) than can be obtained with electrical-resistance strain gages.

Figure 23 illustrates the microyield strength data for Ti-5Al-2.5Sn. A microyield strength of 75,000 psi is indicated.
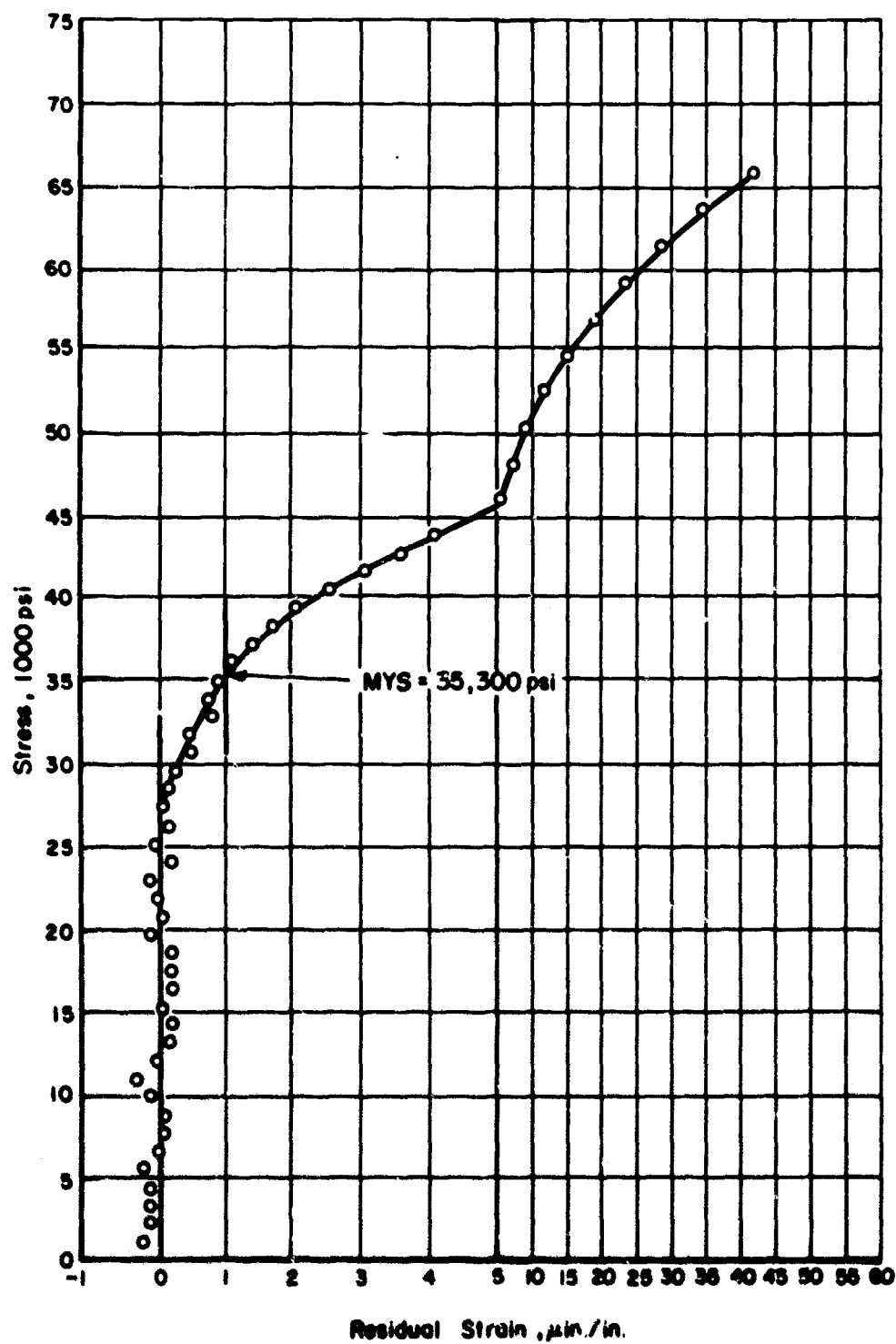
FIGURE 15. MICROYIELD STRENGTH OF Ni-SPAN-C SPECIMEN 5

1-1/4 hr at 1800 F, WQ; 21 hr at 1250 F, AC.

30
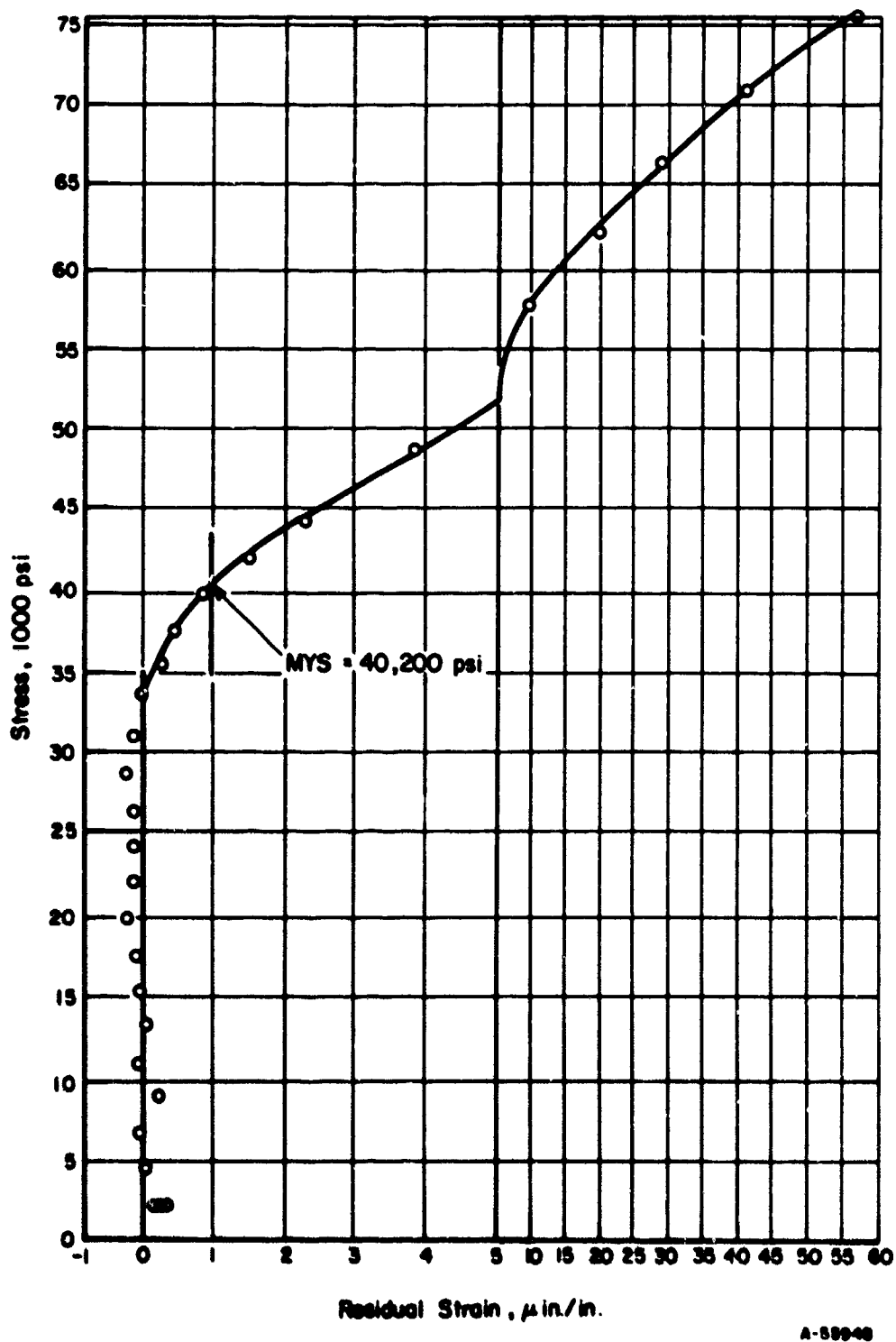
FIGURE 16. MICROYIELD STRENGTH OF Ni-SPAN-C SPECIMEN 6
1-1/4 hr at 1800 F, WQ; 21 hr at 1250 F, AC.

31
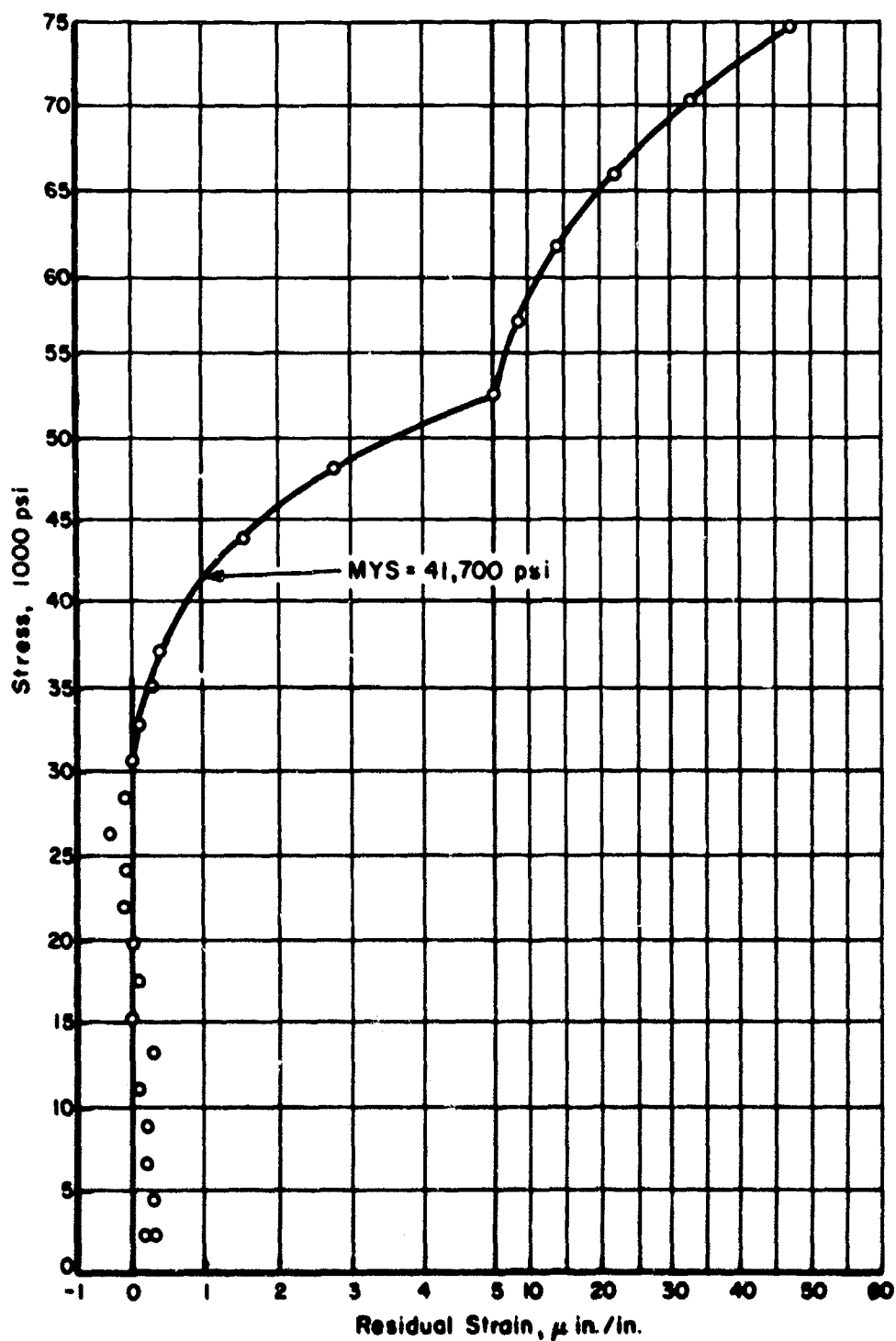
FIGURE 17. MICROYIELD STRENGTH OF Ni-SPAN-C SPECIMEN 16

1-1/4 hr at 1800 F, WQ; 21 hr at 1250 F, AC.

FIGURE 18. MICROYIELD STRENGTH OF 440 C STAINLESS STEEL SPECIMEN 9
1/2 hr at 1900 F, OQ; 1 hr at 500 F, AC.

33

FIGURE 19. MICROYIELD STRENGTH OF 440 C STAINLESS STEEL SPECIMEN 7
1/2 hr at 1900 F, OQ; 1 hr at 500 F, AC.

34

FIGURE 20. MICROYIELD STRENGTH OF 440 C STAINLESS STEEL SPECIMEN 4
1/2 hr at 1900 F, OQ; 1 hr at 500 F, AC.

35

FIGURE 21. MICROYIELD STRENGTH OF A356 CAST ALUMINUM SPECIMEN 1
16 hr at 1000 F, WQ; 4 hr at 310 F, AC.
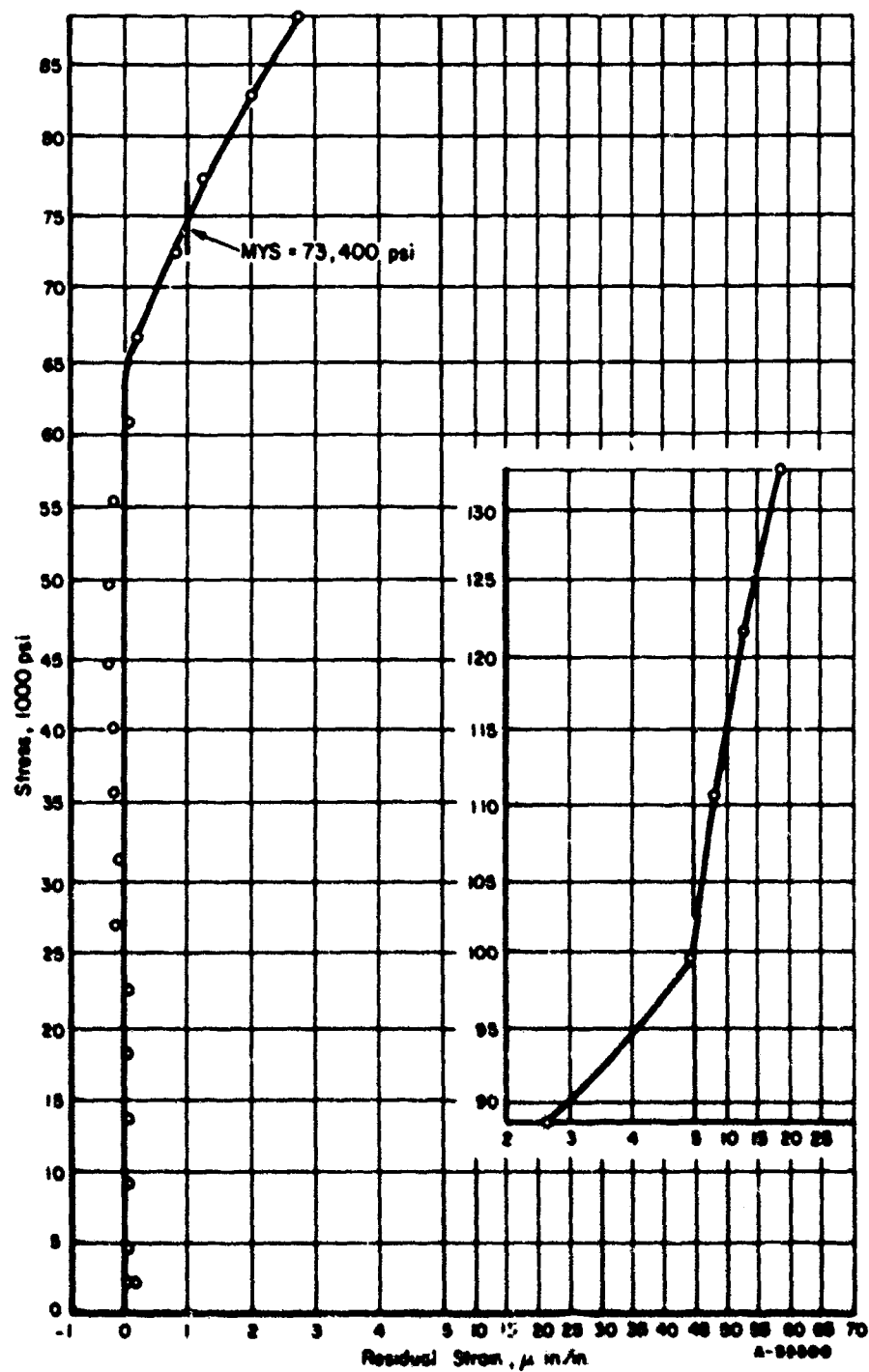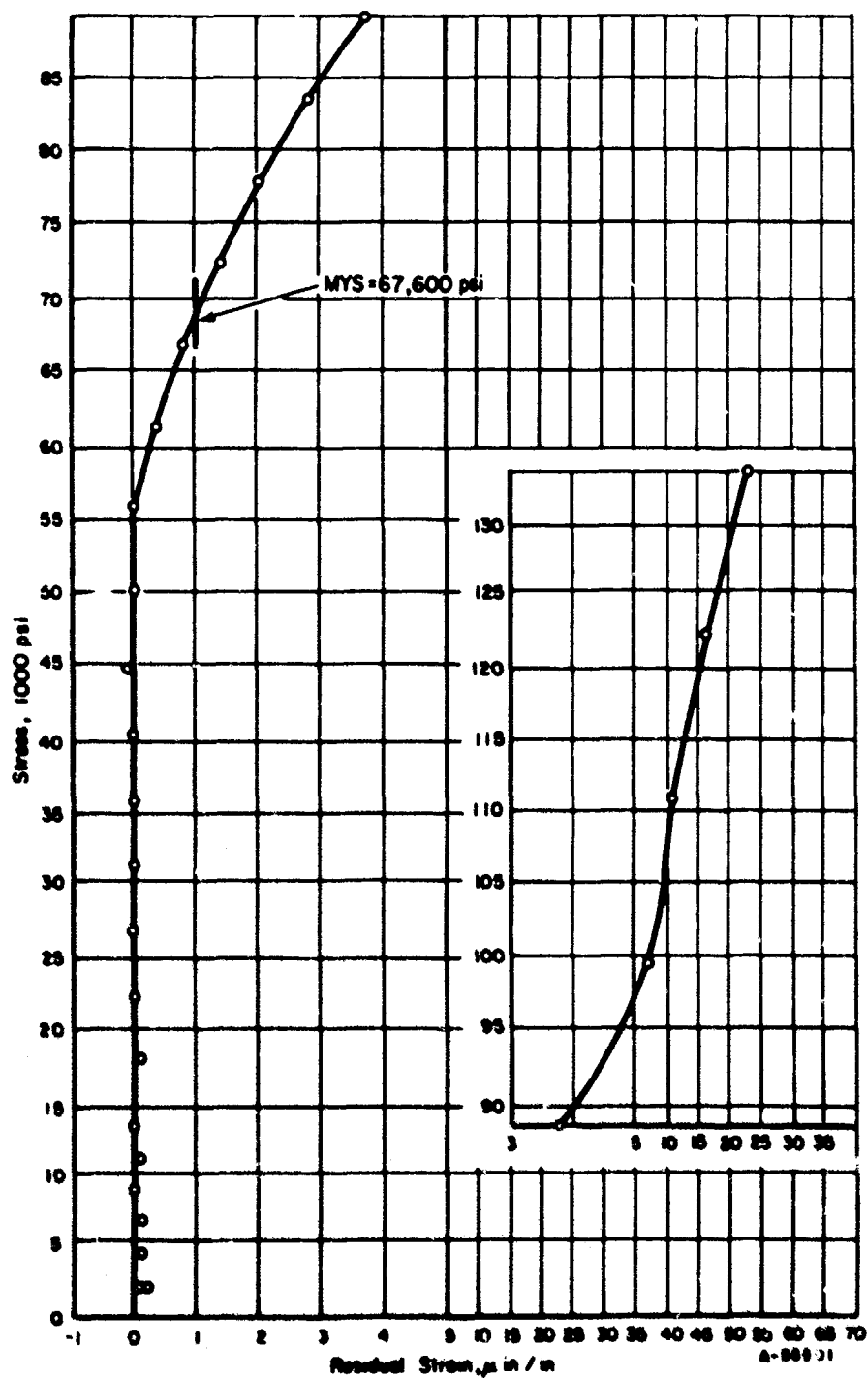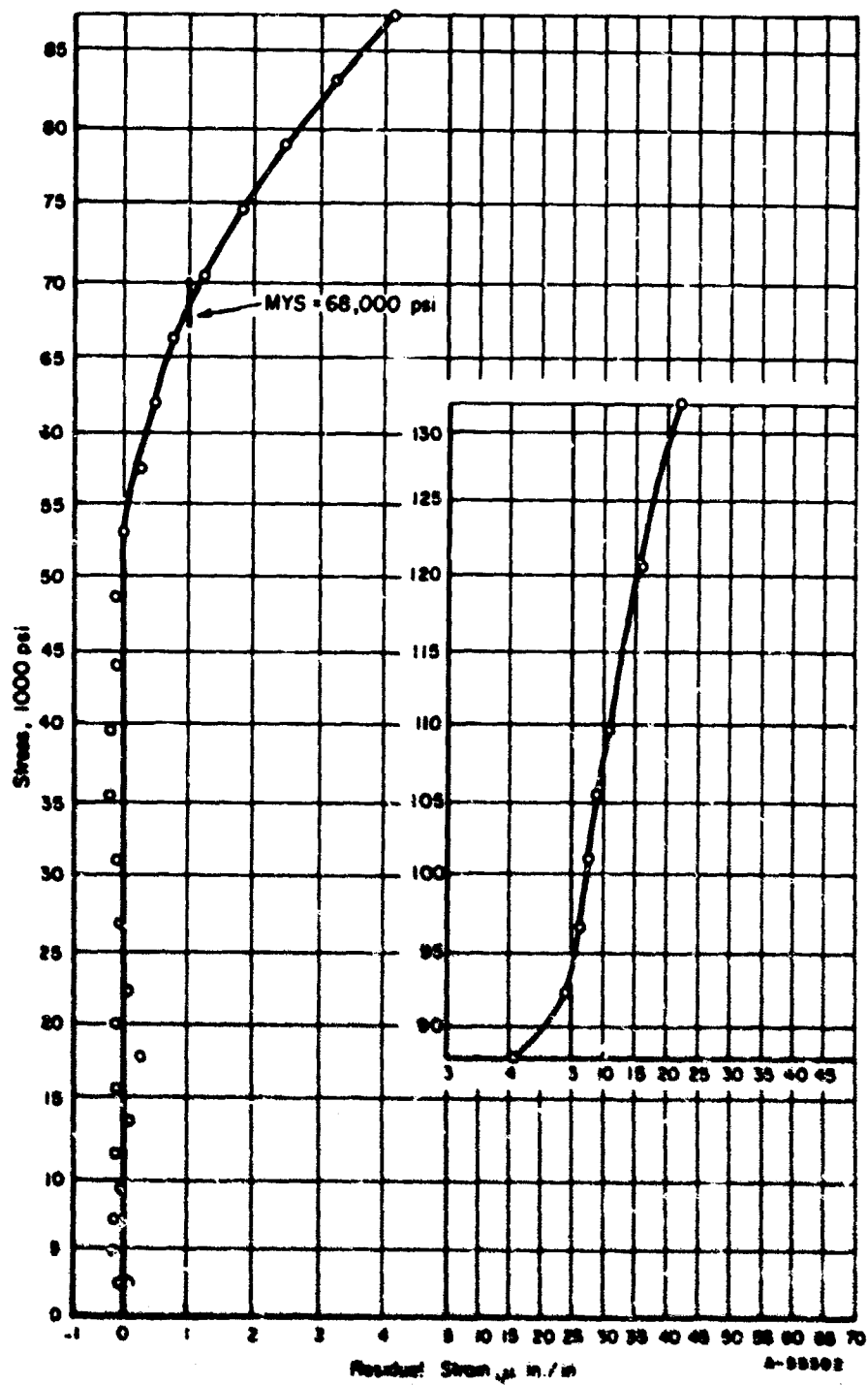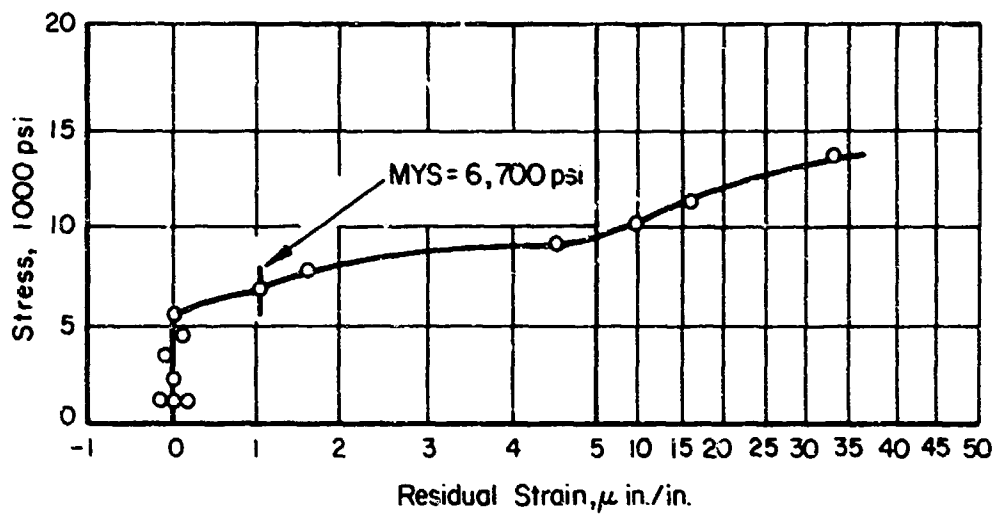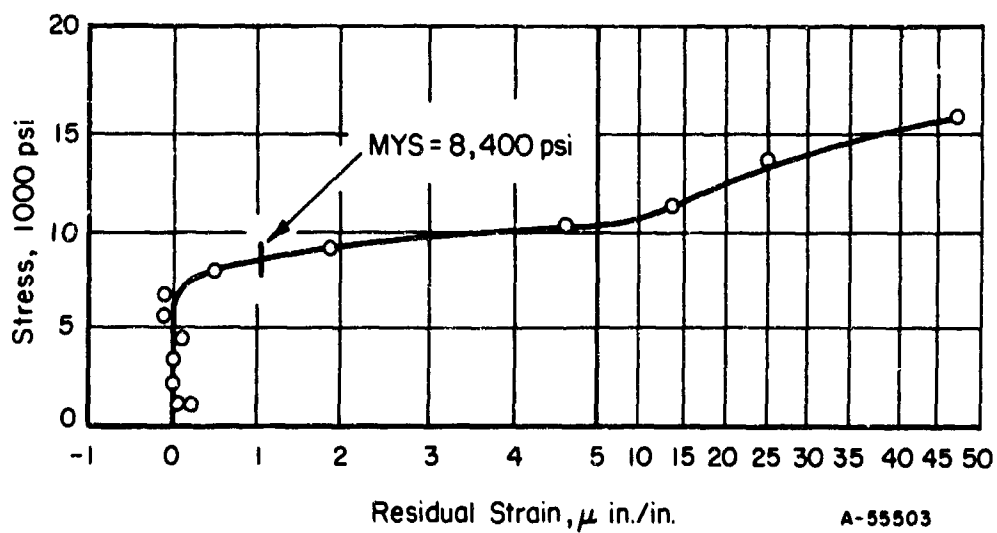

FIGURE 22. MICROYIELD STRENGTH OF A356 CAST ALUMINUM SPECIMEN 2
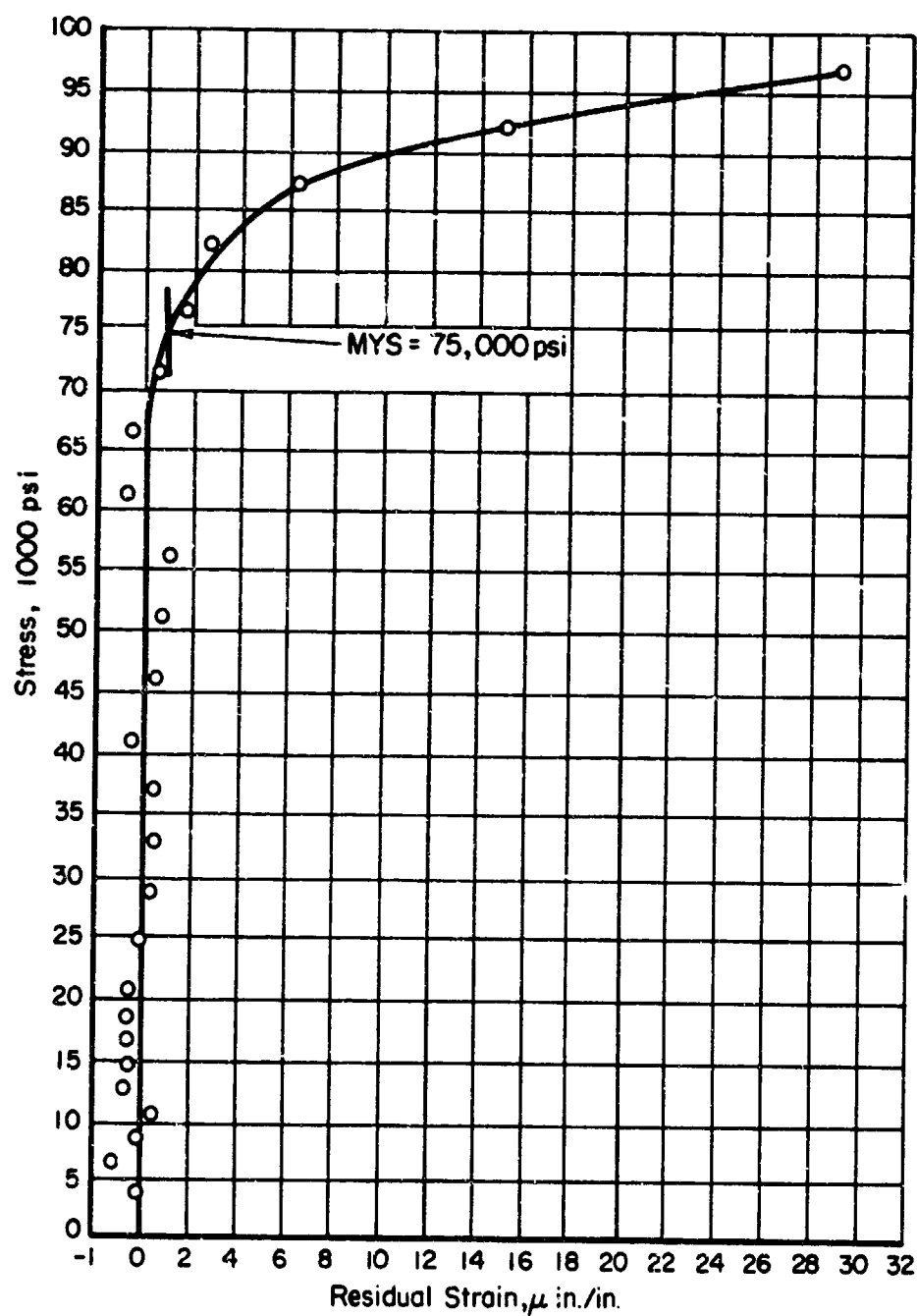16 hr at 1000 F, WQ; 4 hr at 310 F, AC.

FIGURE 23.   MICROYIELD STRENGTH OF Ti-5Al-2.5 Sn

1 hr at 1500 F, FC.

Super PEL Beryllium

Microyield strength data for hot-pressed, Berylco Super PEL beryllium alloy are illustrated in Figures 24 and 25. The indicated average microyield strength is 47,000 47,000 psi. This is considerably higher than the microyield strength of other beryllium alloys and grades as shown in Table VI. However, it is important to note that the Berylco alloy fractured at stresses only slightly higher than those required to initiate microplastic deformation with plastic strains before fracture of only 1 or 2 μin./in.

TABLE VI. COMPARISON OF MICROYIELD STRENGTH OF Be ALLOYS

	Microyield Strength, psi
Berylco Super PEL (1 hour at 1450 F, FC)	45,000-49,000
I 400 Be	5,000-7,000[a]
S 200 Be	6,400-8,300[b]
HP 40	14,400-16,600[b]
Honeywell Be-Ag	14,000-16,800[b]

(a) Determined by Battelle Memorial Institute under Contract No. NAS 5-10267.

(b) Isopressed by Battelle Memorial Institute under Contract No. DAAHOI-68-C-0018.

AD995 Aluminum Oxide

Microyield strength data for AD995 aluminum oxide are illustrated in Figures 26 and 27. The specimens fractured at stresses of 25,300 and 31,800 psi with no indication of microplastic deformation prior to failure.

Comparative Microyield-Strength Behavior

The microyield strength behavior of the five metallic materials studied is compared in Figure 23. 440 C stainless steel and Ti-5Al-2.5Sn exhibited considerably higher microyield strengths than the other three alloys tested. It should be noted that although these two alloys had approximately the same microyield strength, Ti-5Al-2.5Sn offered less resistance to microplastic deformation when loaded above the microyield strength as indicated by the shallower slope of its stress-residual strain curve.

Super PEL beryllium and Ni-Span-C exhibited intermediate microyield strengths. First evidence of microplastic deformation was detected in both of these materials at approximately the same stress level. However, as indicated by the steeper slope of the stress-residual strain curve for Super PEL beryllium, its microyield strength was approximately 10,000 psi higher than that of Ni-Span-C.

A356 cast aluminum displayed the lowest microyield strength of the materials tested. Furthermore, the very shallow slope of its stress-residual strain curve indicated very little resistance to microplastic deformation when loaded above its microyield strength.
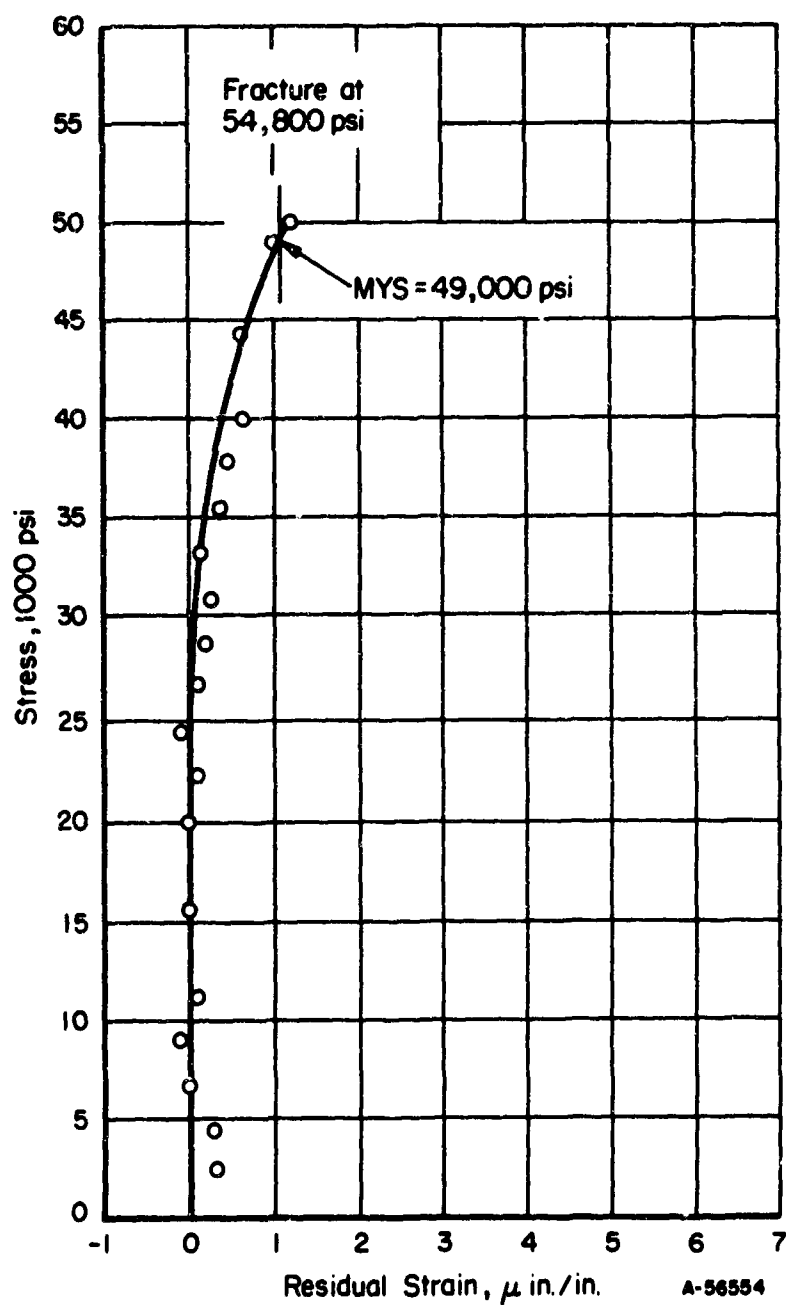
FIGURE 24. MICROYIELD STRESS OF BERYLLIUM SPECIMEN 16
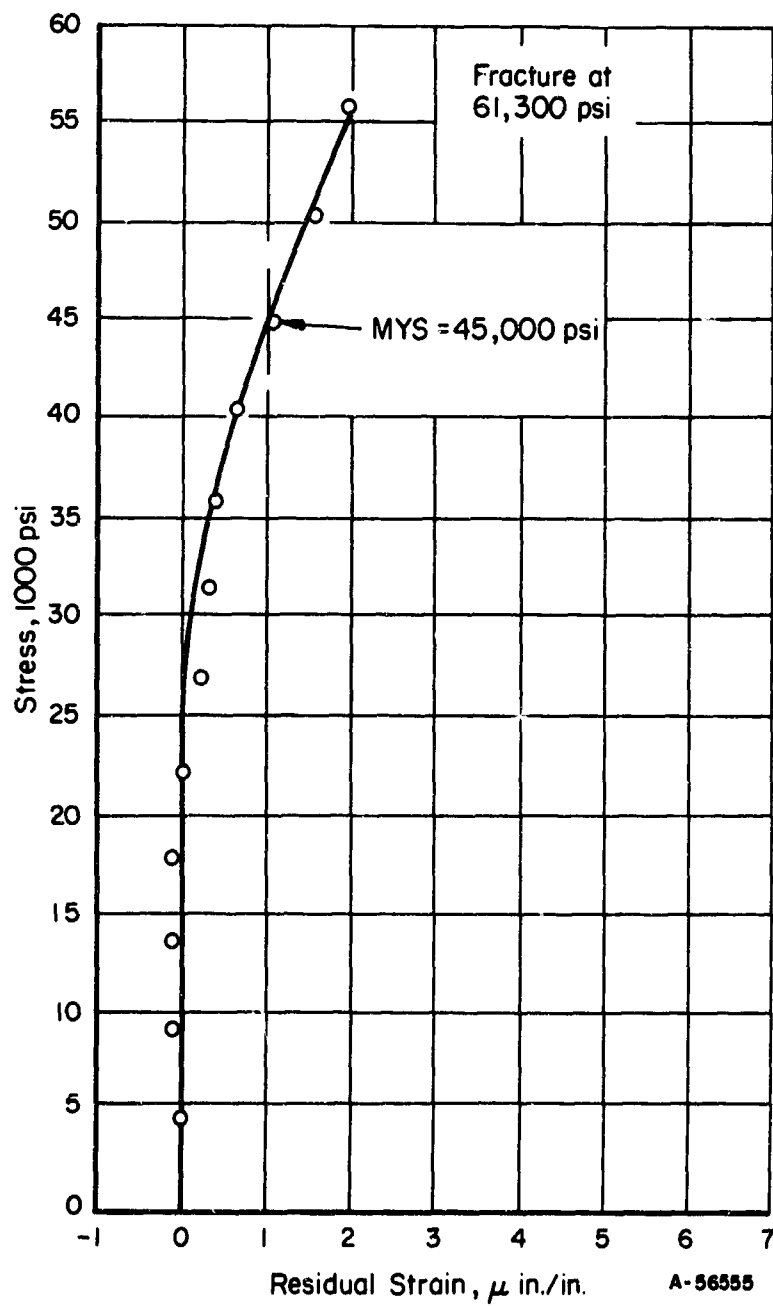
1 hr at 1450 F, FÇ.

FIGURE 25. MICROYIELD STRESS OF BERYLLIUM SPECIMEN 17
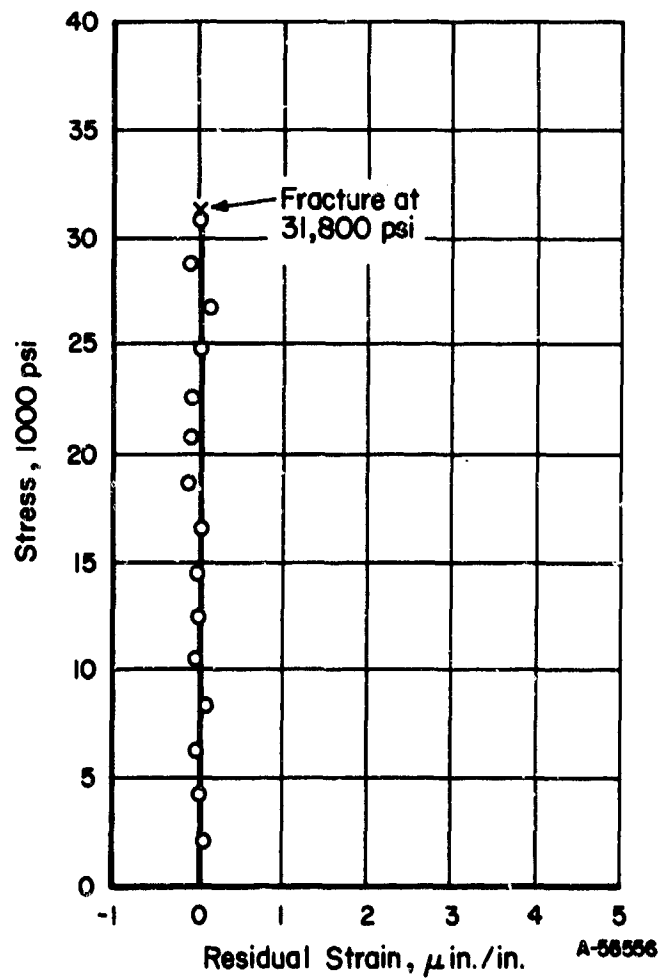
1 hr at 1450 F, FC.

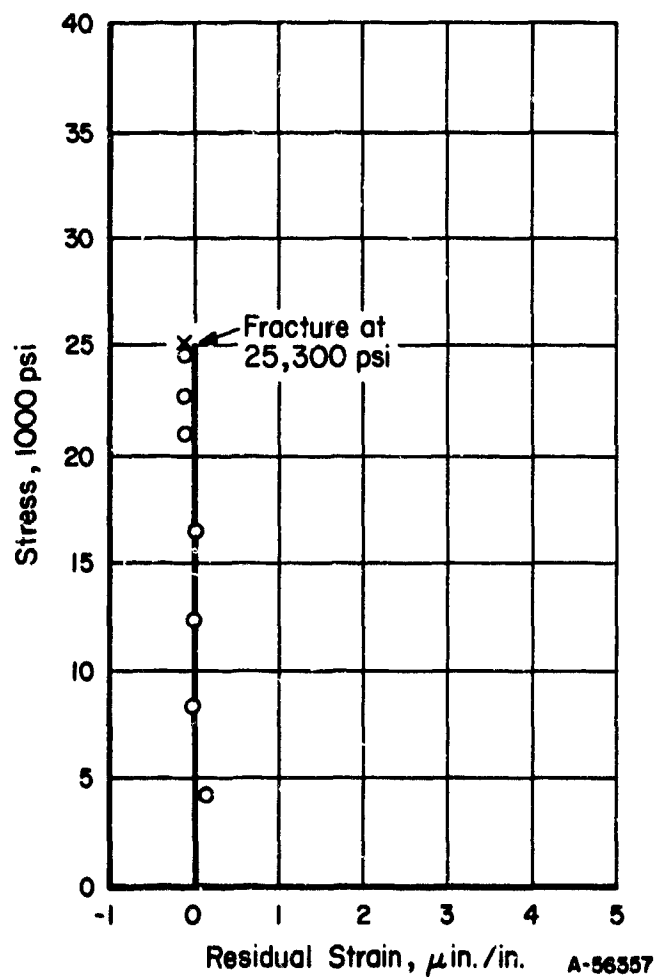FIGURE 26. MICROYIELD STRESS OF AD 995 ALUMINUM OXIDE SPECIMEN 1

41

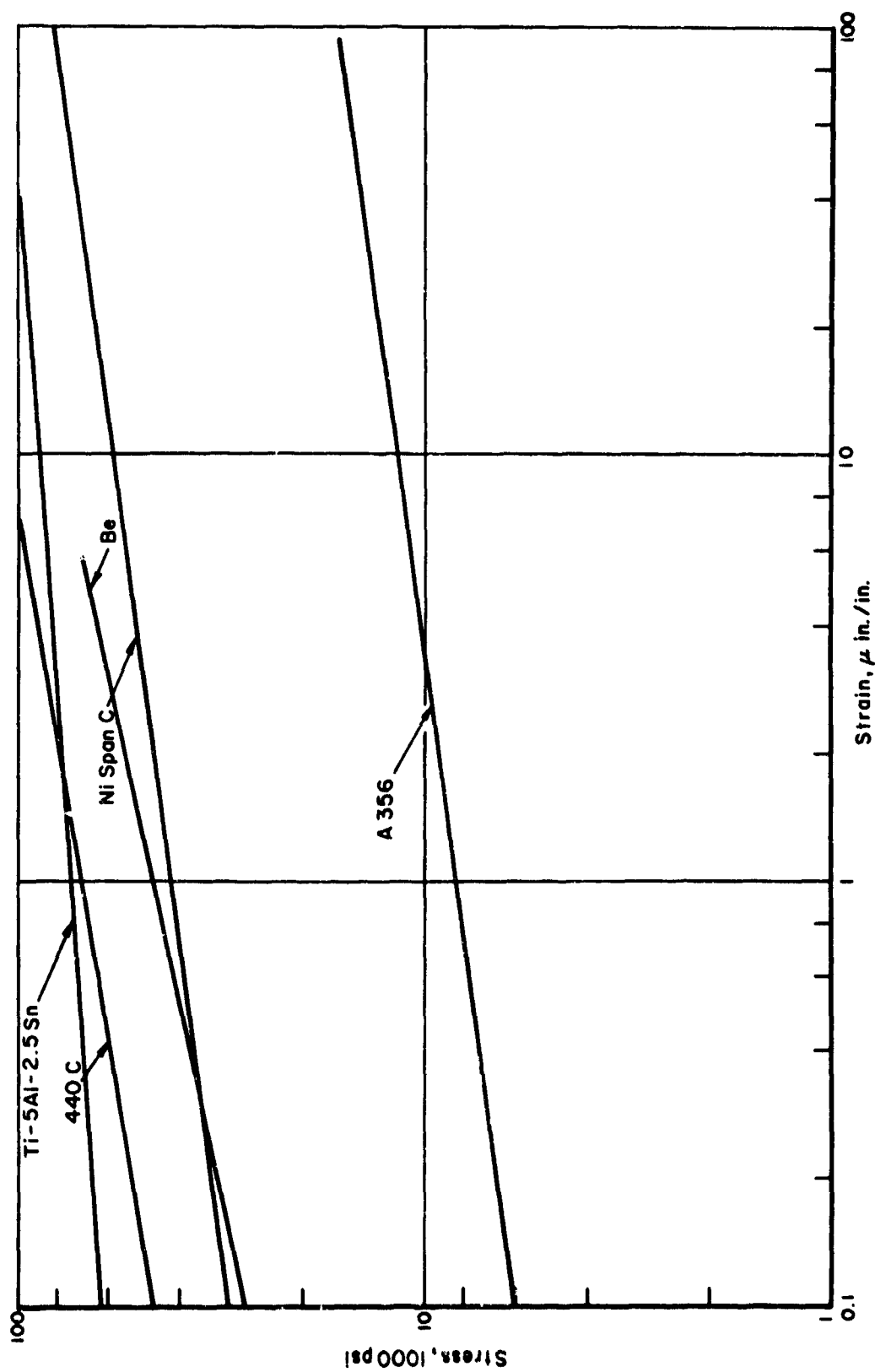FIGURE 27. MICROYIELD STRESS OF AD 995 ALUMINUM OXIDE SPECIMEN 3

FIGURE 28.   STRESS-RESIDUAL STRAIN ON LOGARITHMIC COORDINATES

43

Mechanisms of Microplastic Deformation

Observations concerning the basic mechanisms of microplastic deformation have been made by examining by transmission-electron microscopy thin-foil sections of strained and unstrained portions of tested microyield-strength specimens.

Ni-Span-C

Unstrained foils of Ni-Span-C generally displayed a near absence of dislocations as shown in Figure 29. Second-phase particles were seen in the grain boundaries. Dislocations present were not distinctly associated with any other microstructural feature as can be seen in Figure 29. Observations on foils taken from microstrained Ni-Span-C (40 μin./in.) suggest that microstrain is the result of dislocation generation or movement away from microstructural stress raisers under an applied load. Figure 30 illustrates dislocations emanating from second-phase particles in grain boundaries, the intersection of a twin and a grain boundary, and a jog in a grain boundary. Second-phase particles in grain boundaries appeared to be prime locations for the nucleation of microplastic flow. This is in general agreement with the work of Davies and Ku who studied dislocation generation in Fe-3-1/4 Si by etch-pit techniques.[7] It is also of interest that little evidence of dislocation interaction with other dislocations or defects was detected.

A356 Cast Aluminum

Evidence of microplastic flow in A356 cast aluminum is somewhat more subtle than for Ni-Span-C. Foils of unstrained material revealed rod-like precipitate particles (probably Mg_2Si) in the grain interiors, as shown in Figure 31. The relatively diffuse contrast around the particles indicated a distortion of the matrix lattice due to the presence of the particles. Foils of material strained 40 μin./in. generally exhibited a somewhat sharper contrast around the particles as illustrated in Figures 32a, 32b, and 32c. This sharper contrast suggests that microstrain could be a result of a transformation of lattice distortions around the particles into interfacial dislocations under an applied load. Many of the dislocations appeared to form spirals or loops around the particles. In some instances, as shown in Figures 32d and 32e, some dislocations appeared to move away from the original particles and several of the dislocations connected with other particles.

Tangled knots of dislocations were, on occasion, observed around the precipitate particles, as illustrated in Figure 33. However, these knots were noticed in both strained and unstrained foils. Therefore, they probably were either in the material before testing or were introduced during foil preparation, and are not the result of microplastic deformation.

440 C Stainless Steel

Thin foils prepared from unstrained 440 C stainless steel revealed carbide particles in a martensitic matrix with a very high dislocation density, as shown in Figure 34. This high dislocation density is characteristic of martensite and prevented any meaningful interpretation of the structure of foils taken from strained material with regard to

44
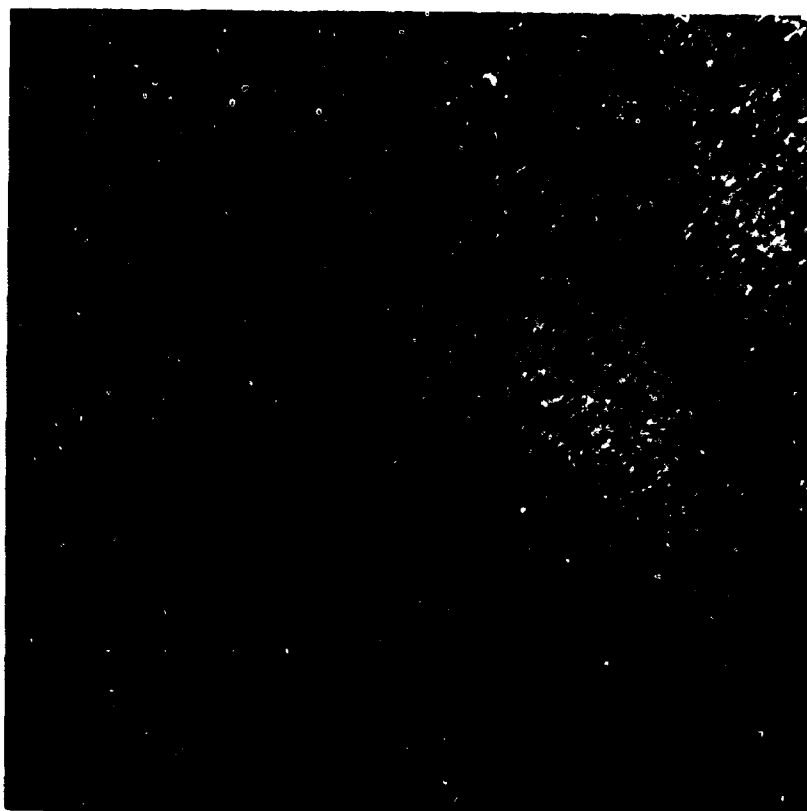
15,000X   a.   E2245d

15,000X   b.   E2246c

FIGURE 29.   UNSTRAINED N₁-SPAN C

45

15,000X   E2244d   15,000X   E2243e
   a. Grain-Boundary Second Phase   b. "Jog" in Grain Boundary
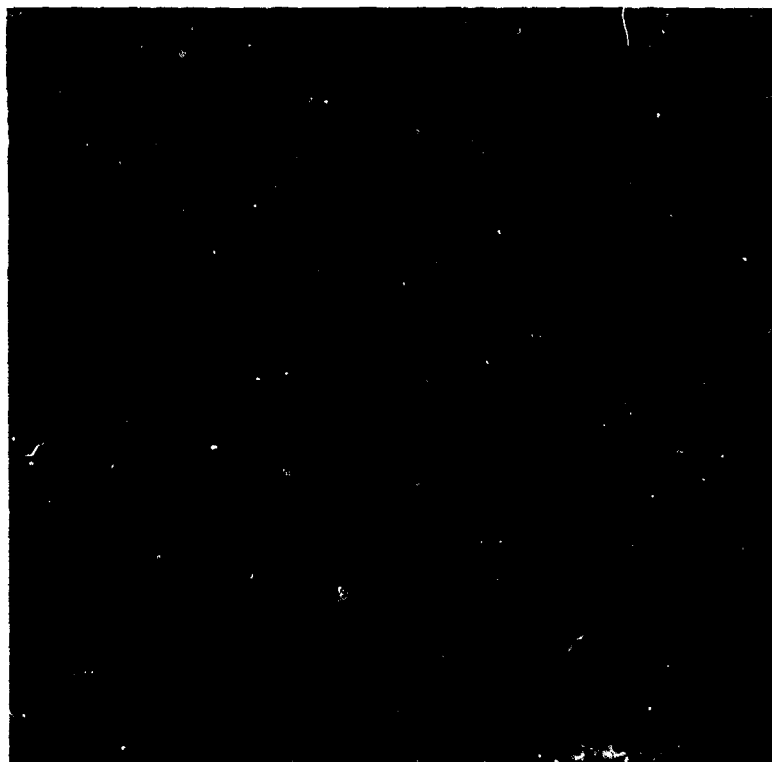
80,000X   E2243a
   c. Intersection of Twin and Grain Boundary

FIGURE 30.   MICROSTRAINED (40 IN./IN.) Ni-SPAN C

46

44,000X   a.   EH421   44,000X   b.   EH431
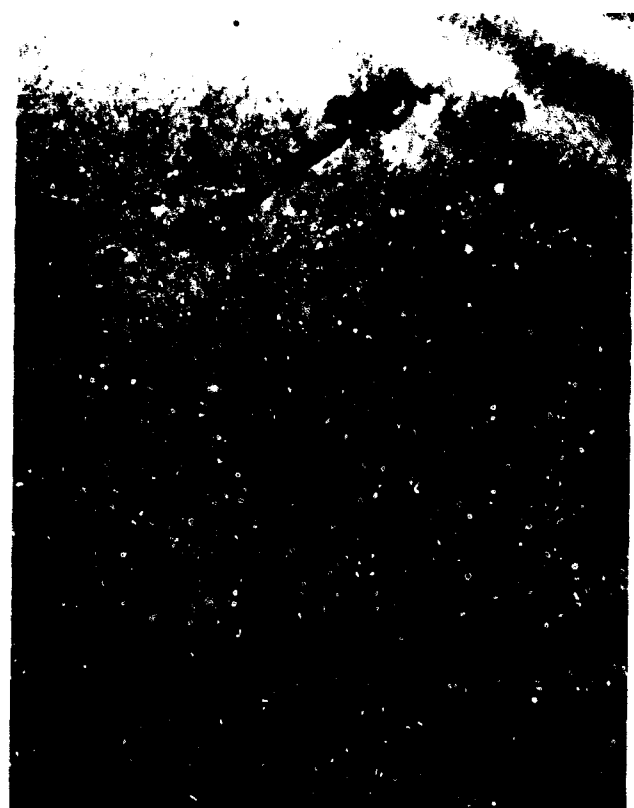
44,000X   c.   EH441

FIGURE 31. UNSTRAINED A356 CAST ALUMINUM

47

42,000X   a.   EH446   42,000X   b.   EH451

42,000X   c.   EH454

FIGURE 32. MICROSTRAINED (40 μIN./IN.) A356 CAST ALUMINUM
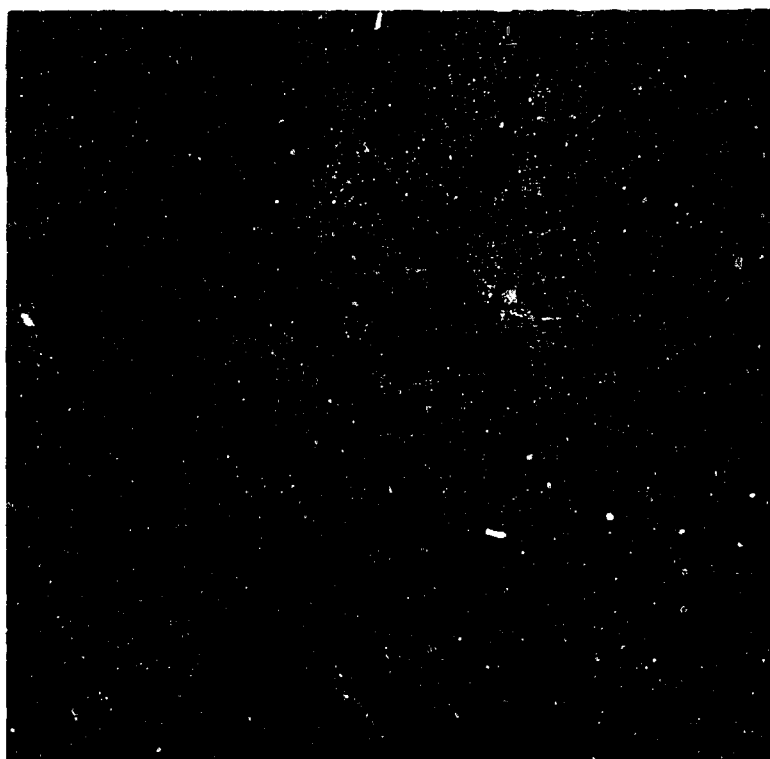
42,000X   d.   EH453
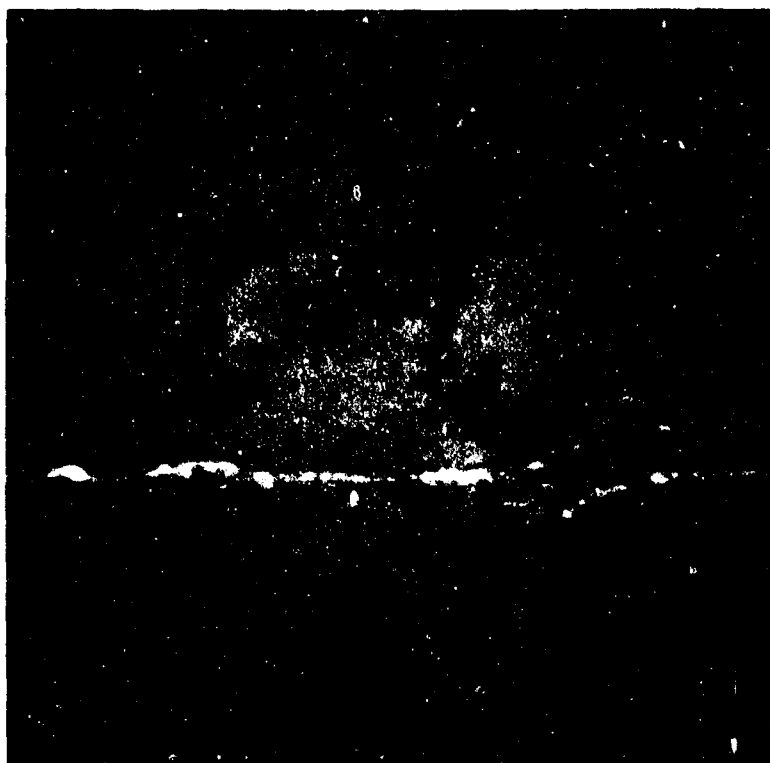
42,000X   e.   EH447

FIGURE 32. (CONTINUED)

44,000X   EH437

FIGURE 33. KNOTS OF TANGLED DISLOCATIONS IN A356
            CAST ALUMINUM
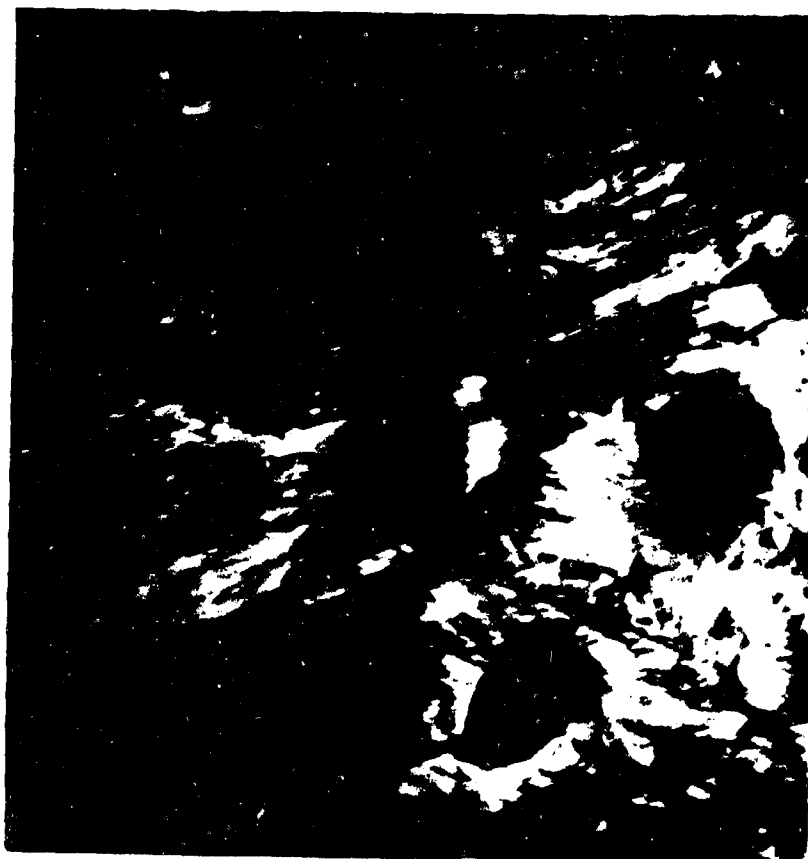
15,000X   E2249d

FIGURE 34.   UNSTRAINED 440C STAINLESS STEEL

micropiastic deformation. However, these foils are still useful in interpreting the micromechanical properties of 440 C stainless steel. The high dislocation density in 440 C stainless steel, as compared to the very low dislocation density of Ni-Span-C, may account for the higher microyield stress and greater resistance to continued microplastic deformation of 440 C stainless steel.

Effects of Plastic Prestrain on Microyield Strength

Microstrain Hardening

Experiments were conducted in which Ni-Span-C and 440 C stainless steel microyield-strength-test specimens were reloaded both immediately and with a 24-hour delay after initial determination of the microyield strength. Examples of such tests are illustrated in Figures 35 and 36. Microyielding occurred in reloaded specimens, with residual strains of approximately 20 to 40 μin./in., at significantly higher stress than the initial microyield strength indicating "microstrain hardening". These data suggest the possibility of increasing the microyield strength by microstraining similar to the way in which cold working increases conventional mechanical properties. It should be noted, however, that some indication of recovery can be observed in both 440 C and Ni-Span-C.

In view of the observation that microstrain in Ni-Span-C is largely due to the generation and motion of relatively unentangled dislocations, the recovery in this material can probably be interpreted as the reverse movement and annihilation of these dislocations. One might anticipate that, associated with this recovery, there would be a dimensional change – a shortening. An attempt to measure such a change was made, as is reported in a later section of this report, but the results were negative.

Plastic Strains of 2.5 and 5 Percent

Plastic strains of 2.5 and 5 percent (i.e., 25,000 and 50,000 μin./in.) were obtained in Ni-Span-C by loading tensile specimens above the 0.2 percent offset yield strength.

Figure 37 illustrates the influence of these relatively large plastic prestrains on the microyield strength of Ni-Span-C. Contrary to the previously observed effects of relatively small amounts of prestrain, plastic strains of 2.5 and 5 percent greatly reduced the microyield strength. In fact, evidence of microplastic deformation was detected at the lowest stress level employed in the test. Equally important, the slope of the stress-residual strain curve was considerably steeper for the prestrained material than for the unstrained specimens.

An electron-photomicrograph of Ni-Span-C strained 2.5 percent is shown in Figure 38. It can be seen that straining 2.5 percent resulted in the generation of numerous dislocations, most of which were confined to relatively narrow, intersecting bands. The dislocations in these bands are, no doubt, severely entangled and relatively immobile. On the other hand, some dislocations are visible in the regions between the bands. These dislocations apparently are not entangled with other dislocations and should, therefore, be able to move at very low stresses, resulting in a lower microyield
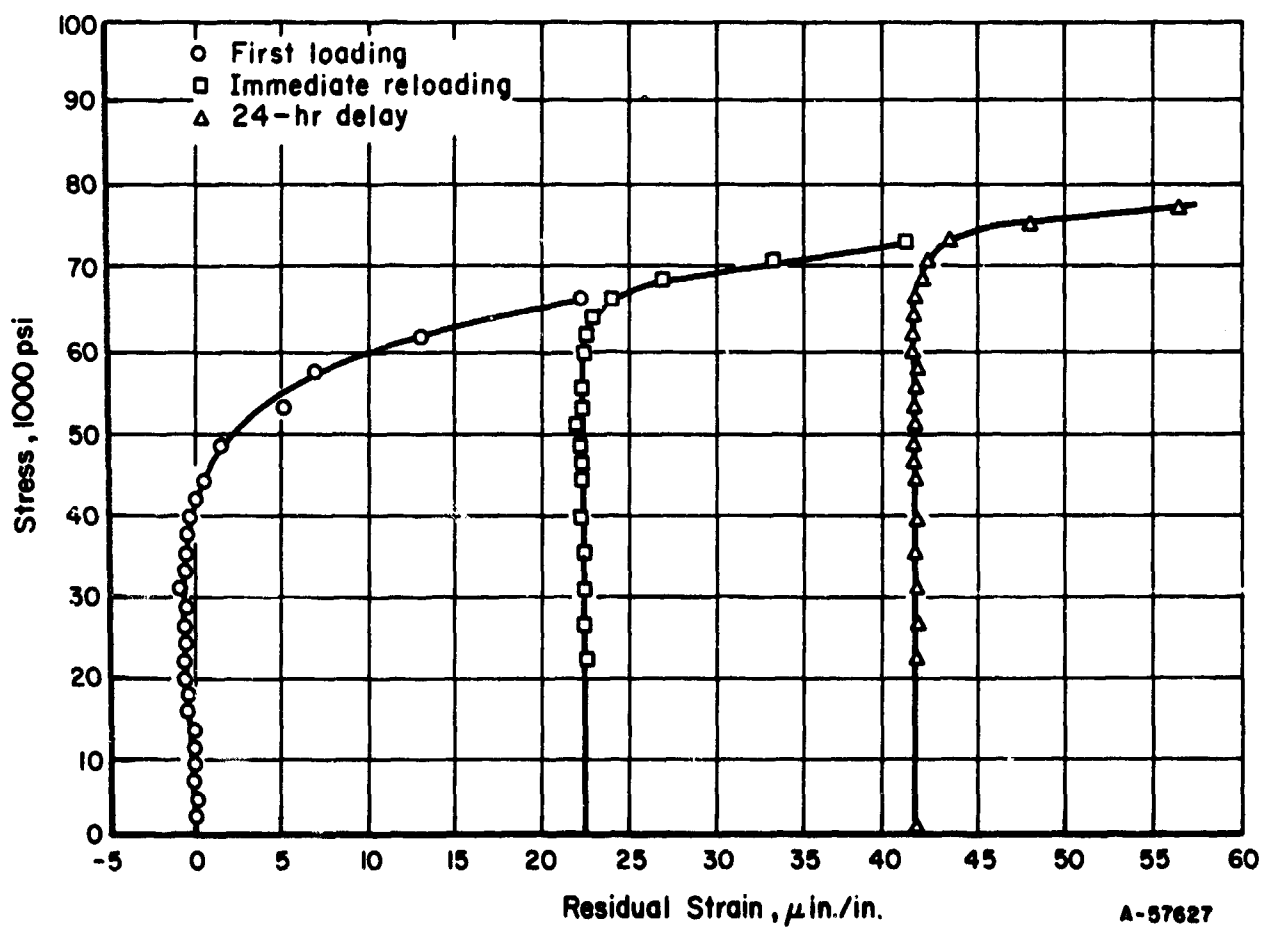
FIGURE 35. MICROSTRAIN HARDENING OF Ni-SPAN-C SPECIMEN 19
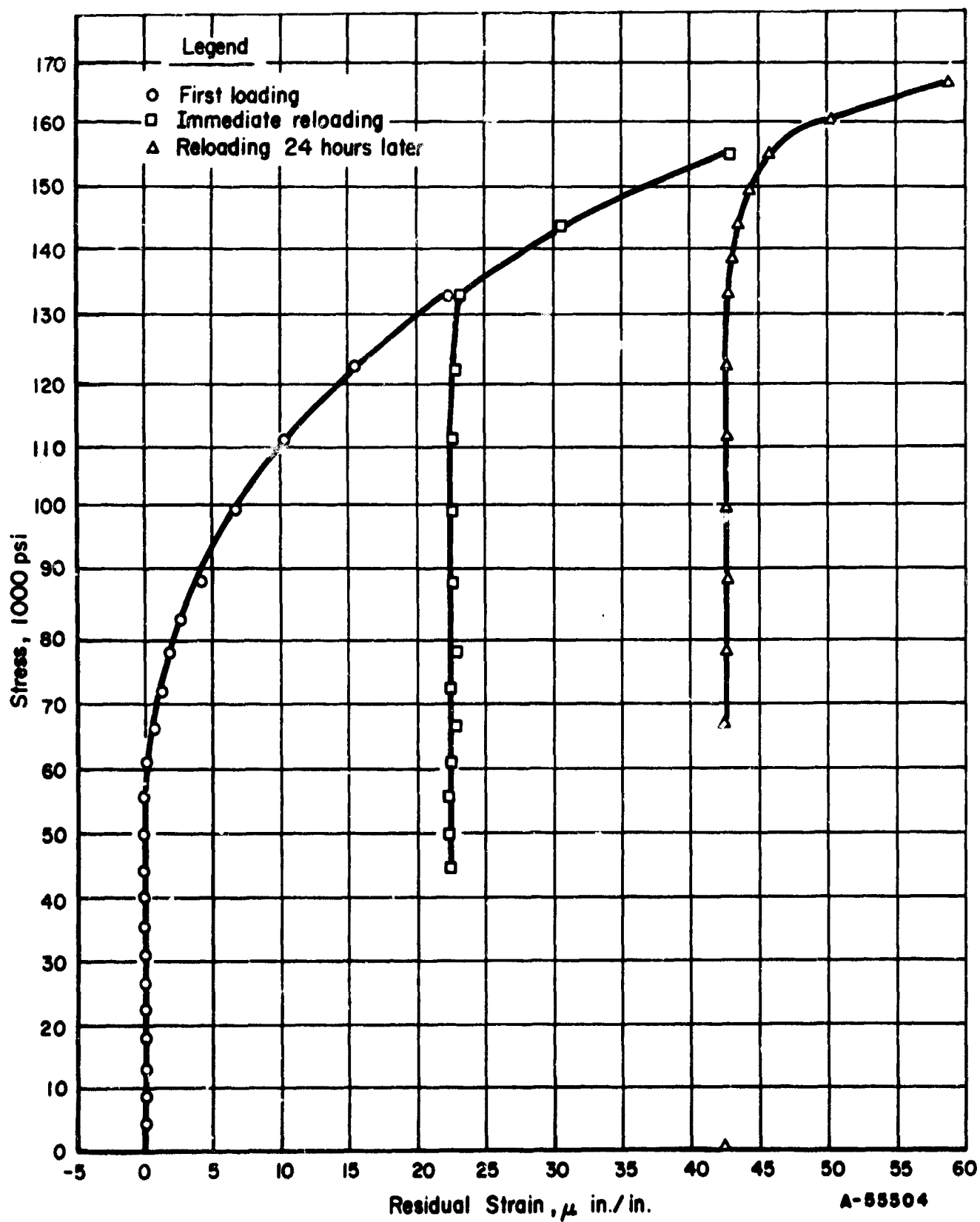
FIGURE 36. RECOVERY OF MICROSTRAIN IN 440 C STAINLESS STEEL
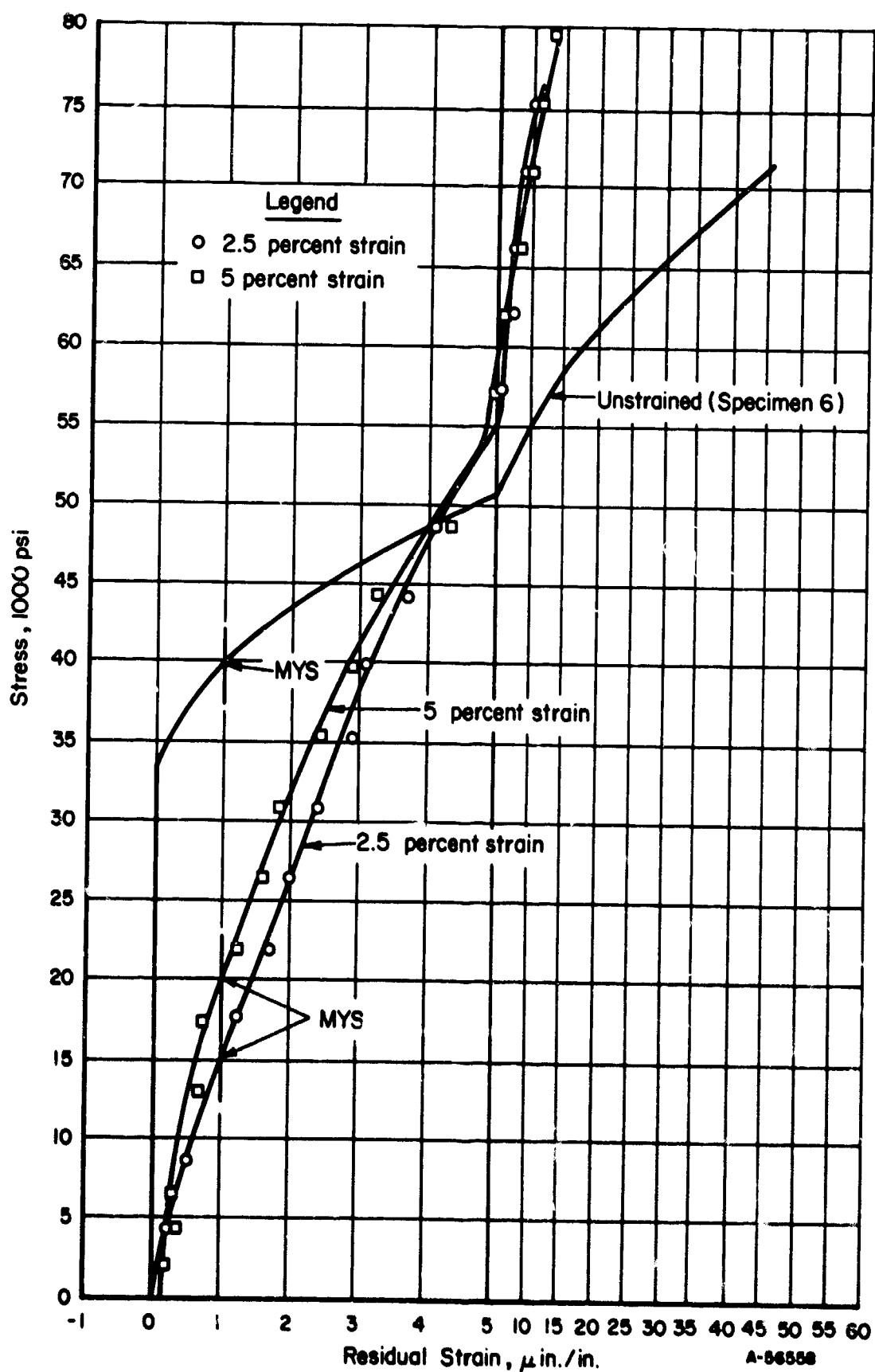SPECIMEN 7

FIGURE 37. EFFECT OF PRESTRAIN ON THE MICROYIELD STRESS OF Ni-SPAN-C
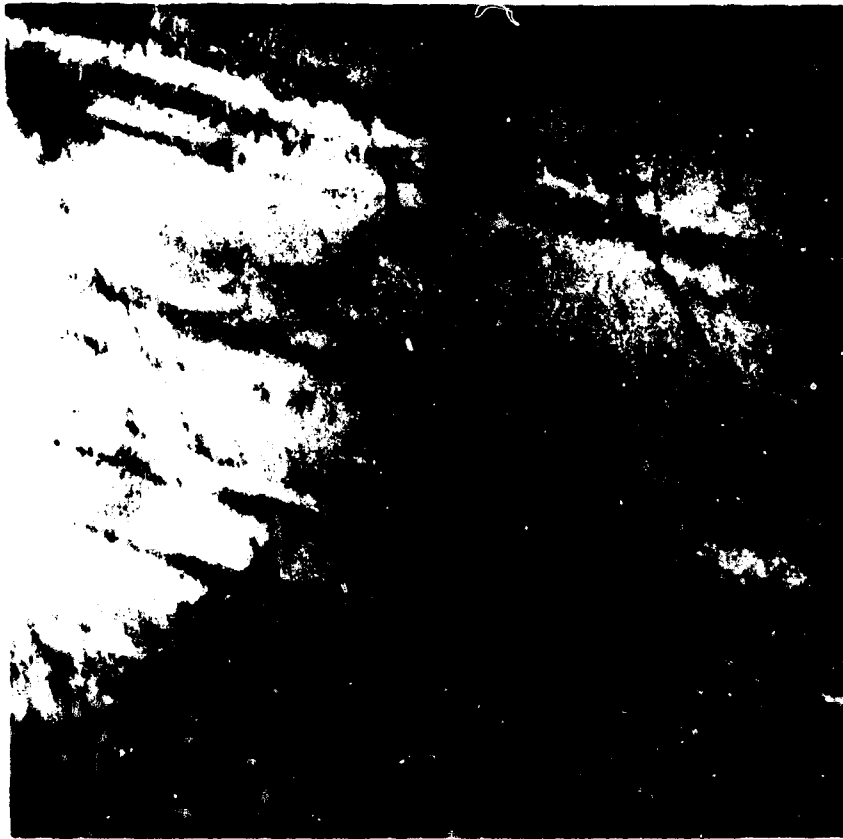
20,000X   3295a

FIGURE 38. NI-SPAN-C STRAINED 25 PERCENT

strength for Ni-Span-C prestrained 2.5 percent than for unstrained specimens. However, once these dislocations move a short distance, they run into the entangled bands of dislocations, and their continued motion becomes considerably more difficult, which accounts for the steeper slope of the stress-residual strain curves for the specimens prestrained 2.5 and 5 percent.

The effects of plastic strains on dimensional stability are discussed in a following section of this report.

Conventional Tensile Properties

The conventional mechanical properties of Ni-Span-C, 440 C stainless steel, A356 cast aluminum, Ti-5Al-?.5Sn, and Super PEL beryllium are given in Table VII and a comparison is made with their microyield strengths. The alloys with relatively high conventional yield strengths also exhibited relatively high microyield strengths. However, no systematic quantitative relationship was evident between the conventional and microyield strengths. Therefore, at our present level of understanding, conventional mechanical-property tests cannot serve as the basis for reliably predicting the microyield strength.

TABLE VII. CONVENTIONAL MECHANICAL PROPERTIES

Material	0.2 Percent Offset Yield Strength, 1000 psi	Ultimate Tensile Strength, 1000 psi	Elongation, percent	Reduction in Area, percent	Average Microyield Strength, 1000 psi
Ni-Span-C	106.7	175.5	12	49	39
	102.1	173.6	12	54	
440 C	(a)	255	0	0	70
	(a)	214	0	0	
A356	22.2	31.2	2	2	
	21.2	31.1	3	2.5	7.5
Ti-5Al-2.5Sn	135.0	137.5	13.5	--	75
	135.2	138.5	10.9	--	
Super PEL Be	(a)	61.3	0	0	47
	(a)	54.8	0	0	

(a) Fracture before yielding.

57

Microcreep Studies

The microcreep behavior of Ni-Span-C, 440 C stainless steel, A356 cast aluminum, Super PEL beryllium, and AD995 aluminum oxide was studied by loading tensile specimens to 50 and 75 percent of their average microyield strengths and measuring the subsequent, time-dependent strains.

Ni-Span-C

Figure 39 illustrates microcreep data for Ni-Span-C. Little difference can be observed in the creep behavior between the 50 and 75 percent stress levels. A creep strain of approximately 1 μin./in. was detected at 100 to 150 hours and the total creep strain at 1000 hours was approximately 10 to 15 μin./in.

440 C Stainless Steel

Microcreep data for 440 C stainless steel are given in Figure 40. No evidence of microcreep (within the precision of creep-strain measurement) was detected at a stress of 50 percent of the microyield strength. At a stress of 75 percent of the microyield strength, a creep strain of 1 μin./in. was observed at approximately 80 hours. A total creep strain of approximately 6 μin./in. was noted at 1000 hours.

A356 Cast Aluminum

Figure 41 gives the microcreep data for A356 cast aluminum. At a stress of 50 percent of the microyield strength, a creep strain of 1 μin./in. was detected at approximately 10 hours and a total creep strain of approximately 17 μin./in. was observed at 1000 hours. The specimen stressed to 75 percent of the microyield strength exhibited less extensive creep than the specimen at the lower stress level. This apparent discrepancy may be attributable to the variability in microyield strength noted previously for A356 cast aluminum. Because of the wide variation in microyield strength, it is possible that the specimen at the higher load level was stressed to a smaller fraction of its specific microyield strength than was the specimen at the lower load level.

Super PEL Beryllium

Microcreep data for Super PEL beryllium are illustrated in Figure 42. Similar to Ni-Span-C, little difference was observed between the behavior of specimens stressed to 50 and 75 percent of the microyield strength.

A creep strain of 1 μin./in. was detected at approximately 100 hours. A total creep strain of approximately 3 to 5 μin./in. was observed at 1000 hours.
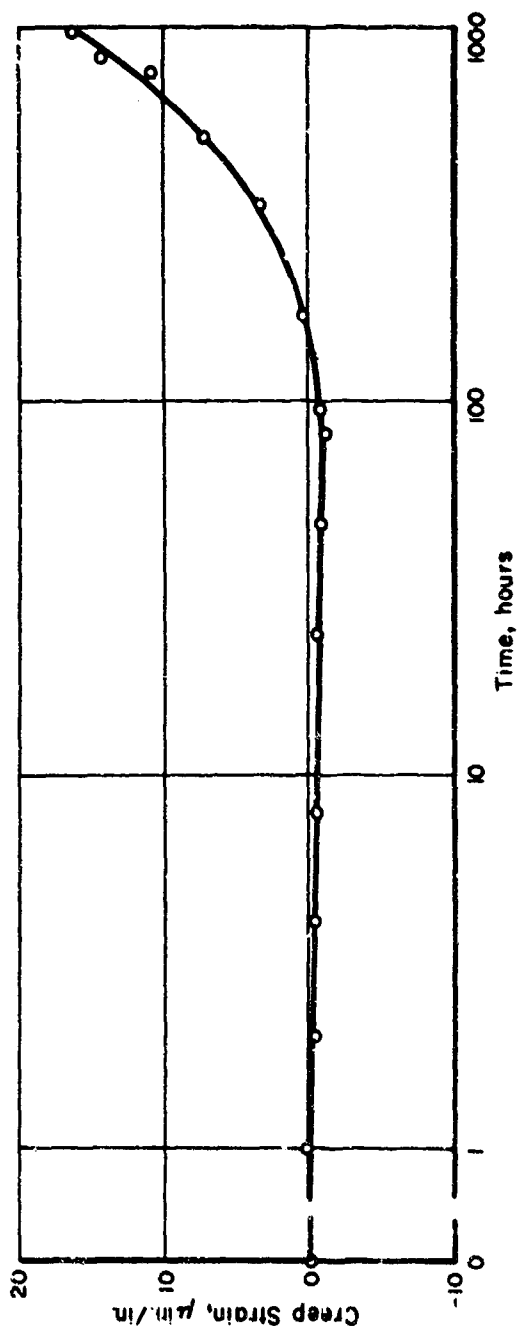
58

FIGURE 39. MICROCREEP OF Ni-SPAN-C

A-37828

a. 20,000 psi (50% MYS)

b. 30,000 psi (75% MYS)

Time, hours

Creep Strain, μin./in.

59
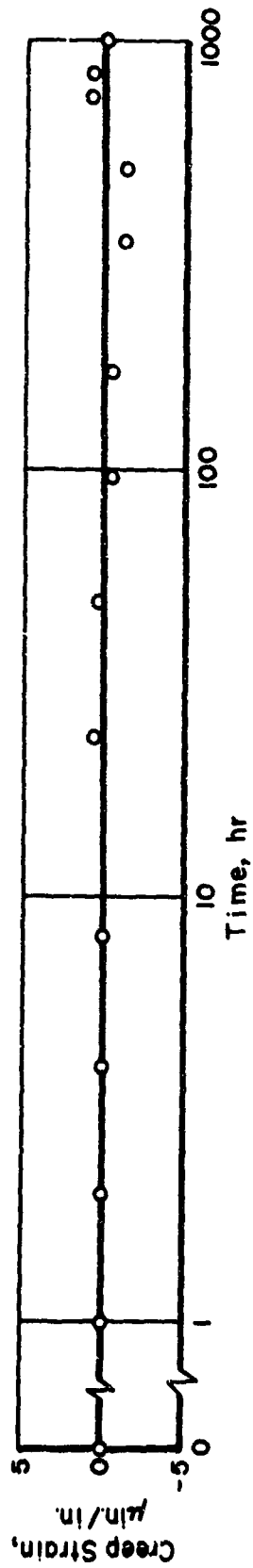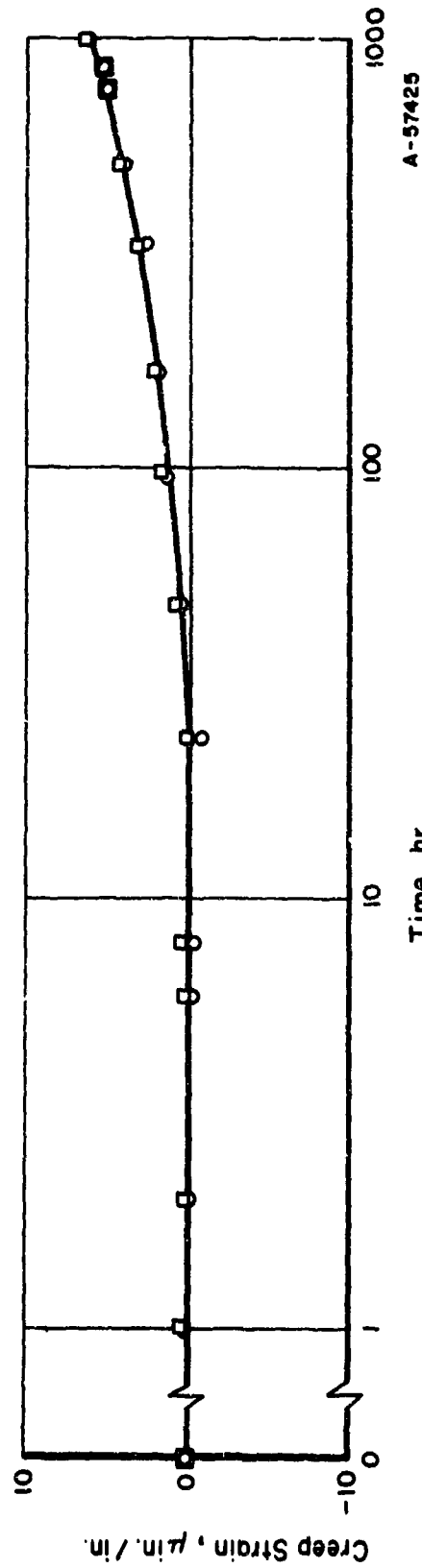
FIGURE 40. MICROCREEP OF 440 C STAINLESS STEEL

(1/2 hr at 1900 F OQ; 1 hr at 500 F, AC)

A-57425

a. 33,500 psi (50 % MYS)

Time, hr

Creep Strain, μin./in.

b. 50,000 psi (75% MYS)

Time, hr

Creep Strain, μin./in.

60
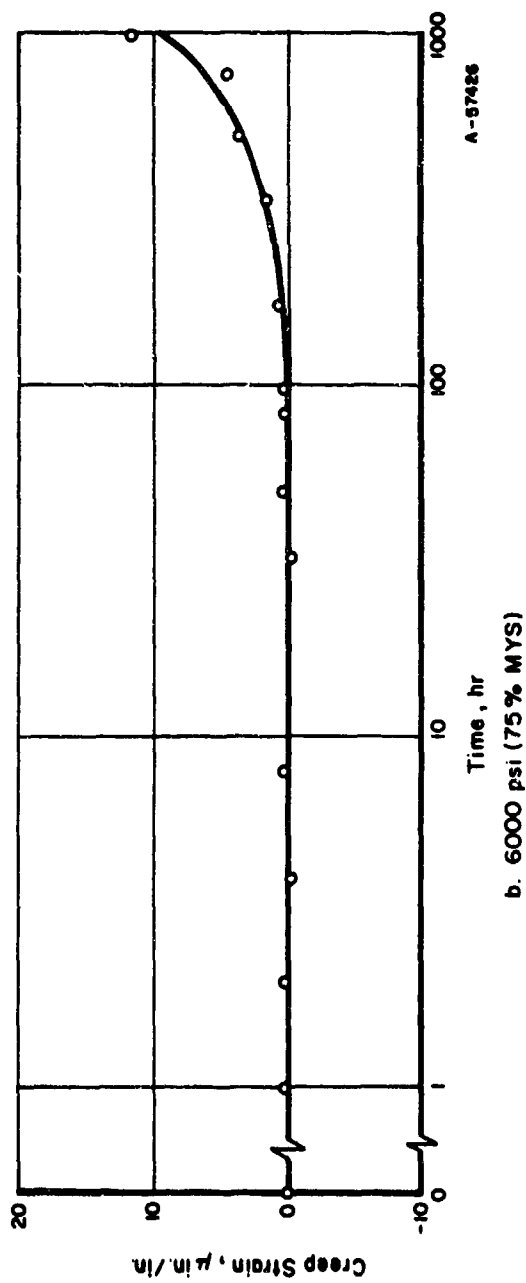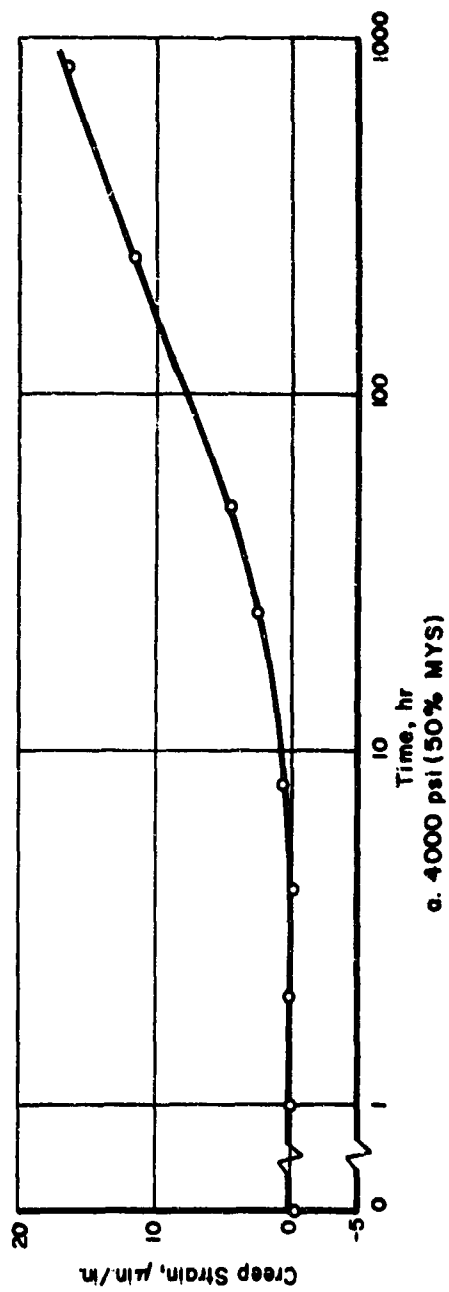
FIGURE 41. MICROCREEP OF A356 CAST ALUMINUM (16 HR AT 1000 F, WQ; 4 HR AT 310 F, AC)

61
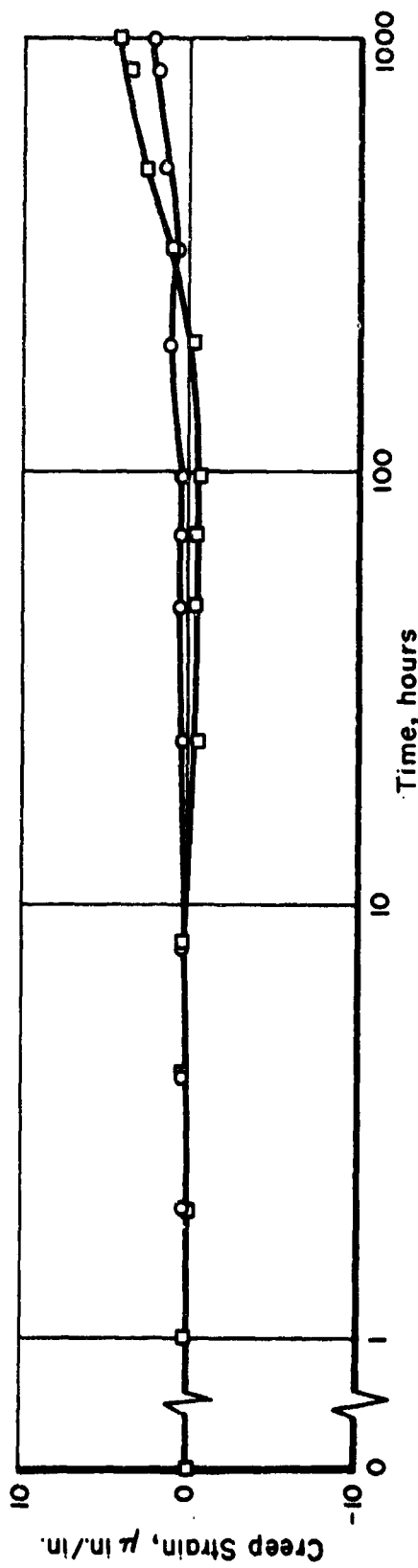
FIGURE 42. MICROCREEP OF SUPER PEL BERYLLIUM

a. 23,500 psi (50% MYS)

b. 35,000 psi (75% MYS)

A - 57629

62

AD995 Aluminum Oxide

Figure 43 illustrates microcreep data for AD995 aluminum oxide. There was no apparent creep of the specimen stressed to 50 percent of the fracture stress for 1000 hours.

Microcreep Rates

The creep strain of some of the various materials at stresses of 50 and 75 percent of their MYS values is plotted on linear time coordinates in Figures 44 and 45. For the most part, these curves appear to be showing a decreasing rate of creep with increasing time. There are some exceptions where the creep rate seems to be accelerating in its early stages (Ni-Span-C and Be), but only one case where the creep rate still appears to be increasing at 1000 hours (A356 at 75 percent of its MYS). Some additional microcreep data on A356, at loads slightly in excess of the MYS also show the rate of creep to be decreasing with decreasing time.[8] Similar behavior has been observed for a variety of materials during a recently completed study for NASA.[9]

Microcreep Mechanisms

A decreasing creep rate is characteristic of low-temperature, low-stress creep and is generally referred to as transient or logarithmic creep.[10] This type of creep is usually attributed to an exhaustion mechanism in which the generation and movement of dislocations is opposed by continuously increasing energy barriers.

One disturbing feature of the microcreep experiments was the general lack of an appreciable difference between specimens stressed to 50 or 75 percent of their microyield strengths. The limited data prevent drawing any significant conclusions from this behavior. Some generally similar behavior was observed in the NASA study, although then a definite stress dependence was apparent.[9] The scatter observed in the NASA studies was attributed primarily to the expected structure sensitivity of the initiation and continuation of plastic flow. Data from the NASA report, with some of the present data added, are shown in Figure 46.

If the microcreep behavior observed is reasonably characteristic of the behavior of these materials, then it is probable that the microcreep is indeed attributable to a dislocation exhaustion, or a dislocation-source exhaustion mechanism. The implications of this are discussed more fully in a later section of this report.

General Comments

The above microcreep tests demonstrated that microplastic deformation can occur in many materials at stresses of only 50 percent of the microyield strength when the stresses are maintained for an extended period. This is important not only with regard to externally applied stresses, but internal, residual stresses of this magnitude, including those introduced by machining, can cause microplastic deformation as well.

An exact, quantitative relationship between microcreep and microyield-strength behavior could not be perceived. However, it was noticed that materials exhibiting the
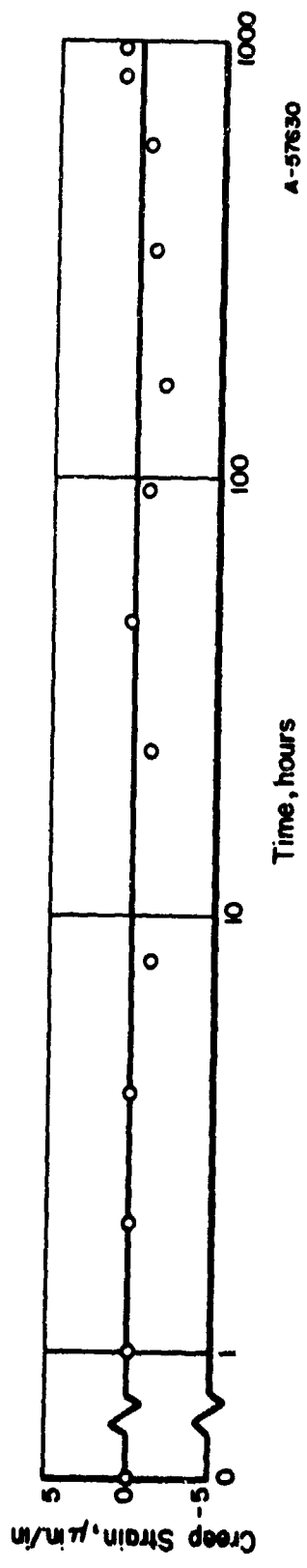
FIGURE 43. MICROCREEP OF A D995 ALUMINUM OXIDE OF 16, 500 PSI (50 PERCENT MYS)
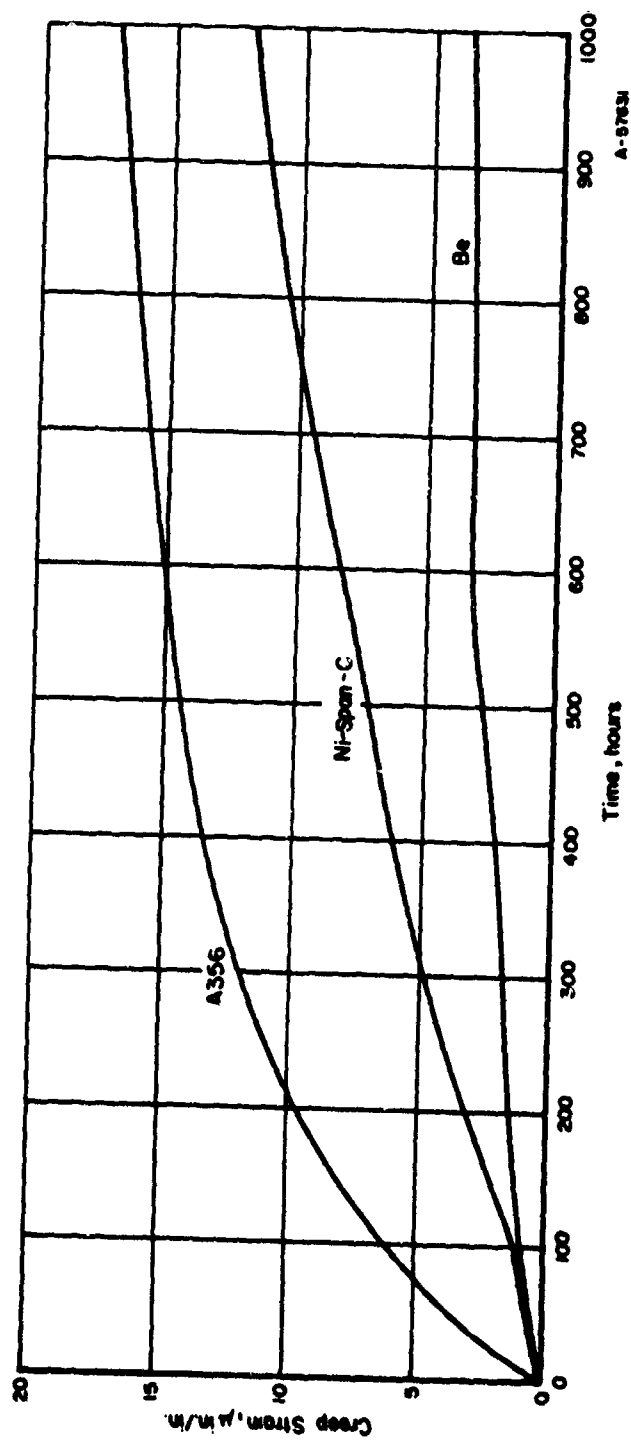
64

FIGURE 44. CREEP STRAIN VERSUS LINEAR TIME AT 50 PERCENT OF THE MICROYIELD STRENGTH
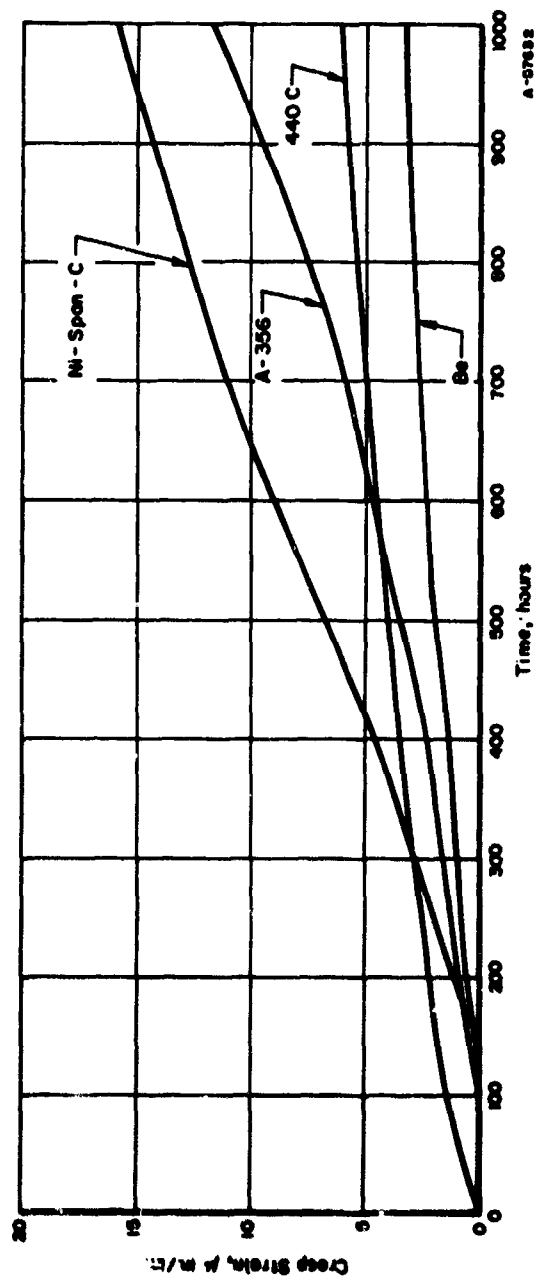
FIGURE 45. CREEP STRAIN VERSUS LINEAR TIME AT 75 PERCENT OF THE MICROYIELD STRENGTH
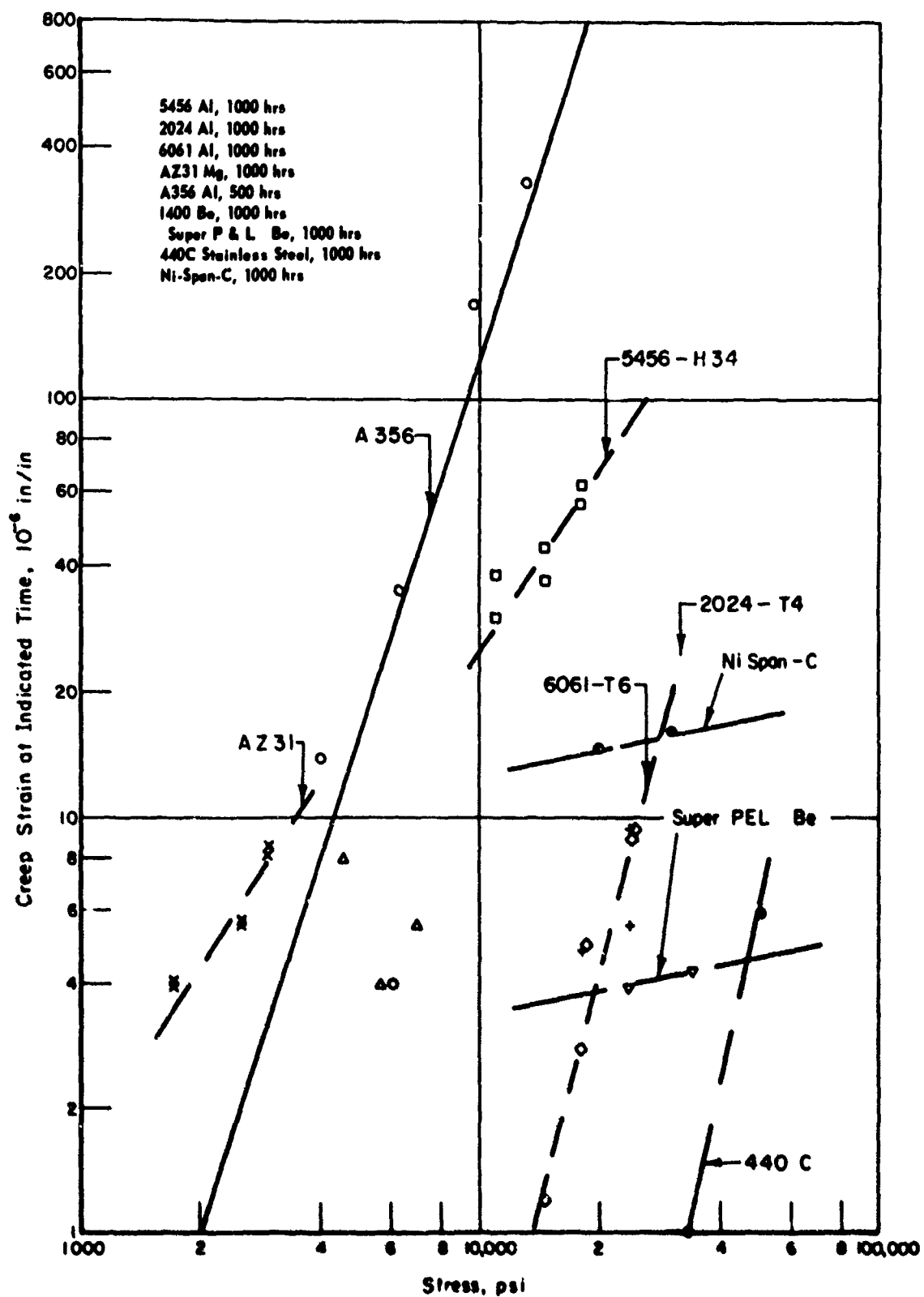
66

FIGURE 46.   TOTAL MICROCREEP STRAIN AT INDICATED TIMES

67

shallowest slopes in the microyield strength, stress-residual strain curves (Ni-Span-C and A356, see Figure 28) also tended to exhibit more extensive microcreep than the 440 C or the Super PEL beryllium. Both the lack of resistance to continued micro-plastic deformation in the microyield-strength test and extensive microcreep could be related to the stress dependence of the generation of dislocations and to the relative ease with which dislocations, once generated, can move through the crystal lattice. For example, dislocations would meet considerable resistance moving through the dense dislocation entanglements observed in 440 C stainless steel, resulting in a steep slope of the stress-residual strain curve, and relatively little microcreep. On the other hand, dislocations could move easily through the almost dislocation-free grains in Ni-Span-C, resulting in a shallower slope of the stress-residual strain curve, and more extensive microcreep than observed with 440 C stainless steel.

Capacitor Strain Gage

Strain measurements on high strength-low modulus materials, such as titanium, are not readily made with electrical-resistance strain gages, since the elastic range of foil gage and adhesive, as noted previously, can be exceeded. A capacitor strain gage lends itself to this application; it is not dependent on adhesives, a high sensitivity is obtainable, and the gage can be used repeatedly. Having cylindrical symmetry, it also gives average strain, which in this case is an advantage.

Based on a paper by Hartman, Bresie and Roberts a prototype capacitor strain gage was designed and built.[11] Small differences in the capacity of a three-plate capacitor were detected by a Wayne-Kerr capacitance bridge, the bridge reading being proportional to the separation of the active and the grounded plate of the gage. Several short-comings became apparent when the gage was attached to a 1/4-inch-diameter annealed drill-rod specimen for evaluation. The active plate had an area larger than could be balanced with the Wayne-Kerr bridge. A capacitor connected in series with the gage was used to bring it within the range of the bridge, but this reduced the gage sensitivity. The main obstacle was, however, the mechanical attachment to the sample. This was done by clamping the gage directly to the specimen test section with set-screws (both cupped and spring-loaded plunger set-screws were tried), but deviations from linearity and lack of a reproducible zero residual strain upon unloading (but main-taining a nominal reference load) were attributed to slippage between the specimen and the gage. A specimen with shoulders for attachment of the gage reduced the slippage, but not enough to make it useful for reliable microstrain measurements.

Therefore, a new gage and a new specimen were made (see Figure 47). Here four pointed screws clamp either half of the gage to a reference face on the sample, perpendicular to the specimen axis and outside the 1-inch gage length. The active plate is the edge of a 2.5 mil brass foil insulated on either side from the guard rings by 3 mil Teflon foil. The outer ring was machined slightly undersize (about 1 mil on the diameter), heated and the foils held in place on the inner guard ring with tape. A small lathe cut was then made to line up the faces again. The gage was connected to the Wayne-Kerr bridge (Model DM 100) with a short, flexible, double-shielded cable; the first shield connected to the guard rings, the second shield to the grounded ad-justable plate. Since the active plate area and the inherent capacity of the gage differ slightly from those for which the bridge scale is calibrated, the gage was calibrated against a known difference (970 μin.) between two nonconductive shims. To increase the sensitivity and to read the bridge more accurately, an electronic voltmeter was used to read the bridge-meter deflection to five decimal places.
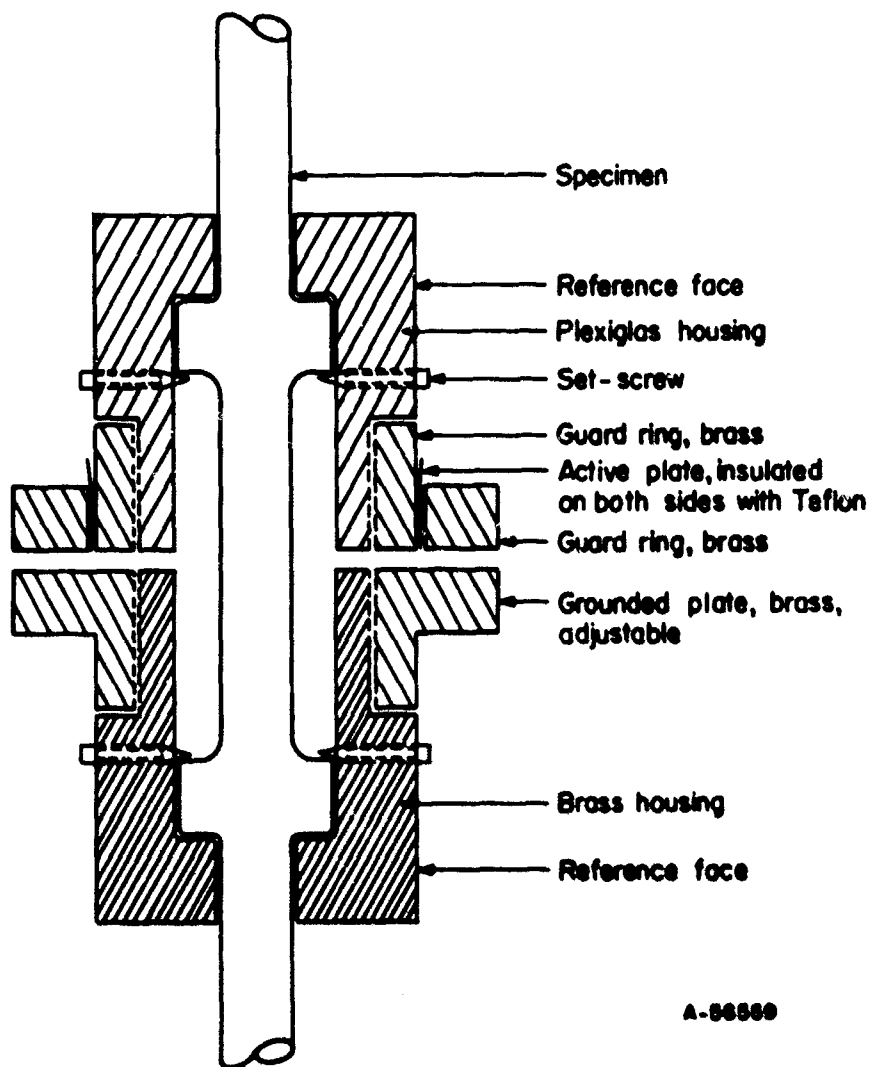
FIGURE 47. CAPACITOR STRAIN GAGE

Scale:

1"

69

Load was applied via loading nuts on the ends of the sample. These nuts rested on a spherical seat in order to minimize eccentricity. The microyield strength of Ti-5Al-2.5Sn (see Figure 23) was obtained using this gage.

DIMENSIONAL STABILITY

Effects of Stress Cycling, Thermal Cycling, and Plastic Strain

Button-head tensile specimens of Ni-Span-C, 440 C stainless steel, A356 cast aluminum, Ti-5Al-2.5Sn, and Super PEL beryllium were subjected to stress cycles, thermal cycles, and plastic strains to evaluate the effect of these variables on dimensional stability. Unlike the specimens used for the micromechanical-property studies, the machined surfaces of these specimens were not removed by chemical etching. Each specimen was measured before cycling to determine the initial length, and after cycling at regular intervals for a period of up to 6 months. The resulting length change data are illustrated in Figures 48, 49, 50, 51, and 52.

Control Specimens

One specimen of each material was not subjected to any additional treatment and its length was monitored over the same period of time as the cycled specimens. These specimens indicated the inherent stability of the various materials as processed (see Experimental Procedures for details) and provided a basis for evaluating the effects of the cycling treatments.

No significant change in length was noted for the control specimens of any of the materials, as shown in Figures 48a, 49a, 50a, 51a, and 52a. Evidently, the residual stresses and metallurgical instabilities in these specimens as processed were insufficient to cause length changes of greater than 1 μin./in. over a period of 4,300 hours (6 months). Therefore, the inherent dimensional stability of these materials can be considered good.

Stress Cycling

A specimen of each material was loaded to 75 percent of its microyield strength ten consecutive times in an Instron Testing Machine using the same load train as for the microyield-strength tests.

Figures 48b and 52b indicate that Ni-Span-C and Super PEL beryllium grew approximately 2 to 3 μin./in. upon stress cycling, but no deterioration in dimensional stability was apparent thereafter for a period of 4,300 hours (6 months). No significant length change upon stress cycling or deterioration in dimensional stability after stress cycling was detected for 440 C stainless steel and A356 cast aluminum, as can be seen in Figures 49B and 50B.

These data suggest that severe distortions and accelerated dimensional instability will not be encountered if these materials are repetitively loaded in one direction at low frequency to stresses up to at least 75 percent of their microyield strengths.

Thermal Cycling

A specimen of each material was placed in a test tube to moderate the rate of temperature change and subjected to the following thermal cycle:
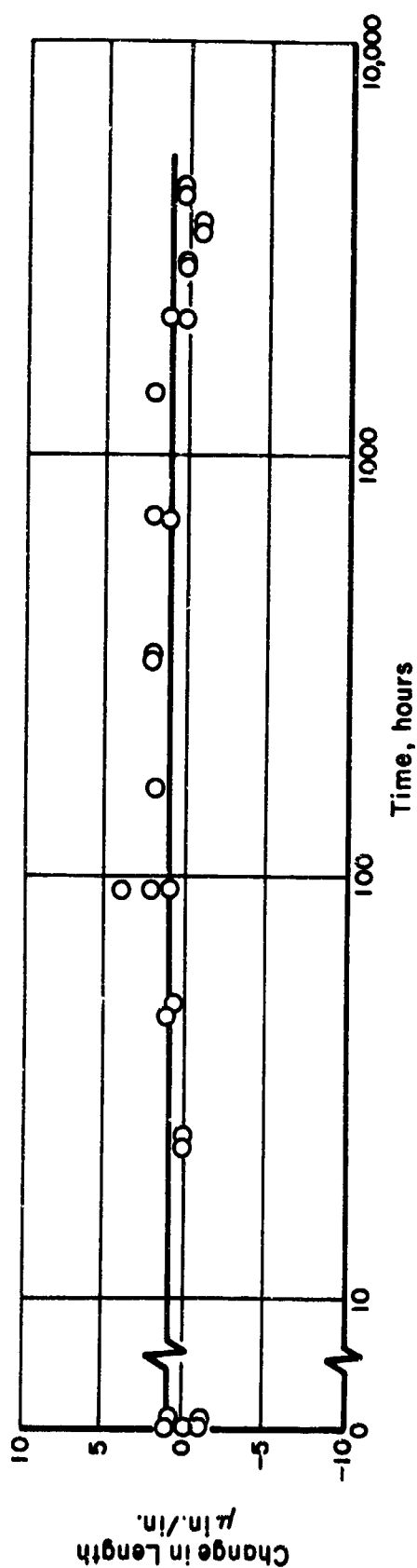
FIGURE 48. EFFECT OF STRESS CYCLING, THERMAL CYCLING, AND PLASTIC STRAIN ON THE DIMENSIONAL STABILITY OF Ni-Span-C (1-1/4 HR AT 1800 F, WQ; 21 HR at 1250 F, AC)
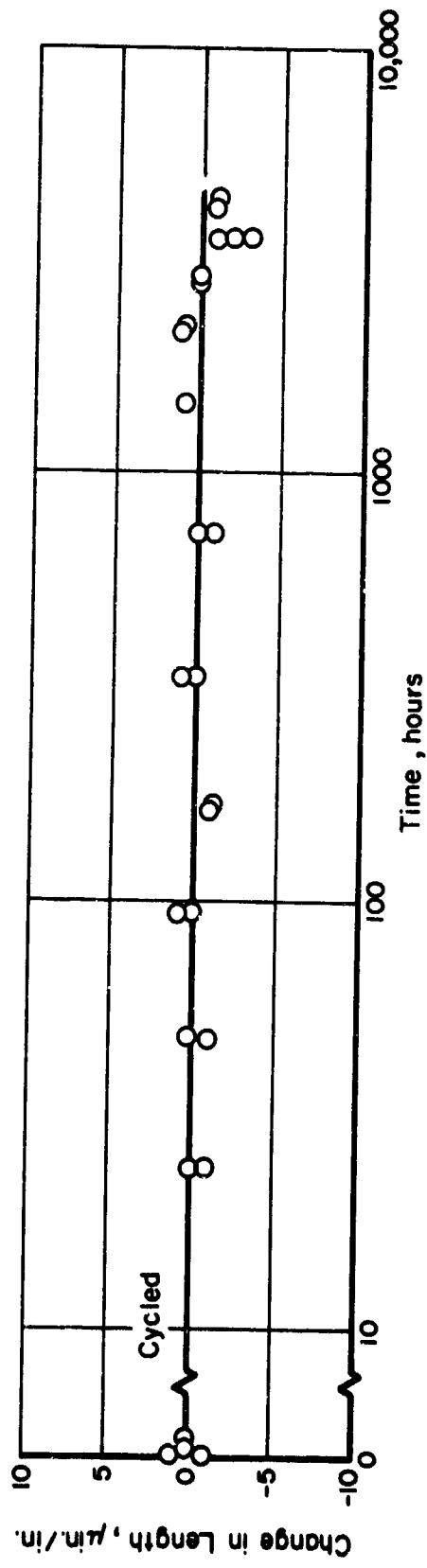
A-57634

c. Thermal Cycled

10 min at 212 F
10 min at RT
10 min at -100 F
10 min at RT

Repeat 5 times

d. 25 μin./in. Plastic Strain

FIGURE 48. (CONTINUED)

A-57656

73

Time , hours
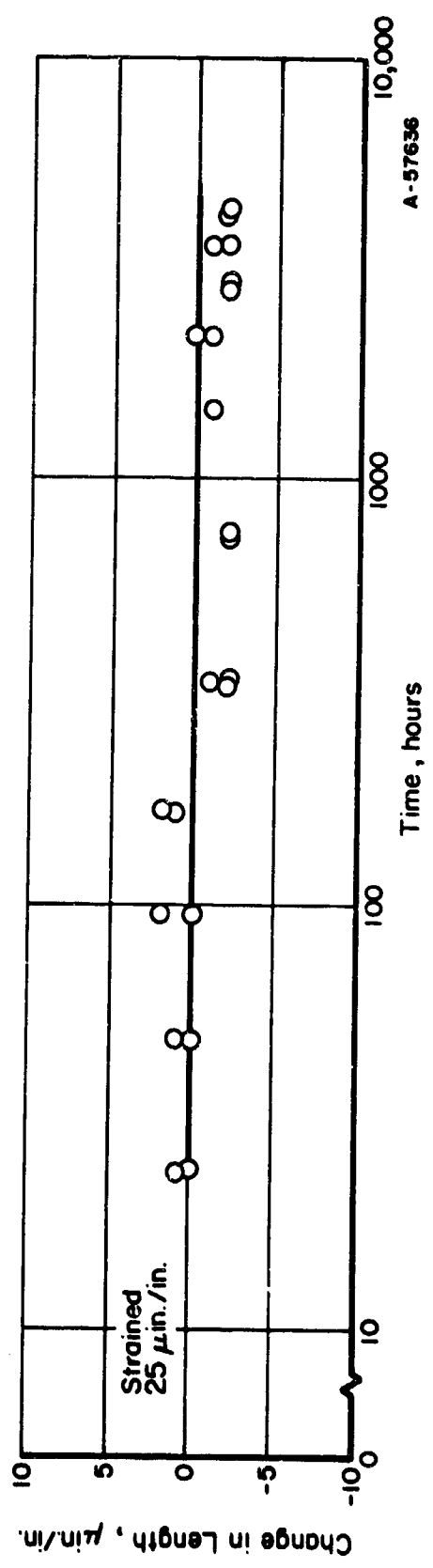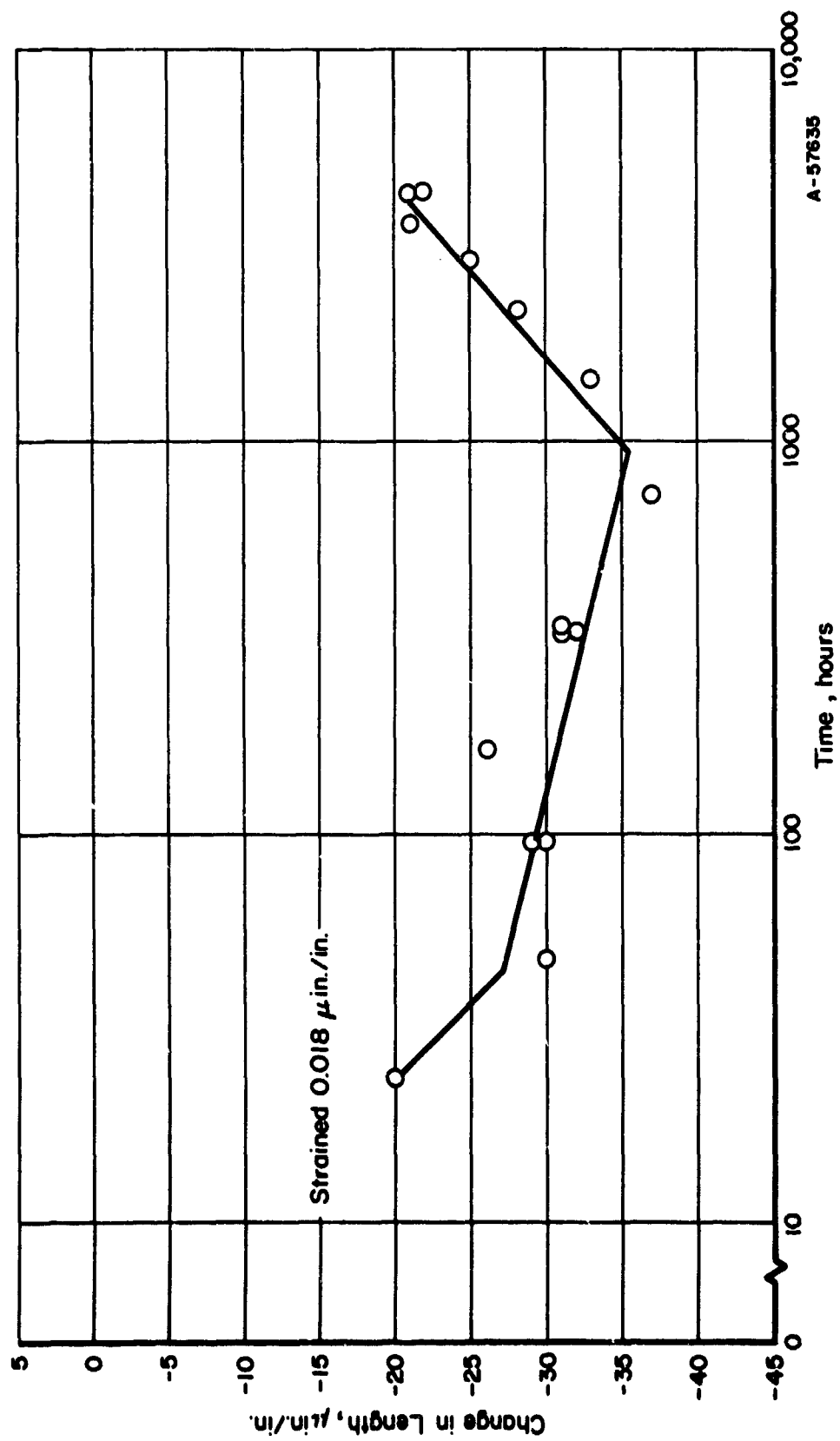
e. 2 % Plastic Strain

FIGURE 48. (CONTINUED)

74
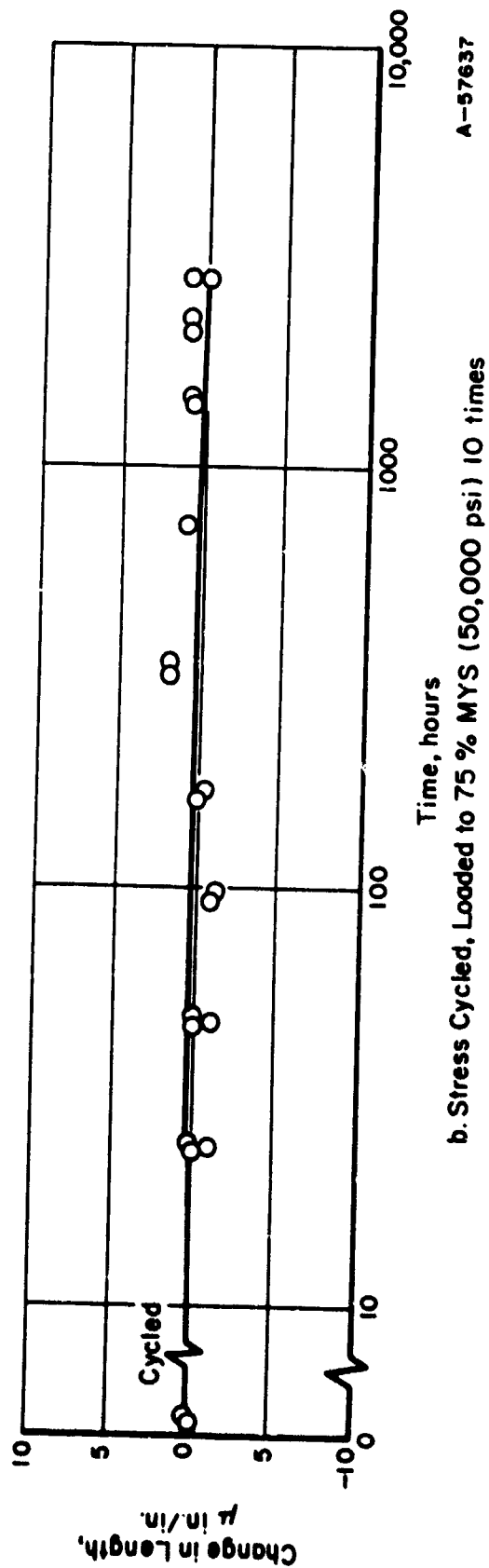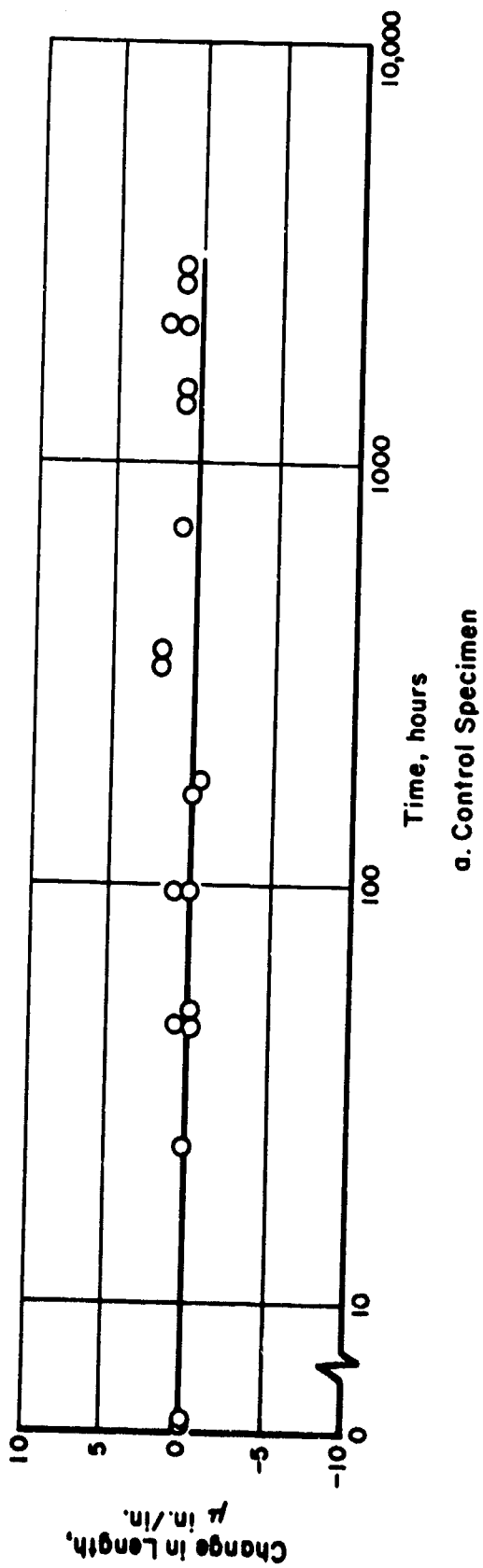
FIGURE 49. EFFECT OF STRESS CYCLING, THERMAL CYCLING, AND PLASTIC STRAIN ON THE DIMENSIONAL STABILITY OF 440 C STAINLESS STEEL (1/2 HR AT 1900 F, OQ; 1 HR AT 500 F, AC)
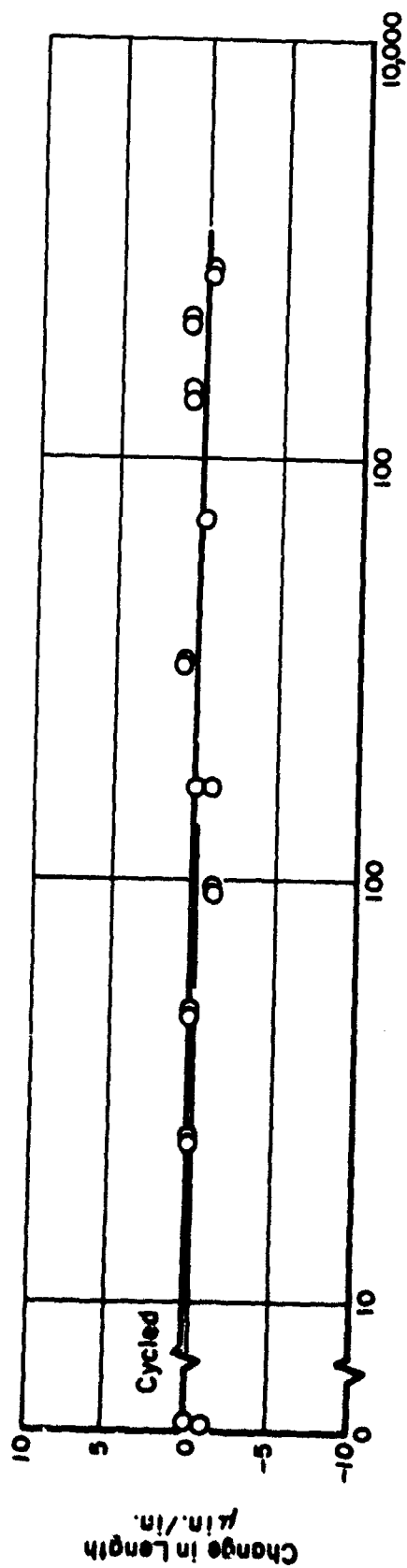
c. Thermal Cycled

10 min at 212 F
10 min at RT
10 min at -100 F
10 min at RT
Repeat 5 times

d. 15 μ in./in. Plastic Strain

FIGURE 49. (CONTINUED)

A–57638

76

Time, hours

a. Control Specimen

Time, hours

b. Stress Cycled, Loaded to 75 % MYS (6,000 psi) 10 times

FIGURE 50. EFFECT OF STRESS CYCLING, THERMAL CYCLING, AND PLASTIC STRAIN ON THE DIMENSIONAL STABILITY OF A356 CAST ALUMINUM (16 HR AT 1000 F, WQ; 4 HR AT 310 F, AC)

c. Thermal Cycled 10 min at 212 F
                   10 min at RT
                   10 min at -100 F
                   10 min at RT
                   Repeat 5 times

d. 50 μ in./in. Plastic Strain

FIGURE 50. (CONTINUED)

78

Time, hours
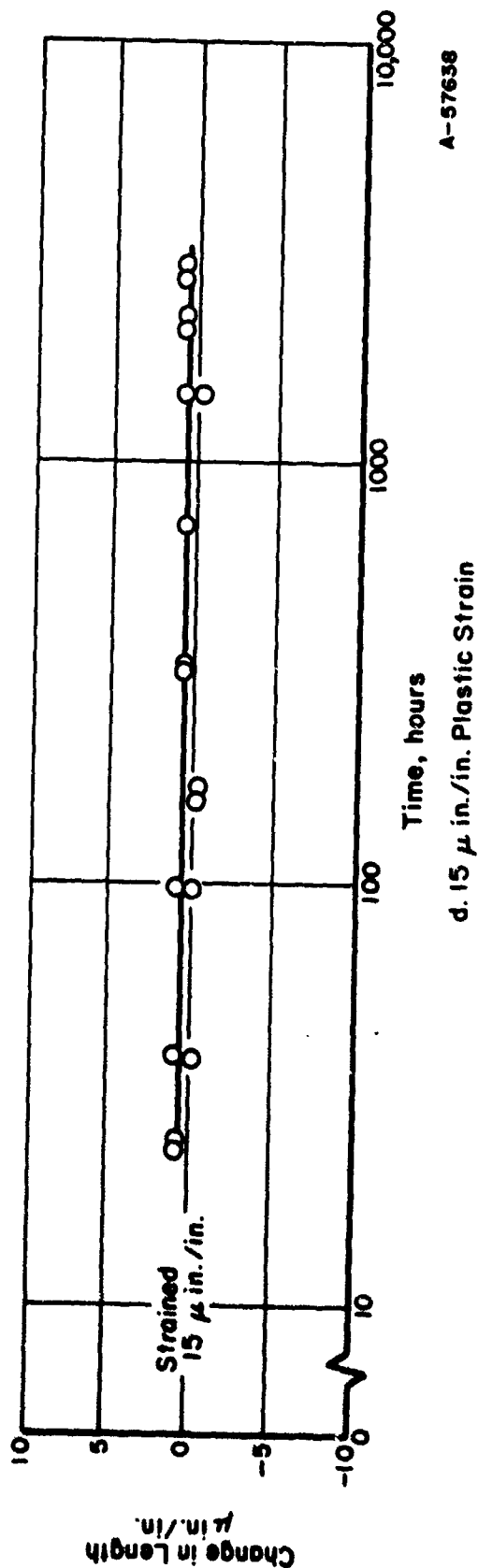
e. 1% Plastic Strain

FIGURE 50. (CONTINUED)

79
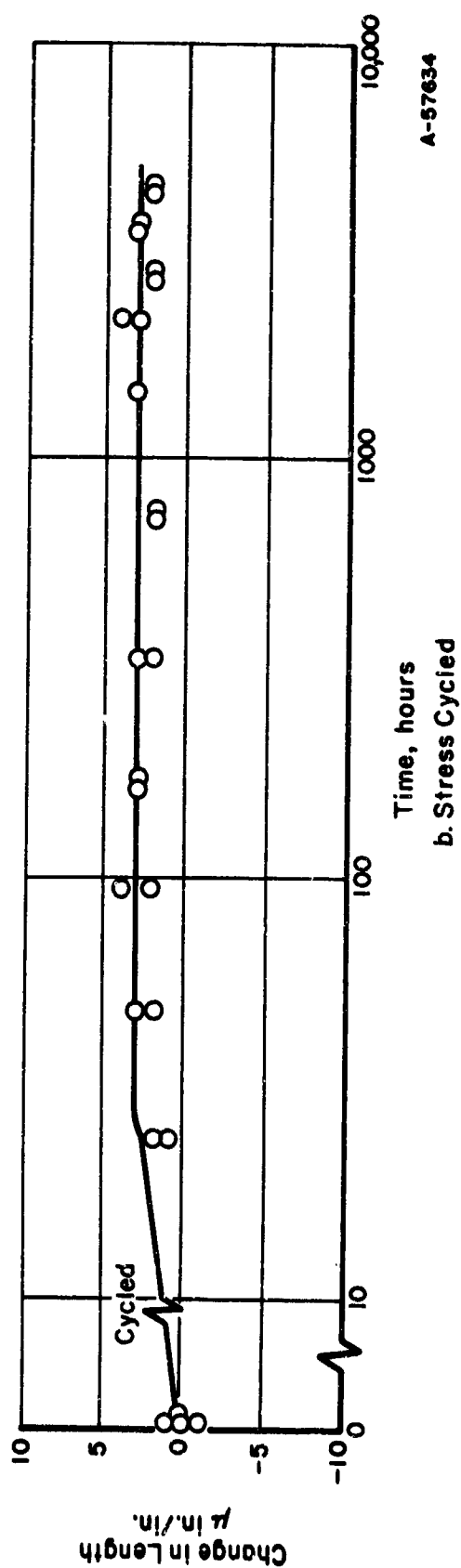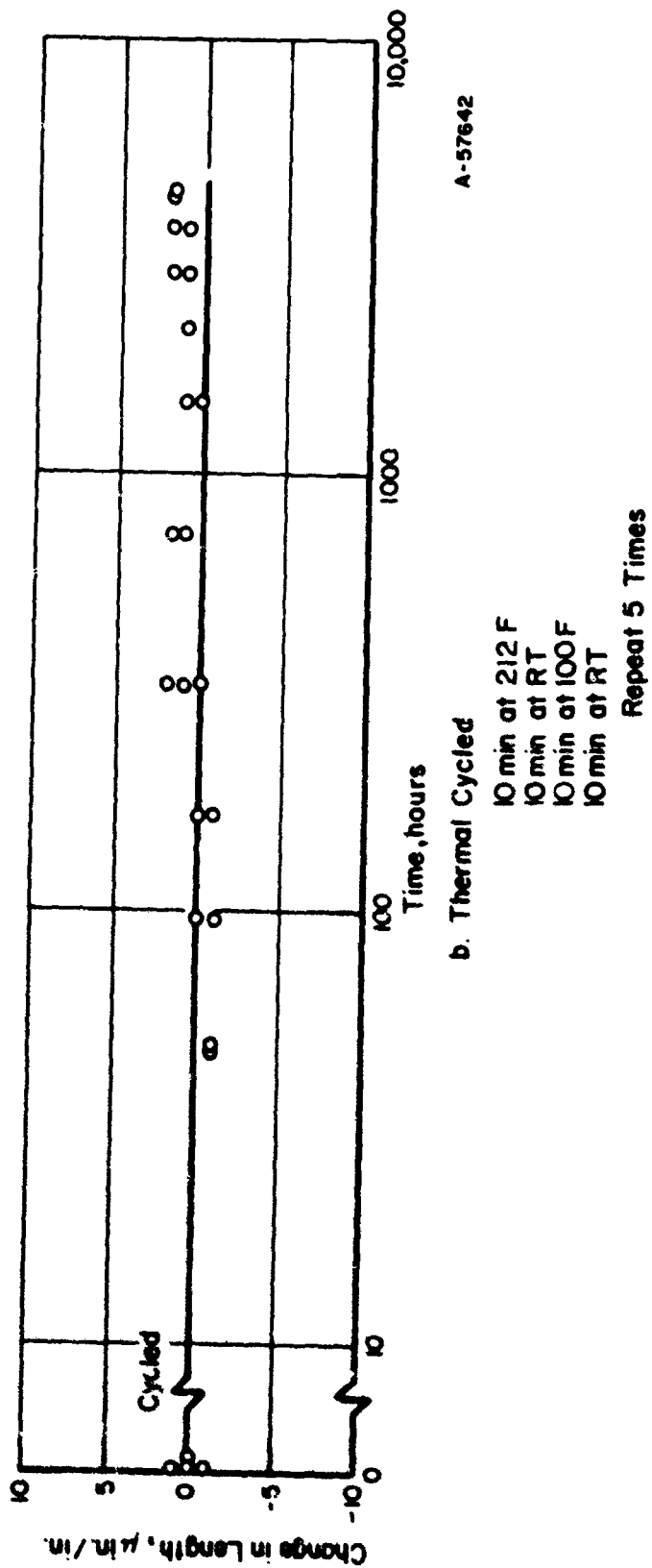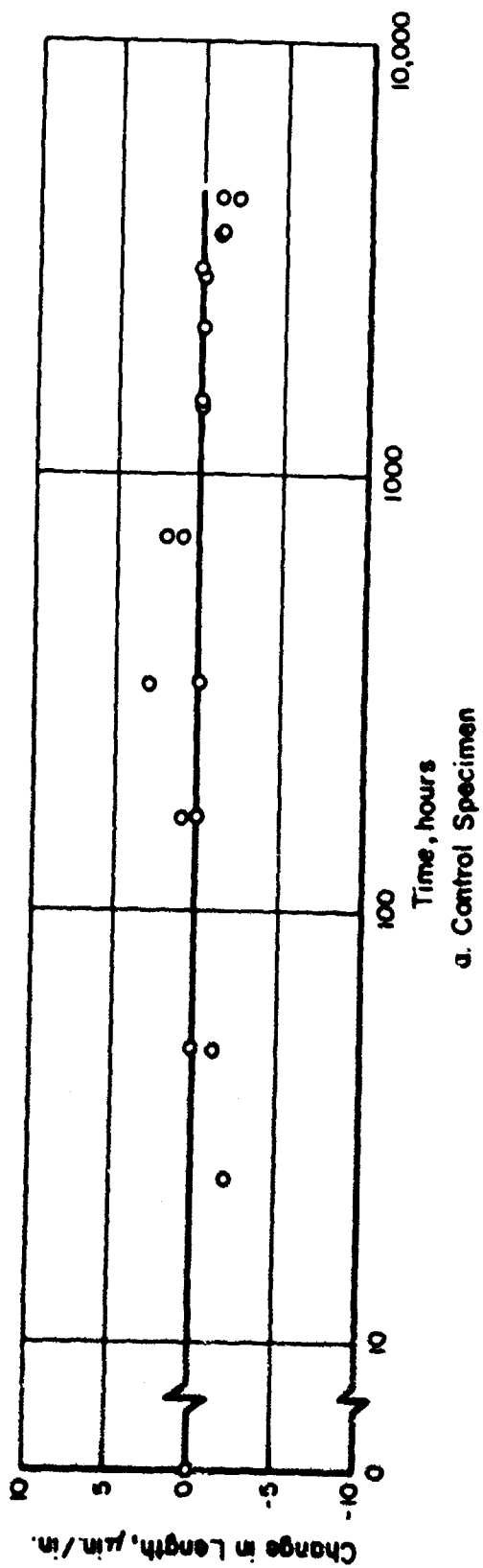
FIGURE 51. EFFECT OF THERMAL CYCLING AND PLASTIC STRAIN ON THE DIMENSIONAL STABILITY OF Ti-5Al-2.5 Sn (1 HR AT 1500 F, FC)

80
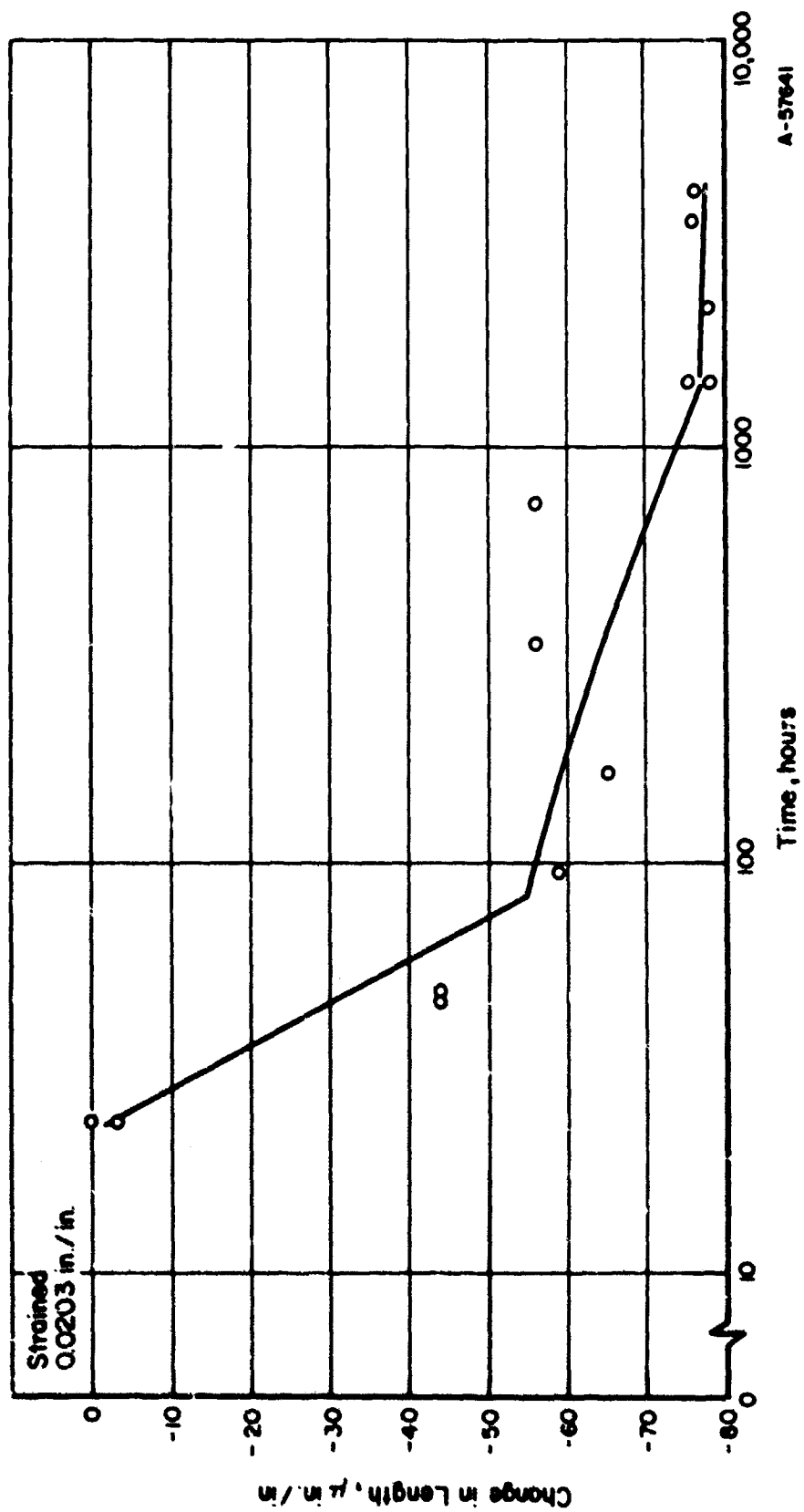
C. 2% Plastic Strain

FIGURE 51. (CONTINUED)

A-57641

81

FIGURE 52. EFFECT OF STRESS CYCLING AND THERMAL CYCLING ON THE DIMENSIONAL STABILITY OF "SUPER PEL" BERYLLIUM (1 HR AT 1450 F, FC)

82

c. Thermal Cycled   10 min at 212 F
                    10 min at RT
                    10 min at -100 F
                    10 min at RT
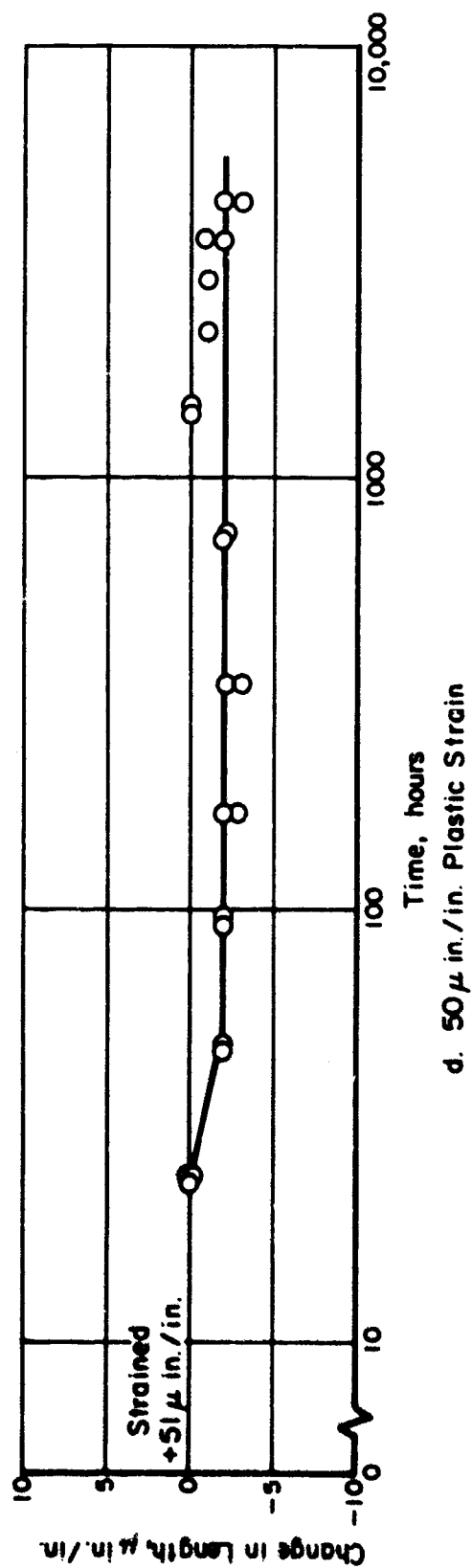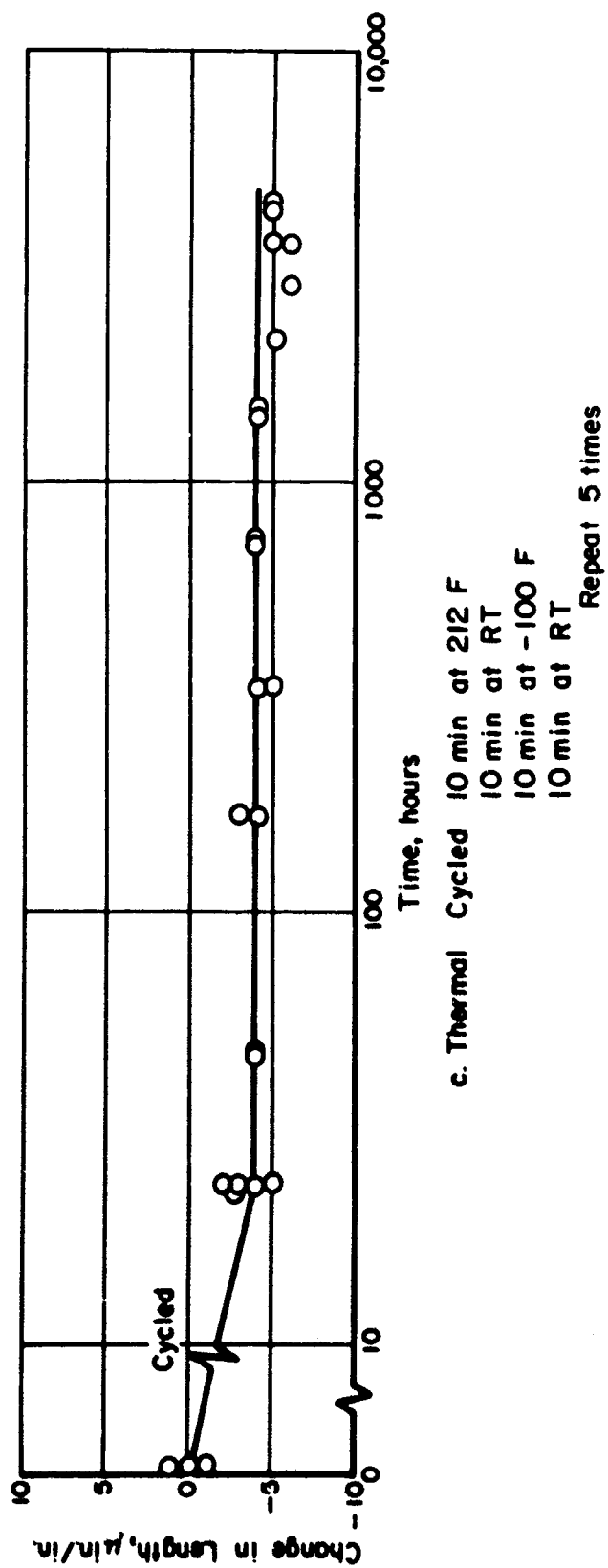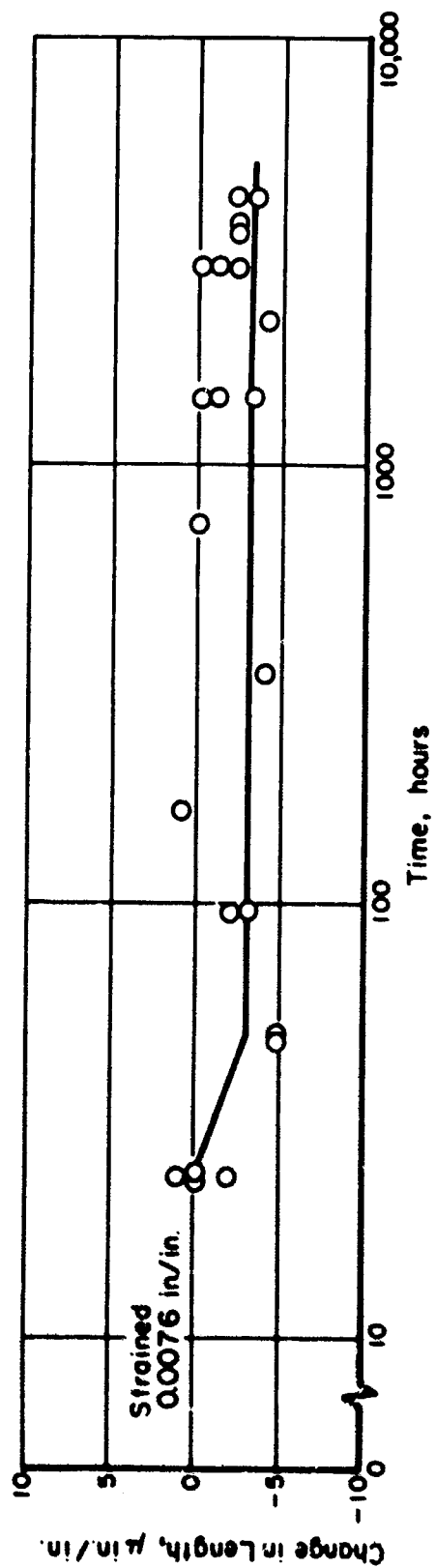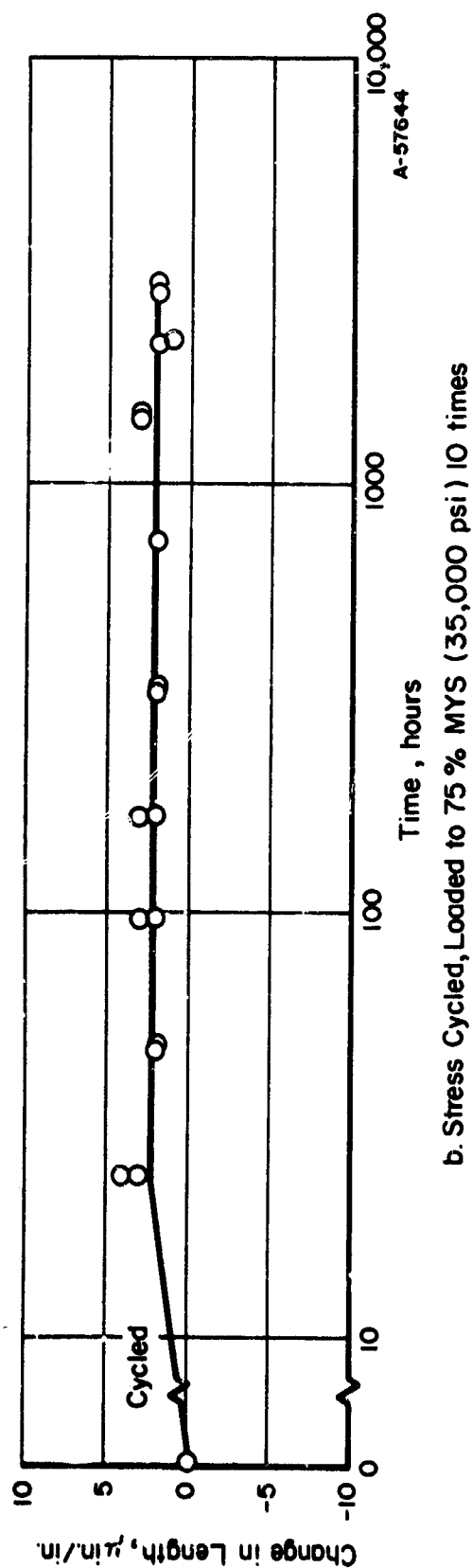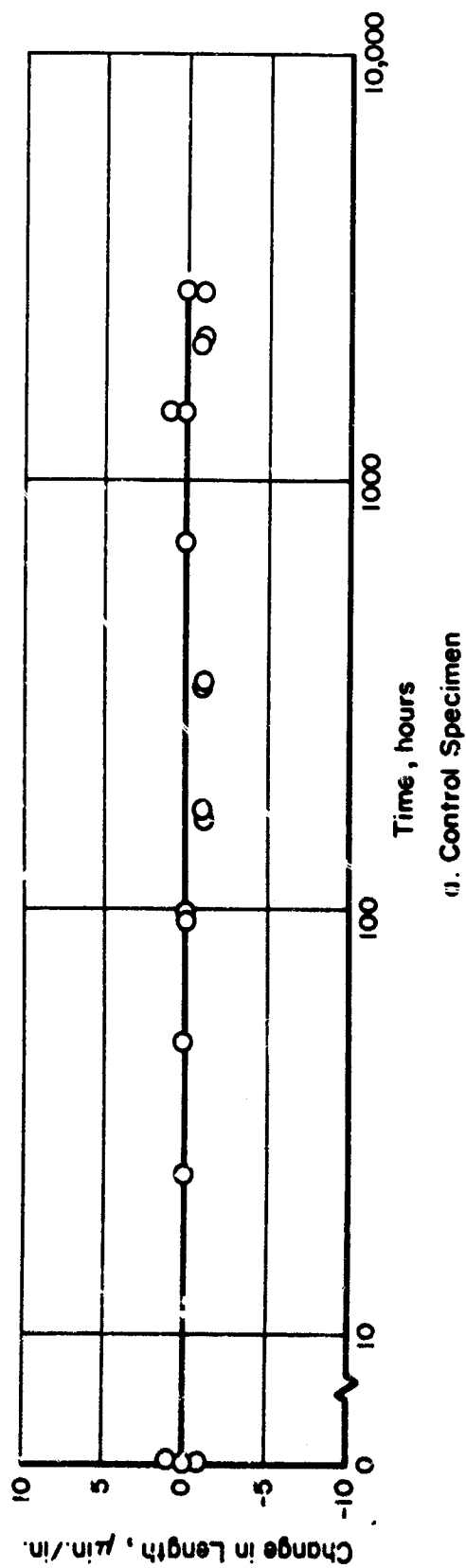   Repeat 5 times
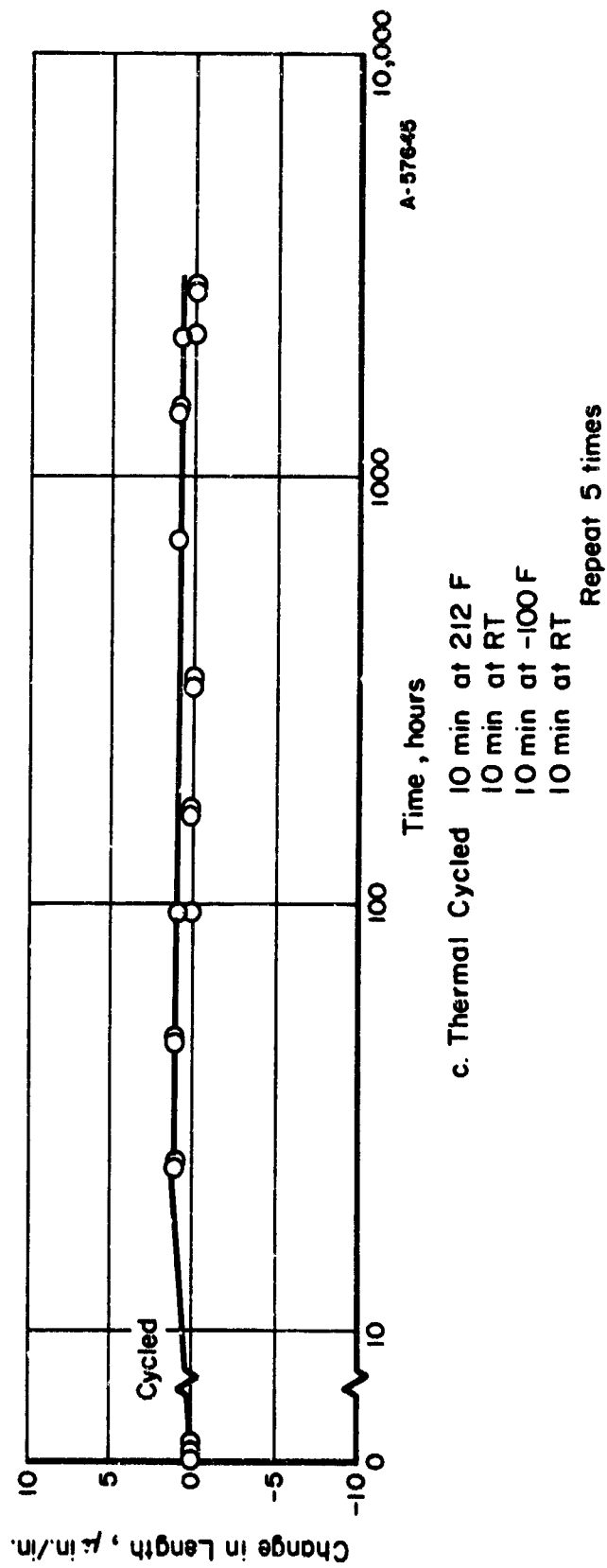
FIGURE 52. (CONTINUED)

83

10 min at 212 F (immersion in boiling water)
10 min at RT
10 min at -100 F (immersion in dry ice and acetone)
10 min at RT
          repeated 5 times.

Figure 50c reveals that A356 cast aluminum contracted approximately 4 μin./in. upon cycling, but no significant change in length was noted thereafter for a period of 4,300 hours (6 months). Figures 48c, 49c, 51b, and 52c show little or no change in length or deterioration in dimensional stability resulted from thermal cycling Ni-Span-C, 440 C stainless steel, Ti-5Al-2.5Sn, and Super PEL beryllium. Therefore, with the possible exception of A356 cast aluminum, severe distortions would not be expected to result in these materials from a relatively mild thermal cycle such as that employed in this study. Any beneficial effects of thermal cycling cannot be assessed due to the good inherent stability displayed by the control specimens of the materials.

Plastic Strain

Plastic strains were applied to specimens of each material by loading them in an Instron Testing Machine to sufficiently high stresses to produce the desired plastic strains.

Figures 48d, 49d, and 50d show that there was no significant change in length of Ni-Span-C, 440 C stainless steel, and A356 cast aluminum specimens for a period of up to 4,300 hours (6 months) after plastic strains of approximately 20 to 40 μin./in. were applied. Therefore, it appears that the increase in microyield strength obtained with Ni-Span-C and 440 C stainless steel by straining 20 to 40 μin./in. described earlier, can be achieved without any appreciable sacrifice in dimensional stability.

Data for Ni-Span-C and Ti-5Al-2.5Sn illustrated in Figures 48d and 51e reveal that quite large length changes occur after specimens are strained approximately 2 percent (20,000 μin./in.). Contractions of from approximately 35 to 80 μin./in. occurred within 1000 hours (6 weeks) after straining. The most rapid period of contraction was within 50 to 100 hours after straining. This contraction is probably in response to residual compressive stresses left in the specimens when they are unloaded after straining. Therefore, large plastic strains can be doubly damaging. Not only do they promote a deterioration in dimensional stability, but they can reduce the microyield strength as was previously discussed for Ni-Span-C.

Residual Stresses Introduced by Machining

Residual stresses introduced by machining in Ni-Span-C, 440 C stainless steel, A356 cast aluminum, and Super PEL beryllium were computed from length-change data as described earlier.

One specimen of each alloy was used to establish base-line data for the evaluation of the residual stresses introduced by controlled machining operations. The surfaces of these specimens were chemically removed in 0.002 to 0.005-inch increments with no intermediate machining. The change in length of these specimens was attributed (1) to

84

residual stresses introduced by the initial machining required to prepare the specimens, and (2) to residual stresses developed by heat treatment.

Additional specimens of each alloy were conditioned for the controlled machining experiments by chemically removing 0.005 inch from their surfaces to remove the damage introduced by the initial machining. The length changes of these specimens were within ±10 μin. of that recorded for the base-line-data specimens. This is considered to be excellent agreement. The residual stresses computed from the base-line data were subtracted from those computed for the machined specimens to assess the magnitude of the stresses introduced by machining.

Figure 53 pictures the setup used for the controlled machining operations. The specimens were held between centers and dogged to the face plate of a high-quality lathe that afforded precise control of machining speeds and cut depths. The specific machining parameters employed for each material are included in the following figures illustrating the length-change data. Care was taken throughout the machining operation not to burr or otherwise marr the lapped measuring surfaces of the specimens.

Ni-Span-C

Figure 54 illustrates length change data for Ni-Span-C specimens with single pass 0.001 and 0.003-inch lathe cuts. The length of the specimens increased upon machining, and then decreased when the machined surface was etched away. A greater length change upon machining was noted for the 0.003-inch cut, but the length decreased more rapidly upon subsequent etching for the 0.001-inch cut. It should be noted that the length change returned very closely to that established by the base-line specimen.

Residual stresses computed from the length-change data are illustrated in Figure 55. The maximum residual stress computed for the 0.001-inch cut (-100,000 psi) was approximately twice as high as that for the 0.003-inch cut (-50,000 psi). However, the stress decreased at a more rapid rate with increasing distance below the machined surface for the 0.001-inch cut. Furthermore, the residual stresses introduced by mcahining penetrated to a deeper depth with the 0.003-inch cut (0.0065 inch) than with the 0.001-inch cut (0.0055 inch). The more rapid decrease in residual stress with the 0.001-inch cut, combined with the deeper penetration of residual stress in the 0.003-inch cut, accounts for the greater length change upon machining observed for the 0.003-inch cut despite the higher maximum residual stress introduced by the 0.001-inch cut.

The residual stresses introduced by both the 0.001 and 0.003-inch cuts exceeded the microyield strength of Ni-Span-C (39,000 psi). The good dimensional stability exhibited by the Ni-Span-C control specimen in the previous series of experiments can probably be related to the resistance to deformation offered by the bulk of the specimen to the highly stressed, but thin, machined surface layer. Severe dimensional instability would be expected in components that have a large machined-surface area to volume ratio.

440 C Stainless Steel

Length change data for 440 C stainless steel with single pass 0.001, 0.002, and 0.003-inch grind cuts are illustrated in Figure 56. The specimen with the 0.001-inch
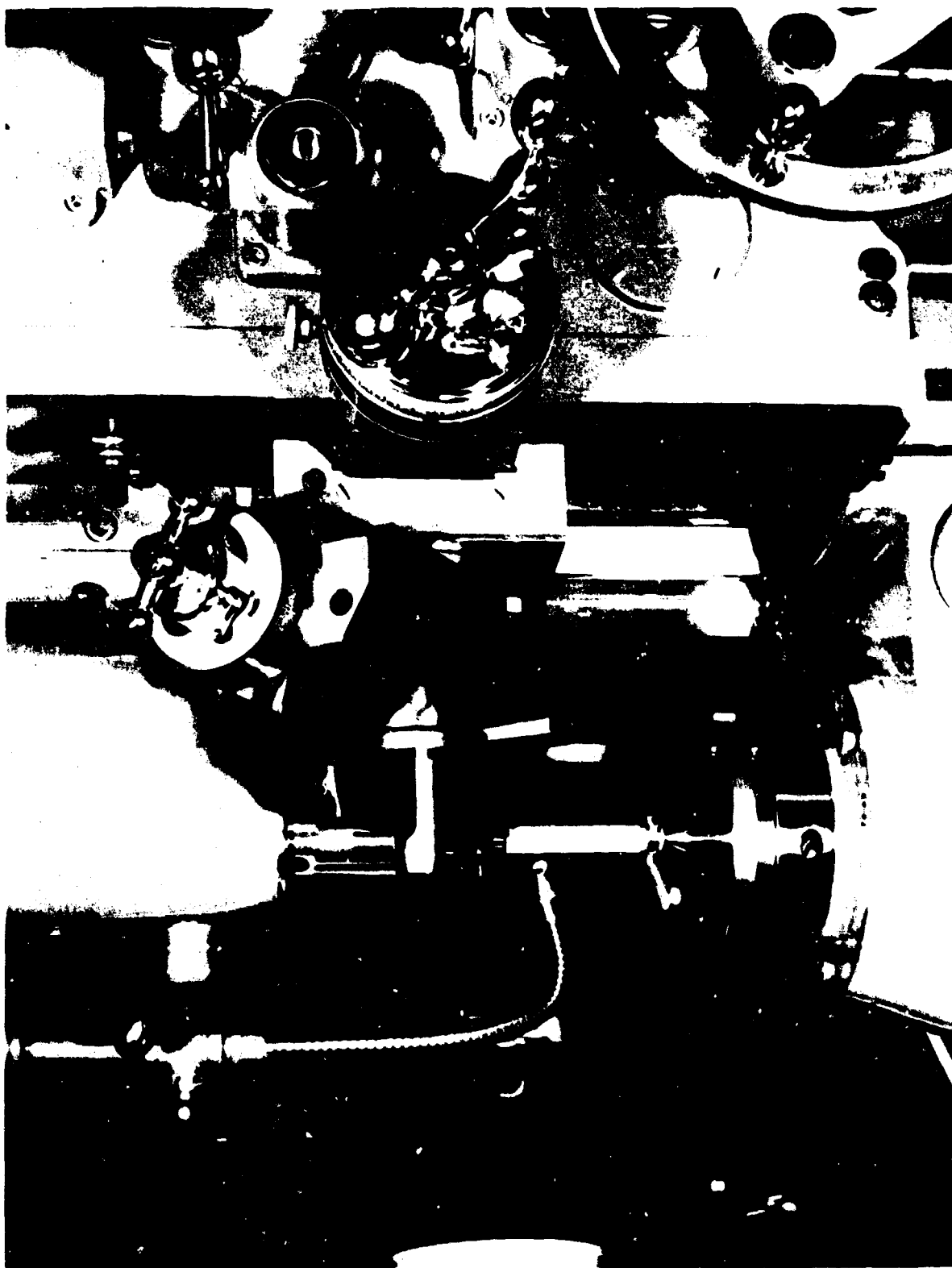
41651

FIGURE 53. MACHINERY SET-UP

86

FIGURE 54. LENGTH CHANGE ASSOCIATED WITH SINGLE PASS LATHE TURNING OF Ni-SPAN-C

1-1/4 hr at 1800 F, WQ; 21 hr at 1250 F, AC.

FIGURE 55. RESIDUAL STRESSES INTRODUCED BY SINGLE PASS
LATHE TURNING OF Ni-SPAN-C

1-1/4 hr at 1800 F, WQ; 21 hr at 1200 F, AC.

88

FIGURE 56. LENGTH CHANGE ASSOCIATED WITH GRINDING OF 440 C STAINLESS STEEL

1/2 hr at 1900 F, OQ; 1 hr at 500 F, AC.
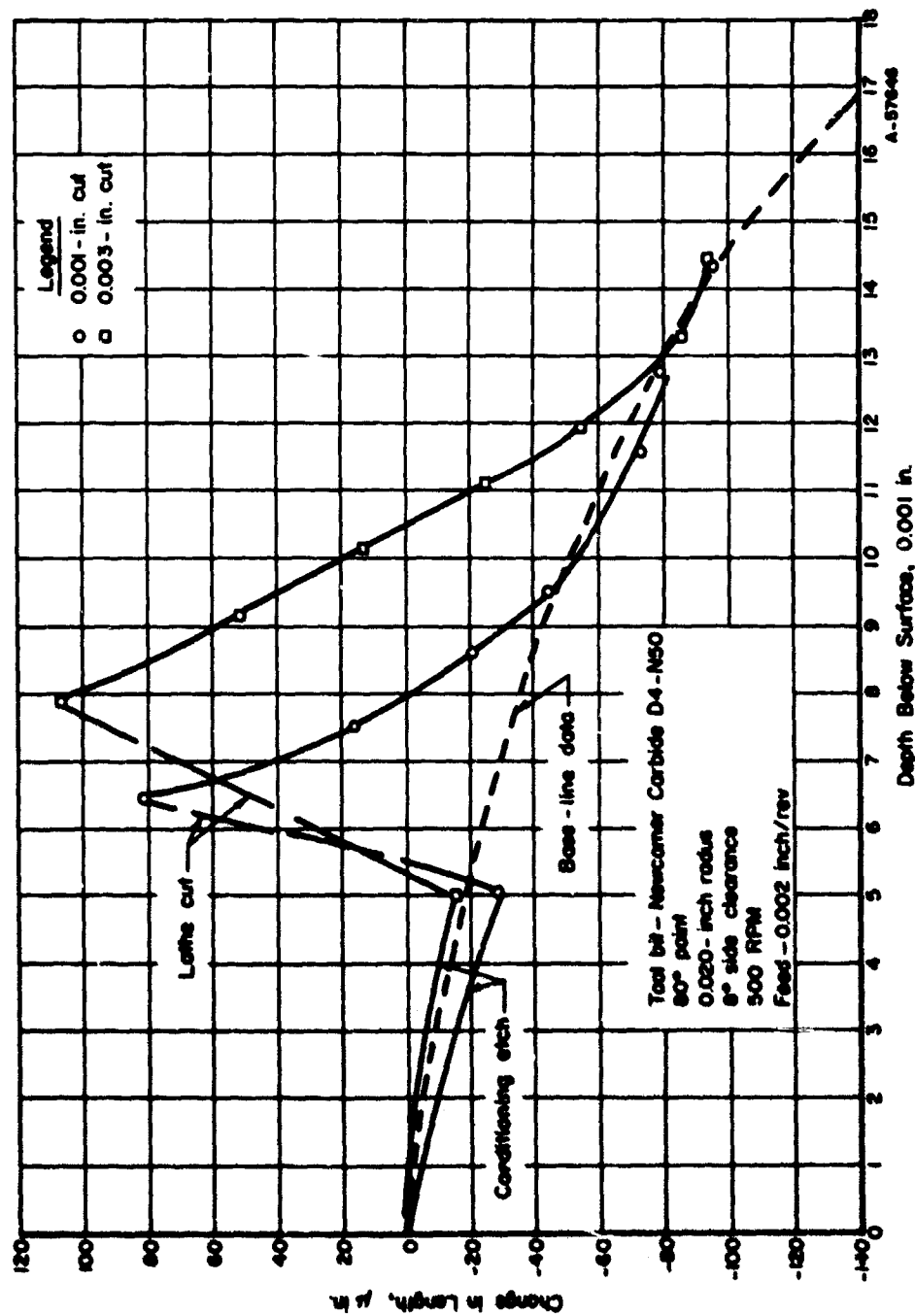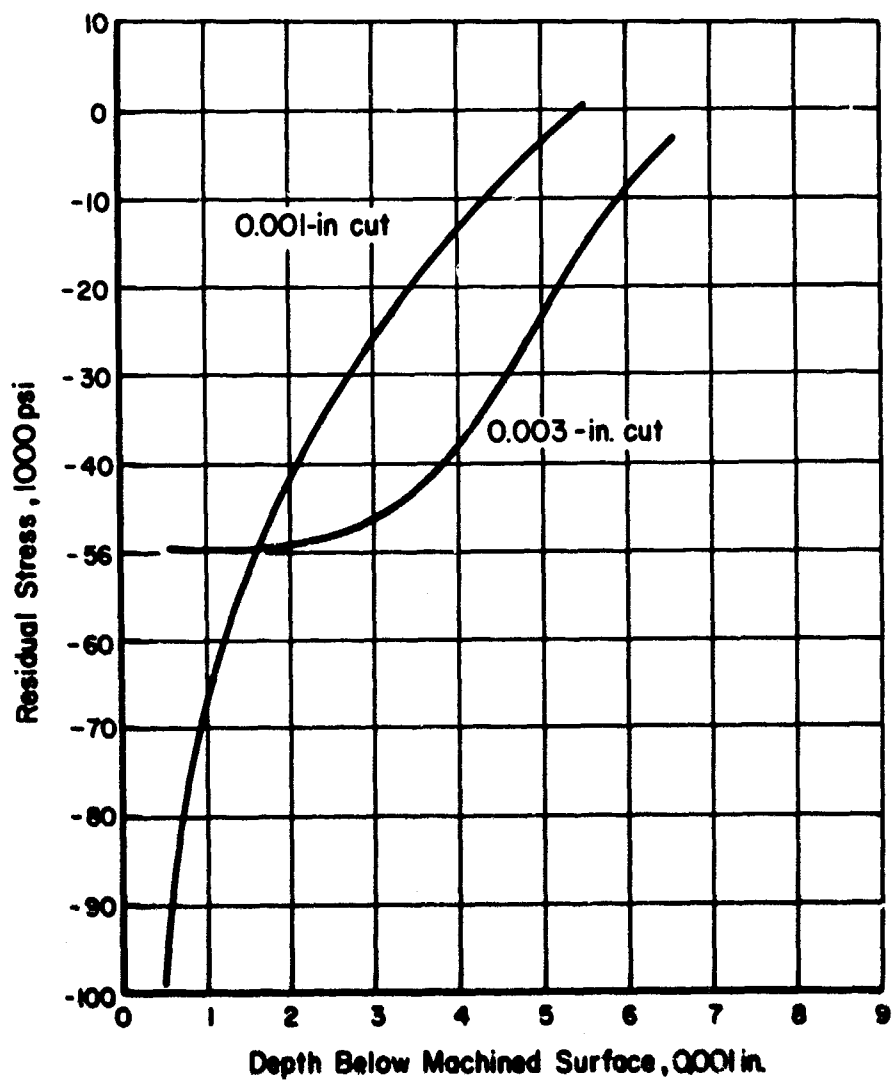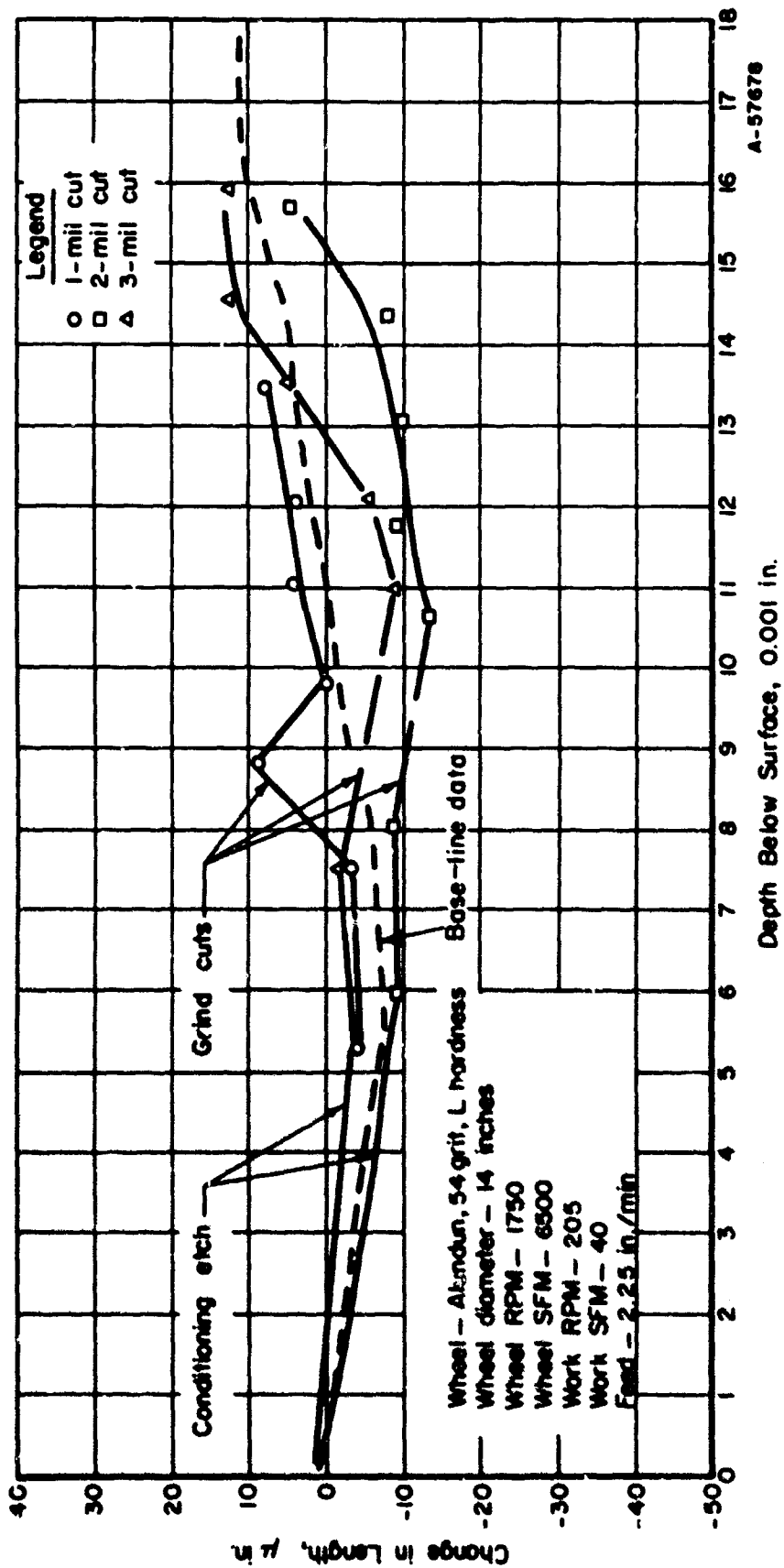
89

grind cut exhibited a positive change in length upon machining, indicating the introduction of a compressive residual stress, whereas the specimens with 0.002 and 0.003-inch grind cuts displayed a negative change in length upon machining, indicating the introduction of tensile residual stresses.

The relatively wide degree of scatter evident in the length-change data makes it very difficult to compute meaningful residual-stress values. However, the maximum residual stress computed was approximately 10-15,000 psi. Since this is considerably less than the microyield strength of 440 C stainless steel (70,000 psi), severe dimensional-instability problems attributable to grinding should not be encountered.

A356 Cast Aluminum

Length-change data for A356 cast aluminum with single-pass, 0.001, 0.003, and 0.005-inch lathe cuts are illustrated in Figure 57. The length change upon machining was observed to increase as the depth of cut decreased. Figure 58 reveals that the maximum residual stresses developed by the three different depth cuts were approximately the same (-10,000 psi). However, the residual stress decreased less rapidly with increasing depth below the machined surface for the shallower cuts. This accounts for the greater length change upon machining as cut depth decreased. Similar to Ni-Span-C, the maximum residual stresses developed by machining were in excess of the microyield strength (7,500 psi), and dimensional-instability problems would be expected in A356 cast aluminum components with a relatively high ratio of surface area to volume.

Length-change data for multiple-pass, sequence lathe cuts are illustrated in Figure 59. A somewhat greater change in length upon machining was noted with the sequence ending with the 0.001-inch finishing cut as compared with the 0.003-inch finishing cut. This is in good agreement with what was described above for the single-pass lathe cuts. Figure 60 shows that somewhat greater residual stresses were introduced by the sequence ending with the 0.001-inch finishing cut.

Super PEL Beryllium

Figure 61 illustrates length-change data for Super PEL beryllium with single-pass, 0.001 and 0.003-inch lathe cuts. The length change upon machining was approximately the same for both cut depths. Furthermore, it can be seen in Figure 62 that the residual stresses introduced by machining are the same for both cut depths. The maximum residual stress was approximately -20,000 psi, which is less than 1/2 the microyield strength (47,000 psi). In addition, the depth of penetration of the residual stresses (0.0015 to 0.0025 inch) was less than that observed for Ni-Span-C and A356 cast aluminum. Therefore, a serious problem of dimensional instability due to residual stresses introduced by lathe turning Super PEL beryllium would not be anticipated.

The same general trends were observed for multiple-pass, sequence cuts of 0.005, 0.003, and 0.001 inch; and 0.005 and 0.003 inch as can be seen in Figures 63 and 64.

90
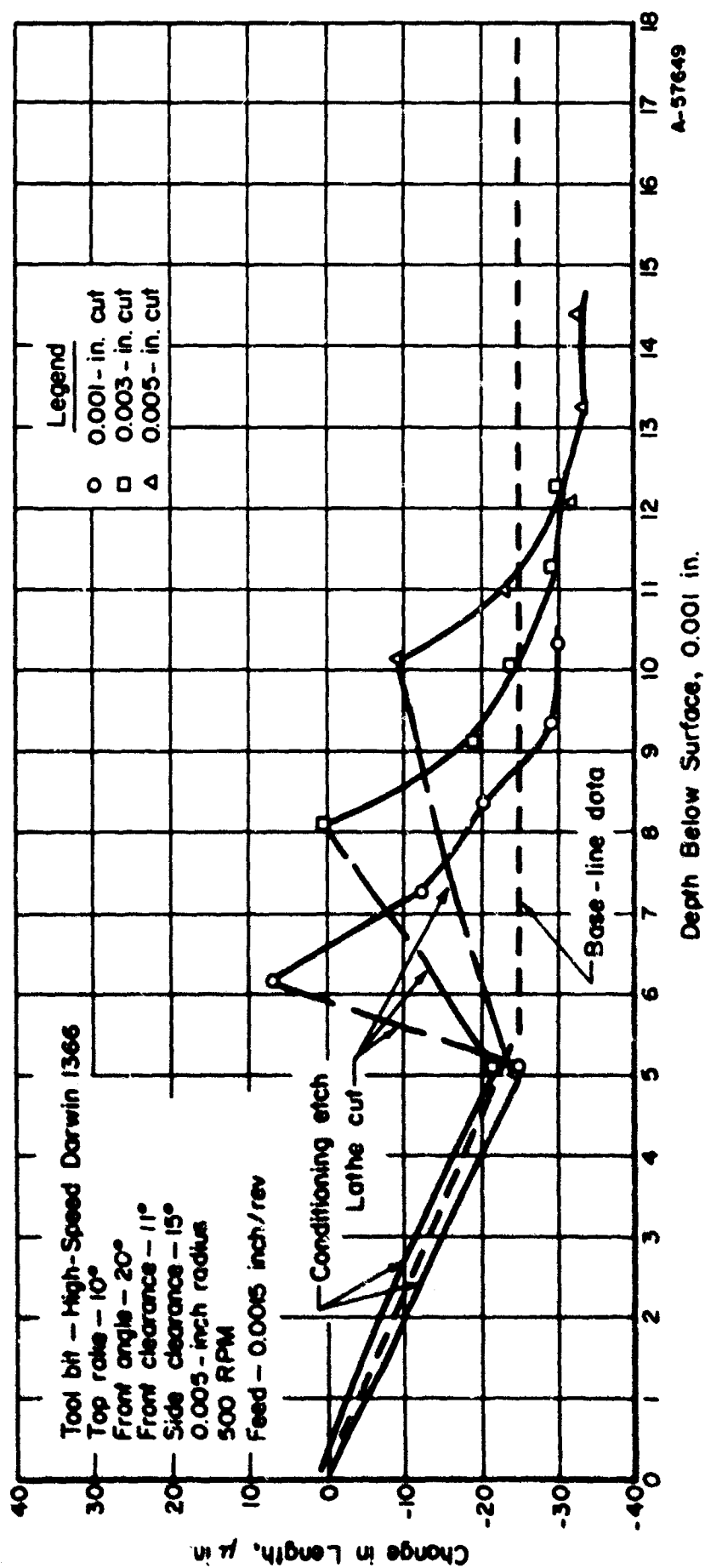
FIGURE 57. LENGTH CHANGE ASSOCIATED WITH SINGLE PASS LATHE TURNING OF A356 CAST ALUMINUM

16 hr at 1000 F, WQ; 4 hr at 310 F, AC.

91
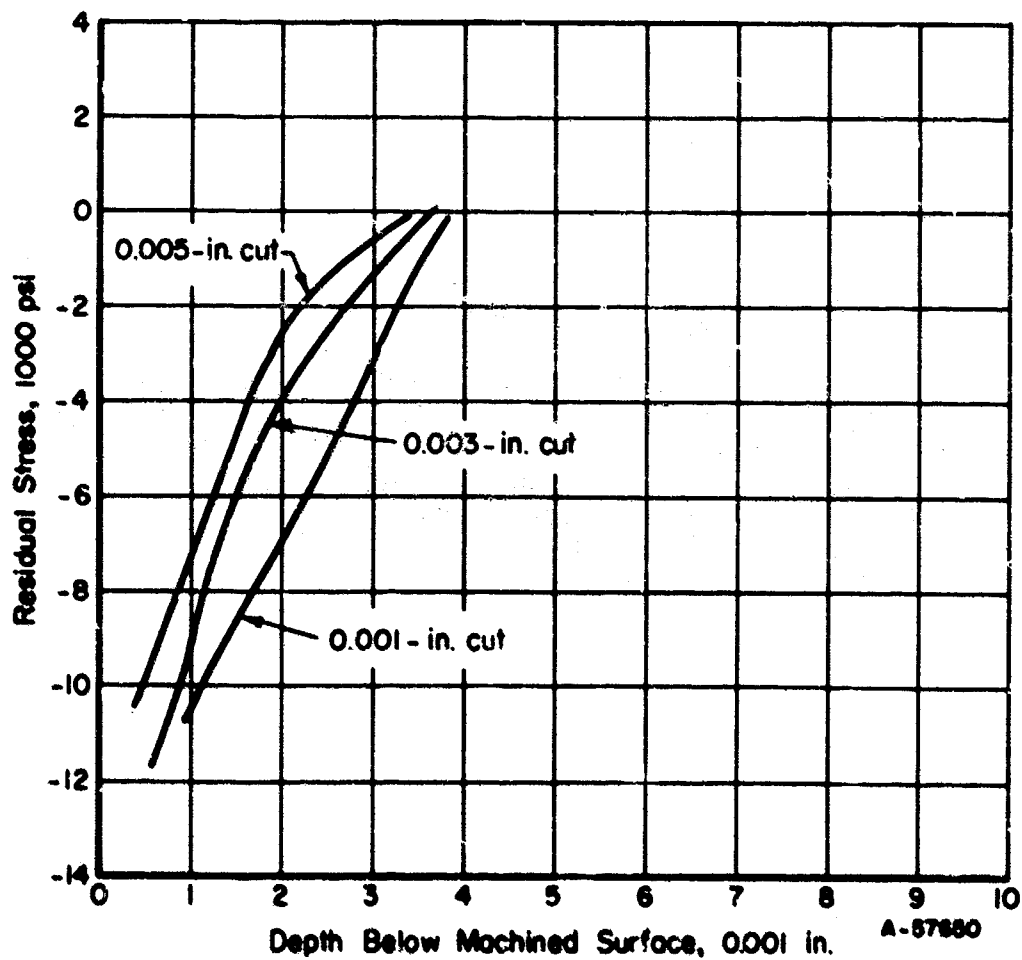
FIGURE 58.   RESIDUAL STRESSES INTRODUCED BY SINGLE PASS
LATHE TURNING OF A356 CAST ALUMINUM

16 hr at 1000 F, WQ; 4 hr at 310 F, AC.
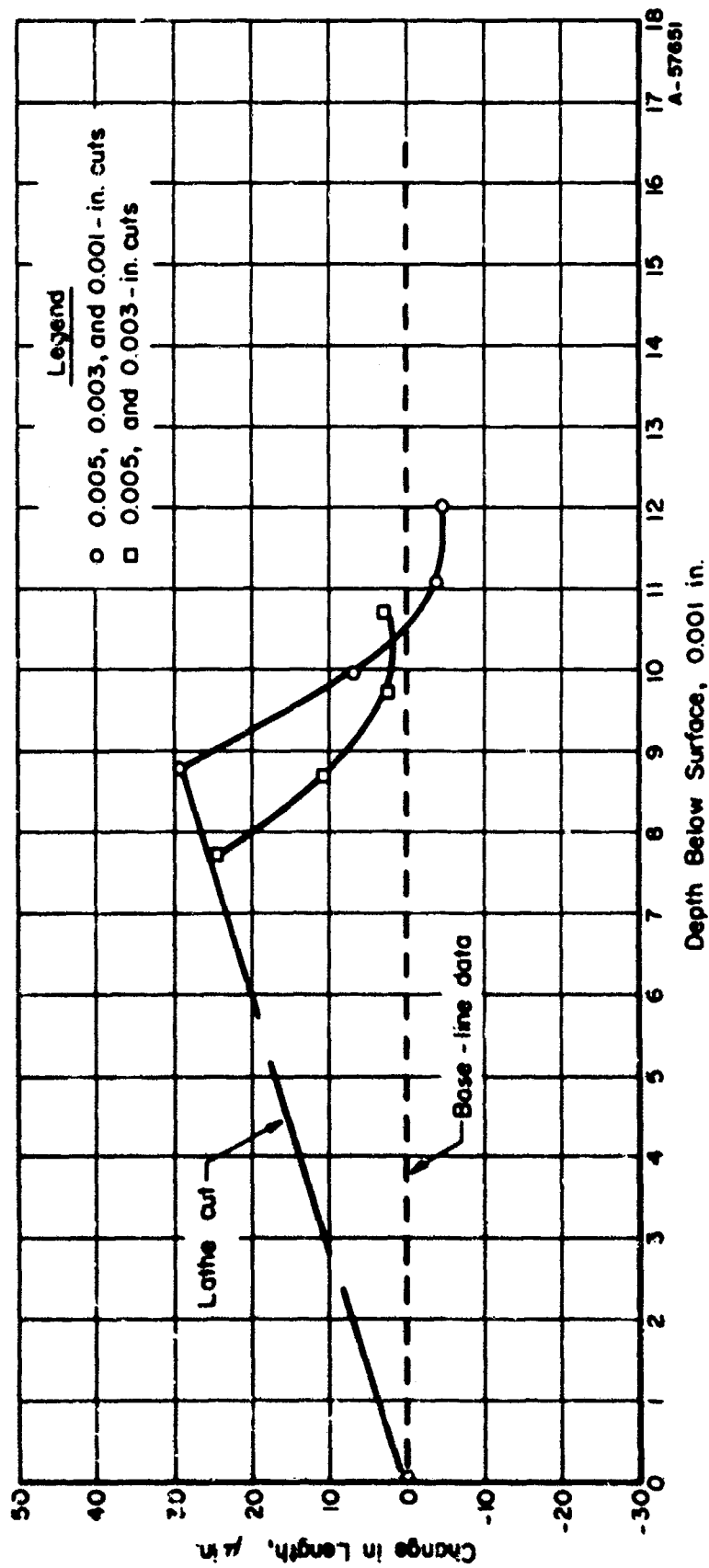
FIGURE 59. LENGTH CHANGE ASSOCIATED WITH MULTIPLE PASS LATHE TURNING OF A356 CAST ALUMINUM

16 hr at 1000 F, WQ; 4 hr at 310 F, AC.
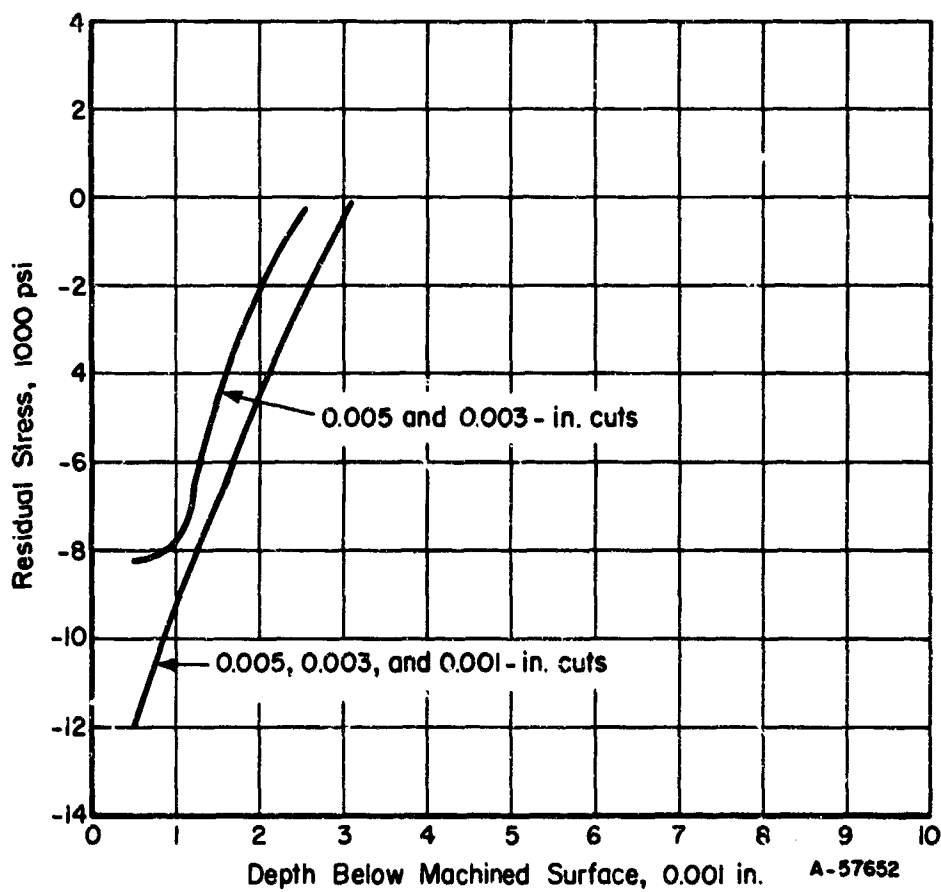
FIGURE 60. RESIDUAL STRESSES INTRODUCED BY MULTIPLE PASS
LATHE TURNING OF A356 CAST ALUMINUM

16 hr at 1000 F, WQ; 4 hr at 310 F, AC.

94
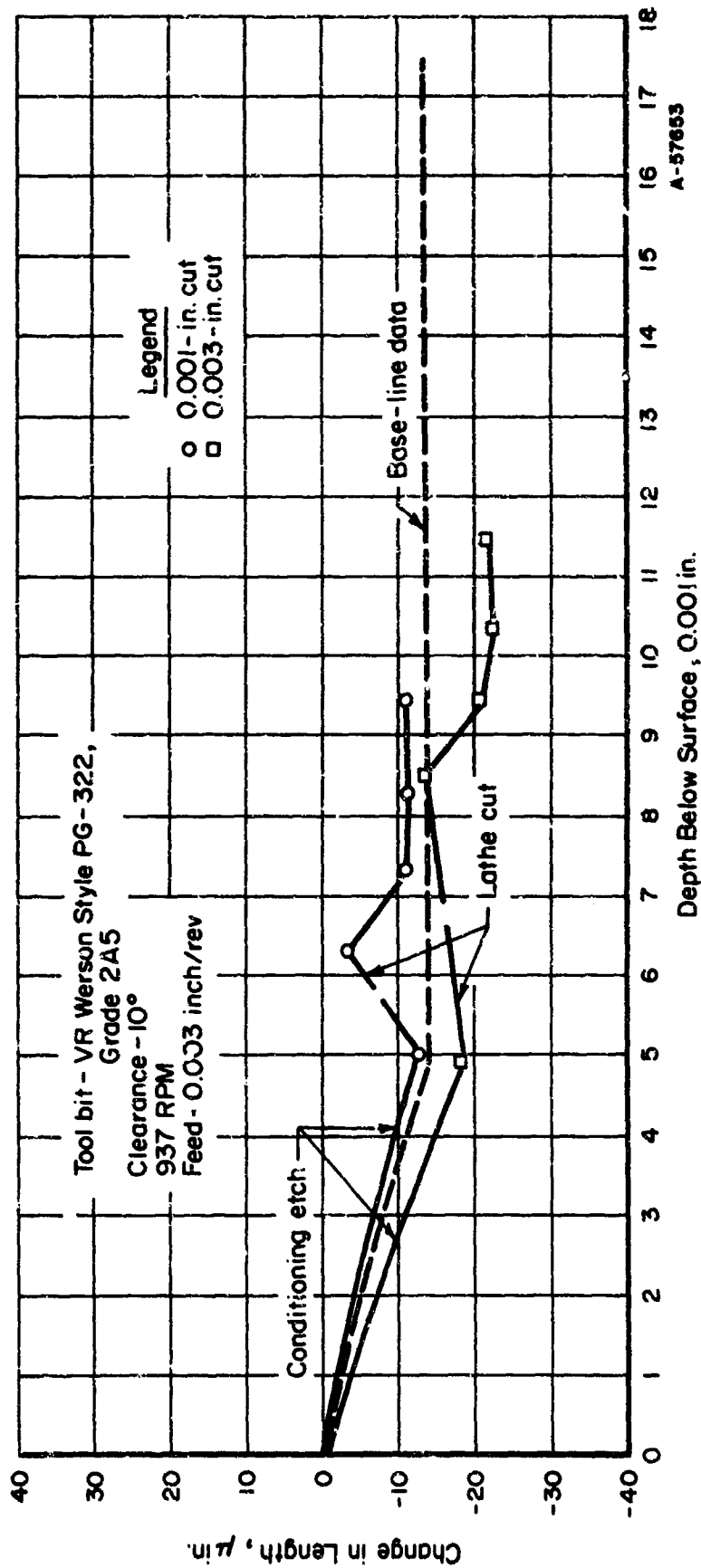
FIGURE 61. LENGTH CHANGE ASSOCIATED WITH SINGLE PASS LATHE TURNING OF SUPER PEL BERYLLIUM

1 hr at 1450 F, FC.

95

Residual Stress, 1000 psi

0.001 and 0.003-in. cuts

Depth Below Machined Surface. 0.001 in.

A-57654
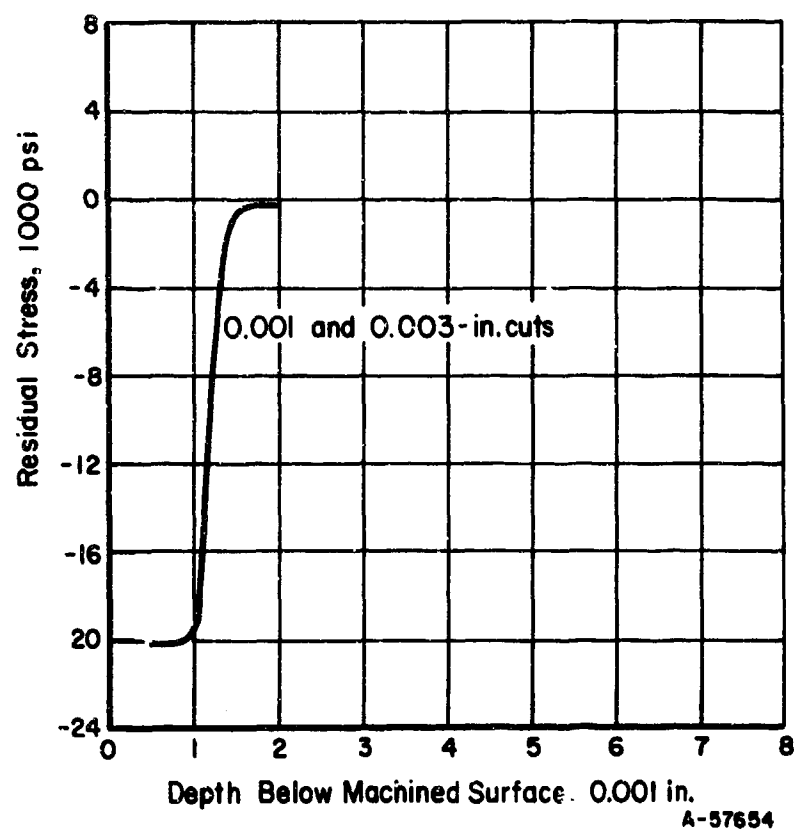
FIGURE 62. RESIDUAL STRESSES INTRODUCED BY SINGLE PASS LATHE TURNING OF SUPER PEL BERYLLIUM

1 hr at 1450 F, FC.

96
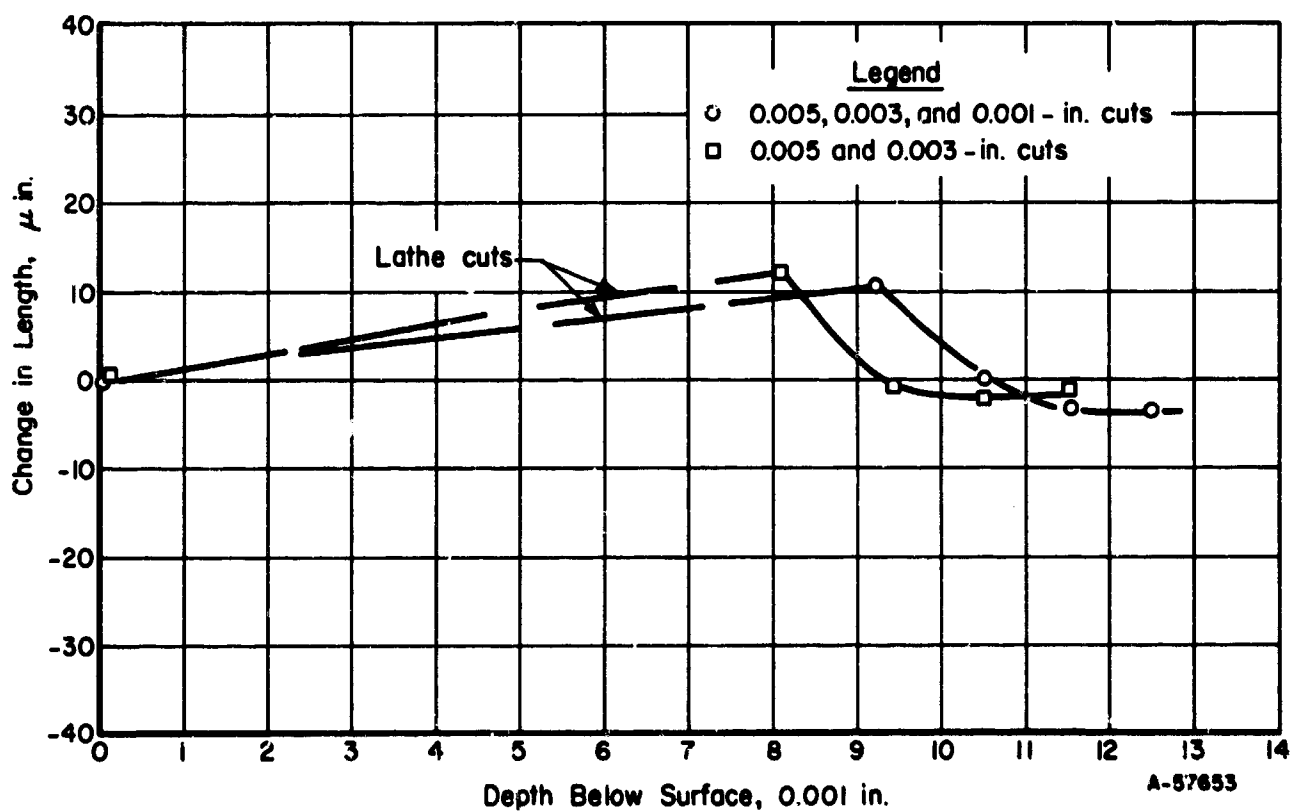
FIGURE 63. LENGTH CHANGE ASSOCIATED WITH MULTIPLE PASS
LATHE TURNING OF SUPER PEL BERYLLIUM

1 hr at 1450 F, FC.

97
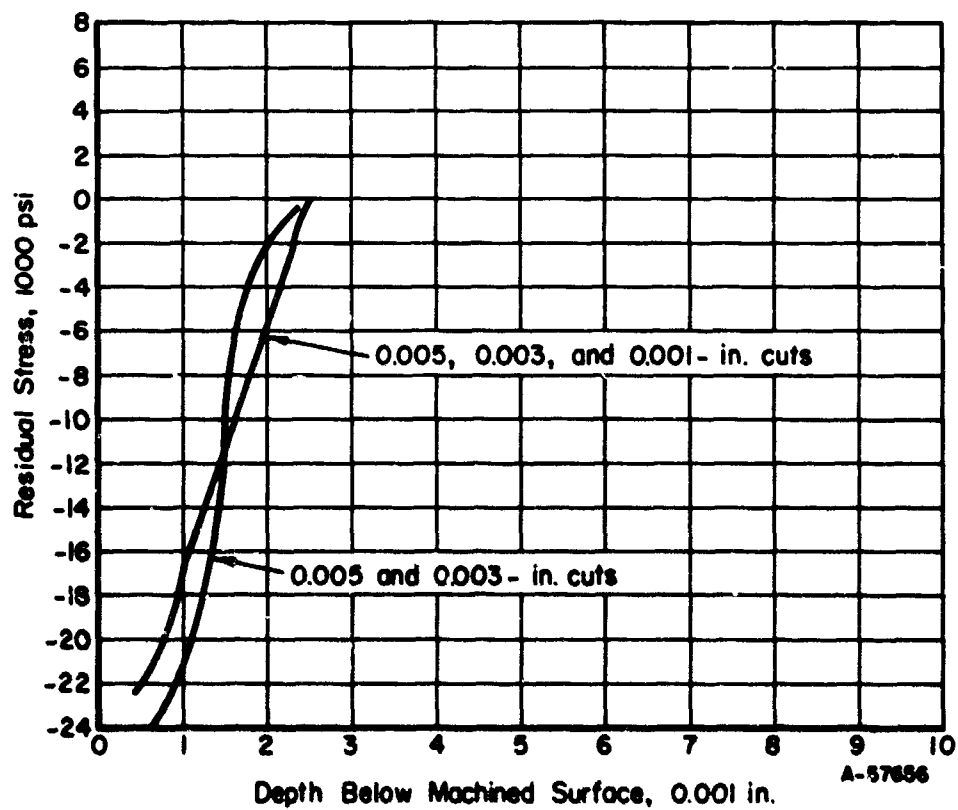
FIGURE 64. RESIDUAL STRESSES INTRODUCED BY MULTIPLE PASS LATHE TURNING OF SUPER PEL BERYLLIUM

1 hr at 1450 F, FC.

98

General Comments

Ni-Span-C and A356 cast aluminum exhibited a trend for higher residual stresses and/or a shallower decrease in residual stress below the machined surface to be associated with relatively light lathe cuts (i.e., approximately 0.001 inch) than for heavier cuts (i.e., 0.003 to 0.005 inch). This same trend has been observed for S200 and I400 beryllium in some related studies at Battelle.[12] This is contrary to the normally accepted concepts of precision machining, and may eventually be of considerable value to the construction of precision instruments. A possible explanation for this behavior is that metal is "rubbed" off the surface with the shallow cut, but is removed cleanly with the somewhat heavier cuts.

DISCUSSION

This research program has provided a basis for evaluating the comparative behavior of several potential candidate materials suitable for the construction of precision instruments. Also, insight has been gained into the basic mechanisms governing micromechanical properties.

Significance of Micromechanical Properties

It is evident that many of the trade-offs and compromises that have to be made when selecting a material for a conventional application also have to be made when selecting materials for precision instruments. Table VIII gives the microyield-strength behavior and selected physical properties of Ni-Span-C, 440 C stainless steel, A356 cast aluminum, Ti-5Al-2.5Sn, and Super PEL beryllium. Ti-5Al-2.5Sn and 440 C stainless steel have approximately the same microyield strength (70-75,000 psi). However, the rate of "strain hardening" above the microyield strength differs considerably. Thus, greater distortions would be expected in accidentally overloaded Ti-5Al-2.5Sn parts. Furthermore, the modulus of elasticity of Ti-5Al-2.5Sn (14.5×10^6 psi) is only approximately 1/2 that of 440 C stainless steel (30×10^6 psi). Therefore, the elastic strains in a stressed Ti-5Al-2.5Sn component would be twice those in a 440 C component functioning under the same load. Another disadvantage connected with Ti-5Al-2.5Sn is the low thermal conductivity (4.5 Btu/ft^2/hr/F) and moderately high thermal expansion (5.25 μin./in./F) characteristic of titanium-base alloys. This means that localized heating or cooling of Ti-5Al-2.5Sn components could develop high stresses and consequent distortions because the heat input cannot be dissipated rapidly into the surrounding material and the size differential between hot and cold areas would be relatively large. On the other hand, the density of Ti-5Al-2.5Sn (0.161 lb/in.^{3}) is only a little more than 1/2 that of 440 C stainless steel (0.28 lb/in.^{3}). The importance of constructing an instrument of minimum weight might more than outweigh any disadvantages of using Ti-5Al-2.5Sn if a material with a high microyield strength is required.

TABLE VIII. MICROYIELD-STRENGTH BEHAVIOR AND SELECTED PHYSICAL PROPERTIES

Material	Average Microyield Strength, 1000 psi	Modulus of Elasticity, 10^6 psi	Density, lb/in.^{3}	Thermal Conductivity at RT, Btu/ft^2/hr/F	Thermal Expansion at RT, μin./in./F
Ni-Span-C	39-40	26	0.293	≈90	4.7
440 C	69-70	30	0.28	14.0	5.6
A356	7.5	10.5	0.097	≈90	11.5
Ti-5Al-2.5Sn	75	14.5	0.161	4.5	5.25
Super PEL Be	47	45	0.067	≈105	6.5

Ni-Span-C and Super PEL beryllium both have somewhat lower microyield strengths (approximately 40-50,000 psi) than 440 C stainless steel and Ti-5Al-2.5Sn. Although Ni-Span-C and Super PEL beryllium have approximately the same microyield strength,

they differ greatly in most other respects. Super PEL beryllium has the lowest density (0.067 lb/in.^{3}) and highest modulus of elasticity (45 x 10^6 psi) of the materials investigated in this program. This makes beryllium especially attractive for applications where light weight and high rigidity are of critical importance.

A356 cast aluminum provides the lowest microyield strength (7,500 psi) of all of the materials studied, and relatively severe distortions would be expected if a component were accidentally overstressed. The alloy has a low density (0.097 lb/in.^{3}) and is castable. Therefore, it should be useful for making lightweight castings of intricate shapes that would be very costly or impossible to machine. However, caution must be exercised because of the inherent variability in the properties of castings. The thermal expansion of A356 is quite high but its high thermal conductivity (90 Btu/ft^2/hr/F) should alleviate any distortion problems associated with localized heating or cooling.

Hypothesis on Mechanisms of Dimensional Instability

The examination of thin foils of Ni-Span-C and A356 cast aluminum by transmission-electron microscopy indicated that microplastic deformation in these two alloys is related to the generation of dislocations at microstructural stress concentrators such as second-phase particles or grain boundaries. Little evidence of interaction among the moving dislocations that is characteristic of straining beyond the 0.2 percent offset yield strength was detected.

If dislocation interactions are not observed, then what is the significance of the "strain hardening" part of the MYS curve? It is certainly not strain hardening in the conventional sense. We believe it to indicate the rate at which dislocation sources are activated. The strain hardening in the micromechanical sense is in reality a dislocation-source exhaustion. This idea is consistent with the microcreep data as well, if one considers the dislocation sources to be thermally activated at a given stress level. As the sources are exhausted, the creep rate decreases. The great majority of the microcreep data generated at Battelle to date, as well as others of which we are aware, show this continually decreasing rate. The hypothesis predicts a relatively strong temperature dependence of microcreep, and this is apparently borne out by Horden and Weirauch's[8] data for A356 cast aluminum.

Both stress cycling and thermal cycling can cause significant dimensional instability. It is not difficult to see why this should happen. If a residual stress exists in a specimen, then a relaxation of this stress can cause a change in dimensions. The most probable mechanism of stress relaxation is the generation and movement of dislocations. The MYS and the microcreep data suggest that this generation and movement of dislocations is stress induced and thermally activated. A cyclic or vibrational stress superimposed on already existing residual stresses could then serve as an "activating" mechanism, simply supplying the small additional stress necessary to operate a source. If this is the case, then a material not containing residual stresses should be relatively stable with respect to any imposed vibrational stress until those stresses by themselves become high enough to activate dislocation sources.

Thermal cycling is much like stress cycling. If the thermal cycle is rapid enough, then the thermal gradient itself will be enough to generate stress. Even on slow thermal cycling, however, significant stress levels can be generated in the sample if the crystal

structure of the alloy gives rise to anisotropic thermal-expansion characteristics or if the alloy is composed of a mixture of phases, each with a different thermal-expansion coefficient.

Some current stabilization procedures call for quenching into boiling water, air cooling, and then quenching into a dry ice-acetone mixture. These are severe conditions that can cause dimensional changes. This procedure can actually deform the specimen plastically. For some applications, however, this seems to be acceptable, especially if the specimen is expected to see severe and rapid thermal cycling in its intended application. For most precision applications, however, quenching as a means of stabilization probably does more harm than good.

Differences in thermal-expansion coefficients, either with respect to crystal direction or phase relationships, are known to cause severe internal stresses when thermal cycling occurs. The thermal cycling of a uranium specimen can cause the length to double or triple. In most materials, however, the mismatch in expansion coefficients is not so severe as to build up stresses that will exceed the MYS. However, in the presence of other residual stresses, the superimposed, thermally generated stresses can be expected to activate dislocation sources that are already close to operative, with consequent dimensional changes.

In the absence of thermal gradients or differences in the thermal-expansion coefficients, thermal cycling is probably effective only in that it exposes a sample to a higher temperature, thereby allowing thermal activation to play a greater role in the generation and movement of dislocations. In this case, of course, the thermal treatment would have no meaning unless a residual stress already existed in the sample.

If this hypothesis is generally true, we must expect dimensional instability in a specimen containing residual stresses of the order of 1/2 the MYS or more. The total dimensional change observed will depend, of course, on the relative volume of the specimen subjected to excessive residual stresses. In the present case, the stresses due to machining, while high, affected only a relatively small volume fraction of the sample and the observed dimensional changes, even after thermal or stress cycling, were small. On the other hand, the residual stresses remaining after a 2-1/2 percent plastic elongation led to severe dimensional changes. This suggests that dimensional changes should be more readily observable (and more troublesome) on the samples where the residual stress is high over a significant volume fraction of the sample. Some preliminary experiments, utilizing a thin disk (1/8 inch thick by 1-1/4-inch diameter) appear very promising as a means of studying this effect. Alternatively, stress-relaxation experiments on samples of any suitable geometry, having a uniform stress across the specimen, should prove more generally useful than the current experiments using as-machined samples. Such experiments, aimed at verification of the effects of time, temperature, stress cycling, and thermal cycling on the relaxation of stresses are the imperative next step to understanding and eliminating dimensional instability due to stress relaxation.

CONCLUSIONS

(1) The techniques of measurement chosen work well for the materials being studied. End measurements are reproducible even on the softest of the specimens. Foil strain-gage measurements of plastic strain are acceptable on all of the metals save the titanium alloy, when a capacitance technique has been used.

(2) The microyield strengths measured are consistently below those reported in the literature. This is, at least in part, attributable to the increased refinement of the equipment and methods used. In particular, the special care taken in preparing the specimen surfaces is believed to have been largely responsible for the more realistic but lower values.

(3) The microcreep data, while limited, demonstrate that significant plastic strain can be observed at stresses as low as 50 percent of the microyield strength.

(4) Conventional machining practice introduces residual stresses near the surface which may exceed the microyield strength. These stresses are often more severe for shallow machining cuts than for deeper cuts, contrary to the reasoning behind current machining practice.

(5) Of the materials examined, all were dimensionally stable (to within ±1 μin./in.) in the as-machined condition, over a period of 6 months. Thermal or stress cycling sometimes led to small dimensional changes (less than 5 μin./in.) but did not appear to alter the time-dependent dimensional stability.

(6) Thermally activated and stress-activated dislocation-source exhaustion can form the basis of a selfconsistent hypothesis to account for the observed data.

(7) Much, if not most, of the observed dimensional instability in materials is the result of the relaxation of residual stresses introduced in processing. The thermal and stress environment imposed upon the material plays a significant role in inducing the relaxation of residual stresses.

REFERENCES

(1) Holden, F. C., "A Review of Dimensional Instability in Metals", DMIC Memorandum 189, Battelle Memorial Institute, March, 1964.

(2) Maringer, R. E., "Review of Dimensional Instability in Metals", DMIC Memorandum 213, Battelle Memorial Institute, June, 1966.

(3) Elsea, A. R., Feron, T. H., and Hall, A. M., "Control of Dimensions in High-Strength Heat-Treated Steel Parts", DMIC Report 163, Battelle Memorial Institute, November, 1961.

(4) Schetky, L. M., "The Properties of Metals and Alloys of Particular Interest in Precision Instrument Construction", R-137, MIT Instrumentation Laboratory, January, 1957.

(5) Dieter, G. E., Mechanical Metallurgy, McGraw-Hill, 1961.

(6) Jennings, C., and Brenner, H. S., "Precision Elastic Limit", Machine Design, April 15, 1965.

(7) Davies, R. G., and Ku, R. C., "Solid-Solution Strengthening in Iron-Base Alloys", Trans. AIME, 236, 1691, December, 1966.

(8) Hordon, M. J., and Weihrauch, P. F., "The Dimensional Stability of Selected Alloy Systems", Alloyd General Corporation, Medford, Massachusetts, December, 1963, to April, 1964.

(9) Maringer, R. E., Cho, M. M., and Holden, F. C., "Stability of Structural Materials for Spacecraft Application", Contract No. NAS5-10267, Battelle Memorial Institute, Final Report (in preparation).

(10) Cahn, R. W., Physical Metallurgy, J. Wiley, 1965.

(11) Hartman, D. E., Bresie, D. A., and Roberts, J. M., "Capacitive Extensometer for Microstrain Measurements", Rev. Sci. Instr., 34 (1963), 1272-1273.

(12) ARPA Contract No. DAAHO-68-L-0018.

DOCUMENT CONTROL DATA - R&D

(Security classification of title, body of abstract and indexing annotation must be entered when the overall report is classified)

1. ORIGINATING ACTIVITY (Corporate author)	2a. REPORT SECURITY CLASSIFICATION
Battelle Memorial Institute	Unclassified
	2b. GROUP

3. REPORT TITLE

Study of Microplastic Properties and Dimensional Stability of Materials

4. DESCRIPTIVE NOTES *(Type of report and inclusive dates)*

Final Report, July 1967 - June 1968

5. AUTHOR(S) *(Last name, first name, initial)*

Ingram, Albert G., Maringer, Robert E., Holden, Frank C., Hoskins, M. E., Sovik, J. H.

6. REPORT DATE	7a. TOTAL NO. OF PAGES	7b. NO. OF REFS
August	104	12

8a. CONTRACT OR GRANT NO.	9a. ORIGINATOR'S REPORT NUMBER(S)
AF 33(615)-5215	
b. PROJECT NO. 7351	
c.	9b. OTHER REPORT NO(S) *(Any other numbers that may be assigned this report)*
d.	

10. AVAILABILITY/LIMITATION NOTICES

This document may be further distributed by any holder only with specific prior approval of the Processing and Nondestructive Testing Branch, Metals and Ceramics Division, Air Force Materials Laboratory, WPAFB, Ohio 45433.

11. SUPPLEMENTARY NOTES	12. SPONSORING MILITARY ACTIVITY
	Air Force Materials Laboratory
	Directorate of Laboratories
	Air Force Systems Command
	Wright-Patterson Air Force Base, Ohio

13. ABSTRACT

Average microyield strengths of 39,000 psi for Ni-Span-C, 70,000 psi for 440 C stainless steel, 7,500 psi for A356 cast aluminum, 75,000 psi for Ti-5Al-2.5Sn, 47,000 psi for Super PEL beryllium, and 29,000 psi for AD995 aluminum oxide were measured. The microcreep behavior of these materials at 50 and 75 percent of their microyield strengths was evaluated also. Experiments showed that plastic strains of 20-40 μin./in. increased the microyield strength of Ni-Span-C and 440 C stainless steel, but plastic strains of 2.5 and 5 percent decreased the microyield strength of Ni-Span-C. Electron-microscope studies indicated that microplastic deformation of Ni-Span-C is the result of dislocation generation at second-phase particles in grain boundaries. For A356 cast aluminum, the generation of dislocation at Mg_2Si particles appeared to be the controlling mechanism.

Dimensional stability studies showed that plastic strains of 20-40 μin./in. did not result in any significant deterioration in dimensional stability, but extensive contraction of specimens strained 2 percent was noted. The mild stress and thermal cycling treatments employed in this research sometimes caused a small change in length upon cycling, but showed no effect on subsequent dimensional stability over a period of at least six months.

Machining experiments revealed that the residual stresses introduced by machining can exceed the microyield strength of an alloy. Furthermore, the highest residual stresses are frequently associated with the finest finishing cuts.

A capacitor strain gage was designed, constructed, and used to measure the microyield strength of Ti-5Al-2.5Sn.

A phenomenological theory has been devised which is selfconsistent with the bulk of the observed behavior.

DD FORM 1473 (1 JAN 64)

Security Classification

14.		LINK A		LINK B		LINK C	
	KEY WORDS	ROLE	WT	ROLE	WT	ROLE	WT
Microplastic Properties							
Microstrain							
Microyield Stress							
Precision Elastic Limit							
Dimensional Stability							
Titanium							
Stainless Steel							
Beryllium							
Aluminum Invar							
Aluminum Oxide							